AFOSR TR FINAL REPORT

CHARACTERIZATION AND MEASUREMENT OF DEFECTS IN THE VICINITY OF FASTENER HOLES BY NONDESTRUCTIVE INSPECTION

PAUL F. PACKMAN
R.M. STOCKTON
J.M. LARSEN

DEPARTMENT OF MATERIALS SCIENCES AND METALLURGICAL ENGINEERING
VANDERBILT UNIVERSITY
NASHVILLE, TN. 37235

This Research was Sponsored by the

AIR FORCE OFFICE OF SCIENTIFIC RESEARCH
Through Contract Number F44620-73-C-0073

September 1975

use VANDERBILT UNIVERSITY
DEPARTMENT OF MATERIALS SCIENCE AND ENGINEERING

(18) AFOSR (19) TR-76-0440

(6) CHARACTERIZATION AND MEASUREMENT OF DEFECTS IN THE VICINITY OF FASTENER HOLES BY NONDESTRUCTIVE INSPECTION.

(10) PAUL F. PACKMAN,
R. M. STOCKTON
J. M. LARSEN

(9) Final rept.,

DEPARTMENT OF MATERIALS SCIENCES AND METALLURGICAL ENGINEERING

VANDERBILT UNIVERSITY
NASHVILLE, TN. 37235

This Research Was Sponsored By The

AIR FORCE OFFICE OF SCIENTIFIC RESEARCH

Through Contract Number (15) F44620-73-C-0073

(11) Sept [redacted] 75

(16) AF-9782 (12) 167p.

(17) 9782b5

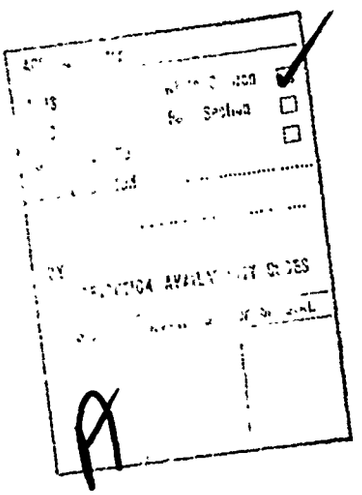

UNCLASSIFIED

SECURITY CLASSIFICATION OF THIS PAGE (When Data Entered)

REPORT DOCUMENTATION PAGE		READ INSTRUCTIONS BEFORE COMPLETING FORM
1. REPORT NUMBER AFOSR - TR - 76 - 0400	2. GOVT ACCESSION NO	3. RECIPIENT'S CATALOG NUMBER
4. TITLE (and Subtitle) CHARACTERIZATION AND MEASUREMENT OF DEFECTS IN THE VICINITY OF FASTENER HOLES BY NONDESTRUCTIVE INSPECTION		5. TYPE OF REPORT & PERIOD COVERED FINAL 6. PERFORMING ORG. REPORT NUMBER
7. AUTHOR(s) P F PACKMAN R M STOCKTON J M LARSEN		8. CONTRACT OR GRANT NUMBER(s) F44620-73-C-0073
9. PERFORMING ORGANIZATION NAME AND ADDRESS VANDERBILT UNIVERSITY P O BOX 3245, STATION B NASHVILLE, TENNESSEE 37235		10. PROGRAM ELEMENT, PROJECT, TASK AREA & WORK UNIT NUMBERS ~~681307~~ 9782-05 61102F
11. CONTROLLING OFFICE NAME AND ADDRESS AIR FORCE OFFICE OF SCIENTIFIC RESEARCH/NA BUILDING 410 BOLLING AIR FORCE BASE, D C 20332		12. REPORT DATE Sept 1975 13. NUMBER OF PAGES 64
14. MONITORING AGENCY NAME & ADDRESS(if different from Controlling Office)		15. SECURITY CLASS. (of this report) UNCLASSIFIED 15a. DECLASSIFICATION/DOWNGRADING SCHEDULE

16. DISTRIBUTION STATEMENT (of this Report)

Approved for public release; distribution unlimited.

17. DISTRIBUTION STATEMENT (of the abstract entered in Block 20, if different from Report)

18. SUPPLEMENTARY NOTES

19. KEY WORDS (Continue on reverse side if necessary and identify by block number)

DEFECT DETECTION
NONDESTRUCTIVE INSPECTION
ULTRASONICS
EDDY CURRENTS
BOLT HOLES
FATIGUE CRACKS

20. ABSTRACT (Continue on reverse side if necessary and identify by block number)

This report describes the ~~work conducted~~ under a program designed to develop advanced nondestructive inspection testing and signal processing techniques that can be used to improve the capability and reproducibility of detection of defects associated with fastener holes. The program consisted of parallel studies designed to investigate those metallurgical and mechanical characteristics associated with flaws in the vicinity of straight shank fastener holes that would influence their detectability. Two NDI procedures were used: shear wave ultrasonics and eddy current. The results show that crack size, local stresses,

DD FORM 1 JAN 73 1473 EDITION OF 1 NOV 65 IS OBSOLETE

UNCLASSIFIED

SECURITY CLASSIFICATION OF THIS PAGE (When Data Entered)

* were investigated.

width of the crack and material within the crack are primary factors influencing their detectability, with the crack size, crack orientation, and local stress being the dominating factors, particularly with ultrasonic techniques. Eddy current technique are particularly sensitive to crack size and crack width, but relatively insensitive to local stresses and orientation. The influence of stress level used to grow the defect was also found to be a factor in its detectability, providing no other stresses were applied. A technique using the concept of a transfer function Tr(s) and corresponding Bode plots has been developed that allows recognition of and detection of small 0.030 inch cracks anywhere within the bolt hole scan region. For normal conditions this means that minimum of two scans must be made for each bolt hole. The sensitivity of this technique decreases as the angle of the normal of the crack to the plane of the shear wave increases, i.e. when the crack is perpendicular to the plane of the wave the sensitivity is highest. The Laplace transfer function approach appears highly useful for detection of the defect, but has only limited usefulness in characterizing the size shape and orientation of the defect. An eddy current bolt hole scan unit has been designed and constructed that allows continuous monitoring of the interior of the surface of the bolt hole area. The technique uses a 5MhZ differential coil scanning in a helical path synchronized with a strip chart recorder. The presence of the defect within the area produces a pertubation that is relatively easy to recognize. The minimum flaw size detectable is 0.030 inches. Preliminary studies using Fourier transfer functions indicated that there is sufficient information within the transfer function to allow some characterization to be made of the orientation, width and length of the defect.

ACKNOWLEDGEMENTS

The authors wish to acknowledge the support and assistance of the faculty and staff of the Department of Materials Sciences and Metallurgy of Vanderbilt University during the conduct of this research program. We also wish to extend our appreciation to the Computer Center of Vanderbilt University for their assistance and patience.

Finally the authors wish to extend their thanks to Mr. William Walker, AFOSR for his continued financial support and patience and encouragement in this program, and to Dr. Pommerantz formerly of AFOSR for his interest and encouragement.

Nashville, Tennessee
September 1975

ABSTRACT

This report describes the work conducted under a program designed to develop advanced nondestructive inspection testing and signal processing techniques that can be used to improve the capability and reproducibility of detection of defects associated with fastener holes. The program consisted of parallel studies designed to investigate those metallurgical and mechanical characteristics associated with flaws in the vicinity of straight shank fastener holes that would influence their detectability. Two NDI procedures were used; shear wave ultrasonics and eddy current. The results show that crack size, local stresses, width of the crack and material within the crack are the primary factors influencing their detectability, with the crack size,crack orientation and local stresses being the dominating factors, particularly with ultrasonic techniques. Eddy current techniques are particularly sensitive to crack size, and crack width, but relatively insensitive to local stresses and orientation. The influence of stress level used to grow the defect was also found to be a factor in its detectability, providing no other stresses were applied.

A technique using the concept of a transfer function $T_f(s)$ and corresponding Bode plots has been developed that allows recognition of and detection of small 0.030 inch cracks anywhere within the bolt hole scan region. For normal conditions this means that a minimum of two scans must be made for each bolt hole. The sensitivity of this technique decreases as the angle of the normal of the crack to the plane of the

shear wave increases, with cracks perpendicular to the plane of the wave, the sensitivity is highest. The Laplace transfer function approach appears highly useful for detection of the occurance of the defect, but has only limited usefulness in characterizing the size, shape and orientation of the defect.

An eddy current bolt hole scan unit has been designed and constructed that allows continuous monitoring of the interior of the surface of the bolt hole area. The technique uses a 5 mhz differential coil scanning in a helical path synchronized with a strip chart recorder. The presence of the defect within the area produces a pertubation that is relatively easily recognizable. The minimum flaw size detectable is 0.030. Preliminary studies using Fourier transfer functions indicated that there is sufficient information within the transfer function to allow some characterization to be made of the orientation, width and length of the defect

CONTENTS

LIST OF FIGURES

LIST OF FIGURES (Continued)

LIST OF FIGURES (Continued)

TABLES

SECTION I

INTRODUCTION

Fatigue cracks are known to develop in fastener holes of structural members of aircraft during the operational lifetime of that aircraft. A great number of these fatigue cracks initiate in holes that are associated with highly stressed joints, containing straight shank fasteners, rivets, taperlok or other patented systems. Even though a great deal of care is usually involved in the design and fabrication of these joints, service history examination and IRAN* procedures have shown that cracks may develop prior to the design lifetime of the aircraft and may necessitate significant curtailment of mission, or decrease in operational characteristics.

Typical examples of this are: (1) the loss in payload and operational lifetime due to the premature formation of fatigue cracks in the top wing surface fastener holes, (2) premature failure of a wing carry-thru-box during cold proof testing; originating at a fastener hole crack (supposedly stress corrosion induced) and (3) cracking of aluminum splice plates observed in accelerated fatigue tests. Current NDT and fracture mechanics programs initiated on the B-1, F-14 and F-15, F-16 have been designed to take positive action designed to minimize unexpected failure of critical structural members due to the presence of such cracks under fasteners. (1)

The fracture mechanics-nondestructive inspection design process uses the concept of the stress intensity factor K_i to determine the design lifetime of a part containing a small flaw. The initial design requirements are such that the combina-

*IRAN-Inspect and Repair as Necessary

tion of mission load spectrum (during the lifetime of the component), initial flaw sizes and material subcritical crack growth potential (da/dN) do not permit the initial crack assumed in the design to grow to a size sufficient to cause failure. This presumes that all flaws larger than the initially assumed small flaw can be reliably and efficiently found, located, identified and removed from the part prior to actual use.(2)

It should be recognized that one of the major problems associated with the detection of small cracks is the detection of fatigue cracks eminating from fastener holes. For the routine inspection of unfilled holes several techniques have been developed and can be used depending upon the acceptance limits required for the inspection.

These include:

1. X-ray analysis. Used where larger cracks can be tolerated or if accessability is difficult.(3)

2. Penetrants. Used w en disassembly and subsequent etch inspection techniques are possible.(4)

3. Optical examination. Used when small cracks must be detected but requires extensive time and cost.

4. Ultrasonics. Can detect small cracks and are used extensively, but difficult to interpret.

5. Eddy current. Used with bolt hole probes, with high sensitivity can detect small cracks.

However, increased requirements of high performance aircraft and newer critical requirements on large cargo aircraft require

the reliable detection of cracks as small as 0.030 in the smallest dimension. This will require a relatively unusual NDT effort and probably cannot be obtained using the standard NDT techniques without a major revision of the techniques for interpretation and analysis of the output signals.

It seems rather ineffective from a cost effective point of view to spend a great deal of time on extremely sophisticated techniques of NDT that have been proposed. It appears extremely unlikely that exotic NDT techniques will find major on-line use for detection of cracks under installed fasteners no matter how successful they may be in the laboratory. Since the problem is directed toward a field inspection problem, techniques such as laser holography, acoustic imagery , liquid heat crystals, etc. cannot be considered viable techniques at this time.

Present inspection techniques require either the removal of the fastener for inspection, or depend on the size of the crack being sufficiant to extend beyond the head of the fastener so that it may be detected visually.

SECTION II

PROGRAM OBJECTIVES

The overall objective of this program was to develop techniques that would be able to reliably detect and characterize small defects in the vicinity of fastener holes, and to develop methods for detecting small cracks with the fastener still in place. The specific objectives were:

- Extension of shear wave ultrasonic indicium analysis and mathematical analysis of signals associated with fastener holes containing small defects, and to characterize those parameters that can influence the detectability of small defects in the vicinity of the fastener hole.
- To determine reliable methods for analysis of signals associated with eddy current bolt hole probe examination of fastener holes to determine if small defects could be reliably detected and characterized.
- To develop fast Fourier analysis signals associated with eddy current helical bolt hole probe scans.

This program included an experimental assessment necessary for understanding the factors that influence the ultrasonic and eddy current techniques ability to find small flaws. The overall program was accomplished in three phases as follows:

Phase I, Ultrasonics

The scope of the ultrasonic technique for characterization of defects was examined. This included comparison of signals from fatigue cracks, EDM notches, as well as a study of the

factors influencing the amplitude of the signal from fatigue cracks, on part through cracks and cracks growing out of fastener holes.

Phase II, Indicia Studies

The scope of this phase was to evaluate the applicability of the ultrasonic indicia, (a measure of the totality of the reflected ultrasonic energy) as to its ability to detect and characterize small cracks in the vicinity of the fastener hole. In particular the impulse analysis technique was used to determine if and when a defect was present in the vicinity of the fastener hole.

Phase III, Eddy Current Studies

This portion of the program concentrated on improving and examining the signals from a unique eddy current scan unit. Signals associated with EDM notches, fatigue cracks, corrosion cracks and other defects associated with the fastener hole with the fastener removed were examined in this portion of the study.

The end aims of Phases I and III were to be the development of computer software and analysis technique for implementation on existing Air Force equipment.

SECTION III

TEST SPECIMENS

Four types of specimens were used.

Part Thru Cracks in Flat Plates

These specimens were made of 7075-T6 Aluminum, Ti6Al-4V and D6AC steel.

The 7075-T65 Aluminum specimens are shown in Figure 1 and tabulated in Table I. They consist of a fatigue cracked, part thru crack, initiated on one side of the plate from a small microweld solidification spot and grown in three point bending by tension-tension fatigue. After the crack had grown to a sufficient size, beyond the weld solidification zone, the central area was polished to remove the crater of the weld spot. Cracks of different length were produced by monitoring the growth with a small microscope of approximately 50X. The test frequency was approximately 10 cps. Crack lengths ranging from 0.015 to 0.4 inches were produced.

Some specimens made of Ti6Al-4V and D6AC steel used in the B-1 inspection program and fatigued in a Amsler high stress fatigue machine were also evaluated in this program. These were provided by AFML & R.I. In these specimens, the initial solidification initiation spot was machined off with a multiple point milling machine. All these specimens had a 0.0005 etch prior to inspection. After fatigue these were subject to some 24 hours of stress corrosion with a mild 5% salt solution.

Part Thru Cracks Eminating From Fastener Holes

The specimens were initially prepared in a manner similar to that described above. The crack was grown to a predetermined

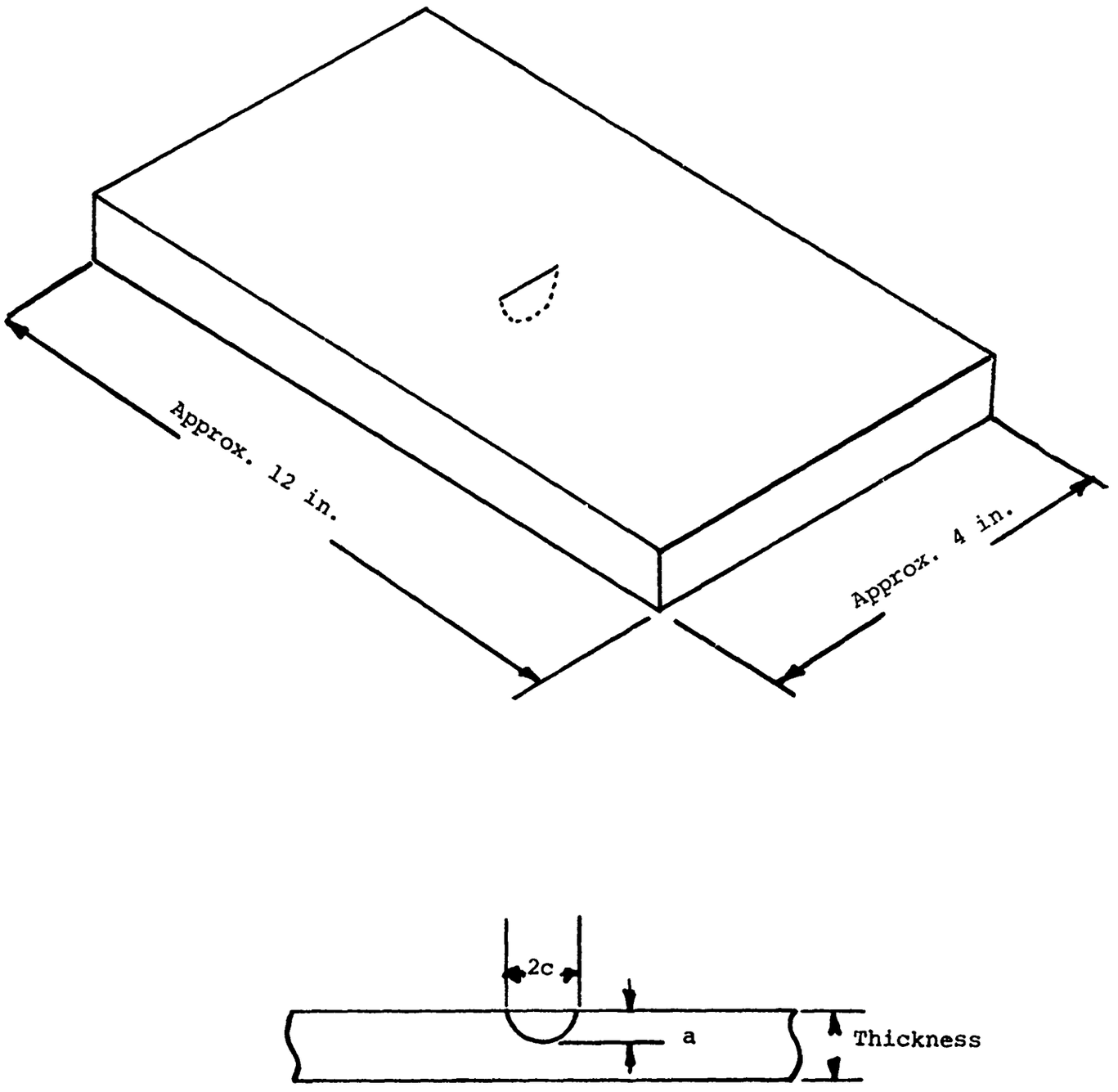

Figure 1

Schematic Showing Part Through Fatigue
Crack in Aluminum Plate

length, then the fastener hole location selected, the hole drilled and reamed. A few additional fatigue cycles were put on the specimen to grow the crack for a short additional distance. The specimen configurations were both part through, semicircular, and thru thickness cracks. Several attempts to grow completely internal cracks by fatigue crack initiation in the interior of the hole were made, but the crack almost always grew in a longitudinal direction considerably faster than in the depth direction and attempts were abandoned. Table III lists typical specimen configurations and sizes for this series.

EDM Notches

A considerable amount of test evaluation was carried out on defects produced by electrical discharge machine (EDM) notches. The use of notches as test specimens was desirable because of the degree of control available over notch size, width and location. However, typical ultrasonic response curves showed that reflections from EDM slots were considerably higher than those found from fatigue cracks.

EDM slots were cut into flaw plates to produce small surface type flaws, as well as cut into predrilled and reamed holes to produce defects in the vicinity of fastener holes. Three types of defects associated with fastener holes were produced. These are (1) through thickness constant depth defect (2) through thickness variable depth defect and (3) part through defect, either emerging on one face or completely internal. Typical specimens are listed in Table IV.

Plates With Fastener and Defect

A limited number of specimens were fabricated with defects

in place and the fastener installed. These were selected from previous drilled and examined plates and the straight shank fastener installed following recommended procedure. In several cases, faying surface sealant Mil S-8802 was installed per recommended practice.

Fastener Hole Defect Configurations

Typical defect configurations associated with highly stressed regions of fastener holes are shown in Figure 2.[4]

There are several common locations for defects associated with the fastener hole. These are:

Part through corner crack eminating from the top or bottom of the fastener hole, either under the head or under the nut.

Completely internal defect in a part through configuration where there is no evidence of the defect on the top or bottom surface. Typical starter defects for this configuration are at the corners of countersunk holes or small scratches or burrs within the fastener hole.

Through thickness defect where the defect has propagated completely through the depth of the plate.

Faying surface cracks that are located in the thickness direction, and lie parallel to the thickness direction. These may not intersect the bolt hole. The primary material used is either 7075-T6511 or 2024-T3 Aluminum plate ranging between 0.25 to 0.65 inches thick. Figure 3 shows simple straight and staggered fastener arrays associated with the B-52 aircraft,[5] while Figure 4 shows typical arrays associated with the KC-130. Fasteners are of the straight shank type with

Figure 2

Typical Defects Associated
With Fastener Holes

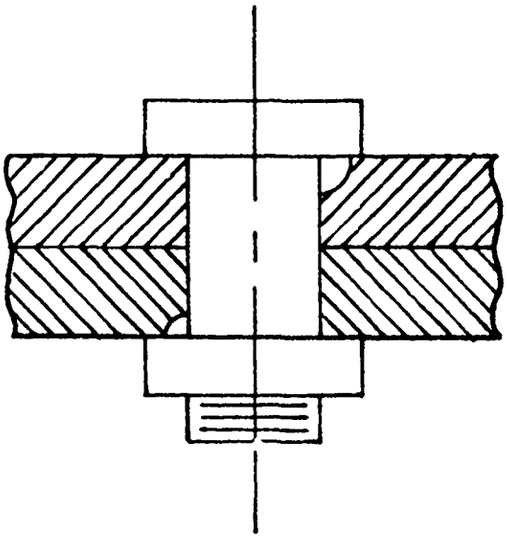

Part Through Corner Cracks

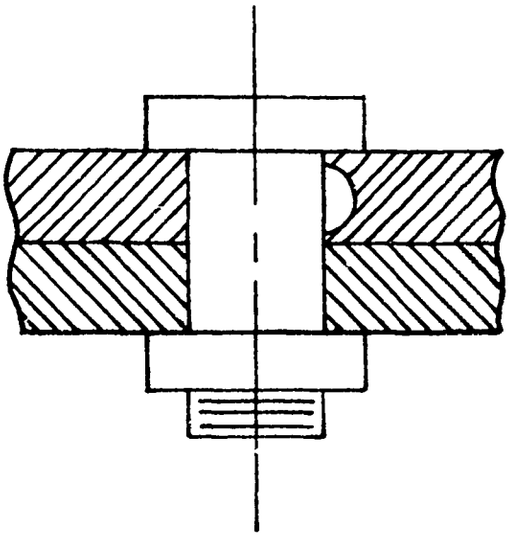

Internal Defect

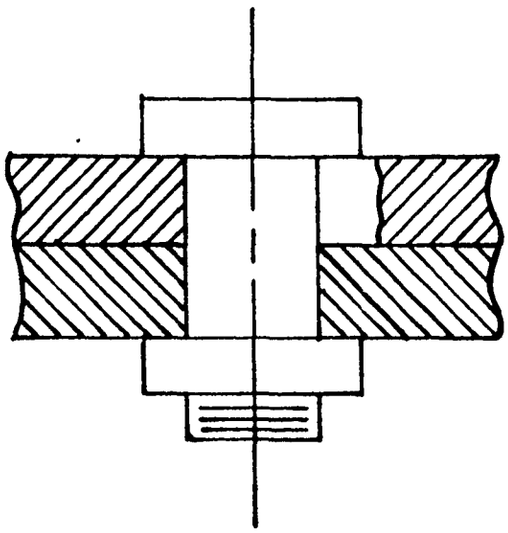

Through Thickness Crack

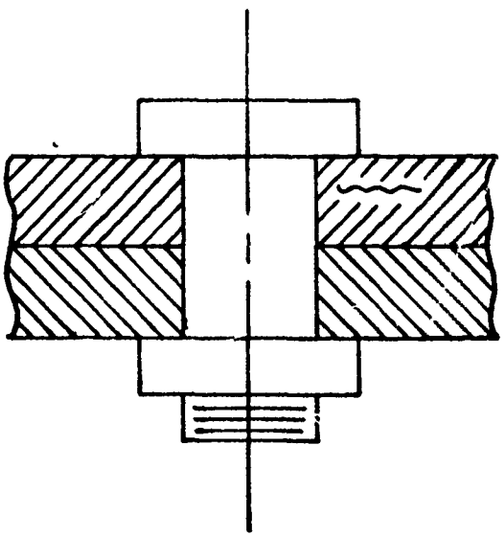

Faying Surface Cracks

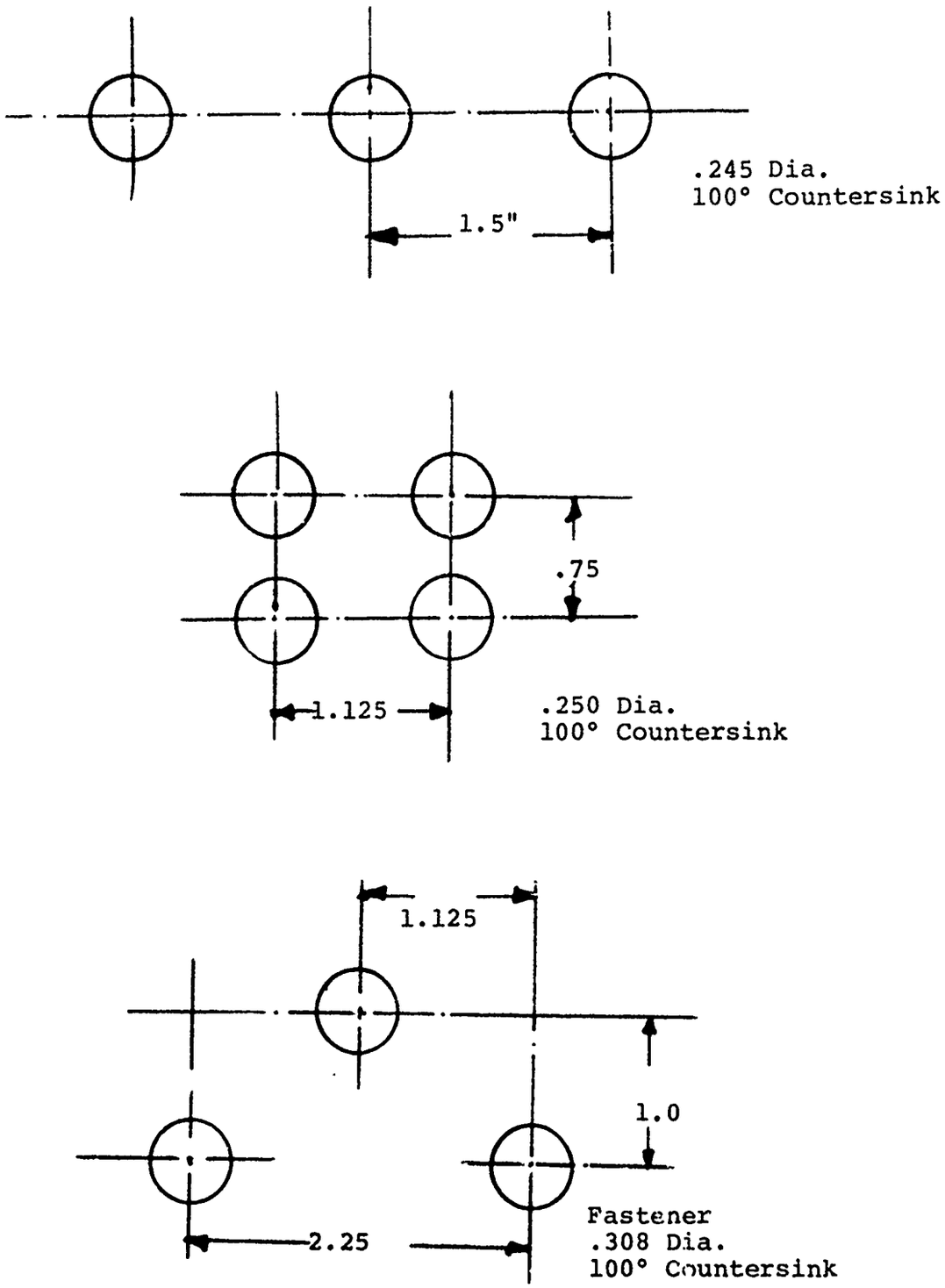

Figure 3

Fastener Arrays; B-52 (5)

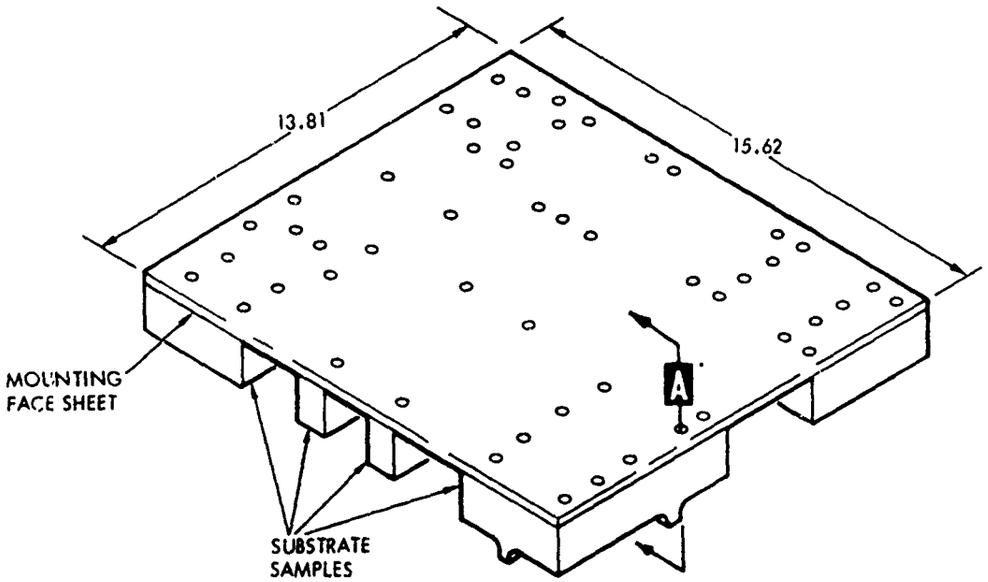

MOUNTED WING FITTING SPECIMENS

NDI- { EDDY CURRENT BOLT HOLE
AUTOMATIC EDDY CURRENT BOLT HOLE

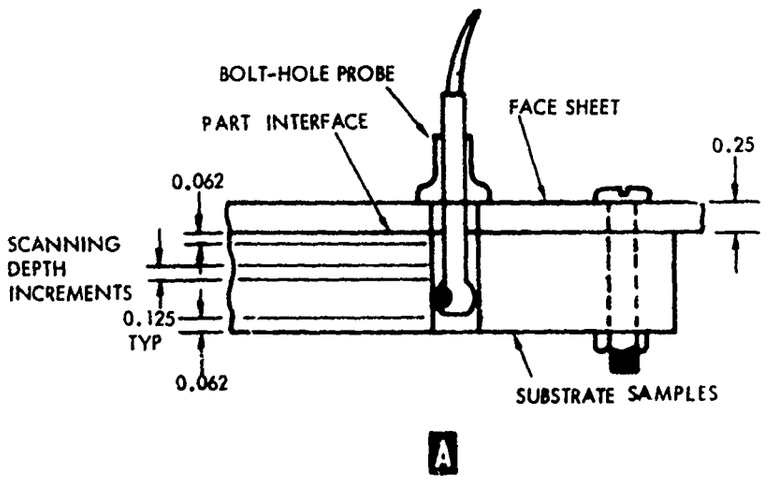

SCAN AT 0.062 INCH FROM EACH END OF HOLE AND AT EACH 0.125 INCH DEPTH INCREMENT BETWEEN THESE.

Figure 4

Fastener Arrays KC 130 (Reference 5)

either protruding or flush heads. The diameters of the actual fasteners range from 0.25 to 0.675. For simplicity all laboratory specimens were produced with a straight shank with a diameter of 0.50 inches. Typical finishing for military fasteners consist of a faying surface sealant of MIL S-8802 and epoxy polymide primer with a top coat of polyurethane enamel. The total thickness of the finish is about 0.002 inches. In laboratory specimens this was produced by a single polyurethane enamel coating without the primer finish. The purpose of the prime is to prepare the surface for adherance of the enamel and it was felt that durability of the enamel finish would not be a problem in this low useage environment. In the initial portion of the program only straight shank fasteners were used containing both part thru and internal defects.

Tapered shank fasteners were examined for comparison and are shown in Figure 5.. These consist of D6AC steel tapered holes with titanium tapered fasteners. These specimens had drilled holes and tapered bores ranging from nominal 0.24 to 0.675 inches in diameter.

Figure 5

Tapered Shank Fasteners

SECTION IV

ULTRASONICS

Introduction

The use of ultrasonics for the detection of defects in structures is well documented.[7] In many applications for detection of unaccessable defects, the use of lucite conversion shoes to introduce shear waves into the material has been in vogue for some time. However, the major thrust of detection techniques for ultrasonics is such that once a method has been developed that will satisfy the requirement, little characterization is performed. In most cases the test specimen used to setup the ultrasonic procedure is either a flat bottom hole calibration or a standard, identical to that required in the actual test. Once the process has been developed to detect the crack, no further study is conducted.

Because of the directness of the application, little coordinated work has been conducted on characterizing those factors that influence the detection and reliability of crack like defects, particularly those associated with fastener holes.

The ultrasonic configuration used in this series of experiments was a standard 45° plastic shoe that was used to convert the normal wave into a shear wave. The unit used was a Sperry UM714 with a fast transigate operating in typical A scan. In all cases the amplitudes reported are scale height readings on the UM 714 Scope. When the signal heights are such that they exceed 4 inches, a sensitivity setting change

was used to reduce the signal to within the scope reading. In these cases a prior calibration curve was constructed using a series of EDM notches that related the scale readings at any densitivity to some magnitude of amplitude height readings on the UM 714 Scope.

Figure 6 shows a typical shear wave ultrasonic setup. The transducer is mounted in a 45° shoe with sufficient oil contact between the transducer and shoe, and between the shoe and the surface of the specimen. The motion of the shoe is such that the magnitude of the defect is the largest value it can assume for a given configuration. If the specimen were examined from the other face, or from the opposite side, that value of reflection would be maximized too.

The ultrasonic interaction between the defect growing out of the fastener hole and the shear wave produced the reflection that is eventually received at the transducer and recorded as a crack. It becomes important to examine each of the variables that can influence the degree of reflection possible from the defect to determine which factors are significant and which can be ignored.

Comparison of Signals Reflected from Cracks and EDM Notches

Shear wave reflections from several EDM notches in steel and aluminum are given in Table V, as a function of the estimated crack length for a through thickness crack. It can be seen that in general the higher the amplitude of the reflection, the larger the defect indication. Assuming that the size of the

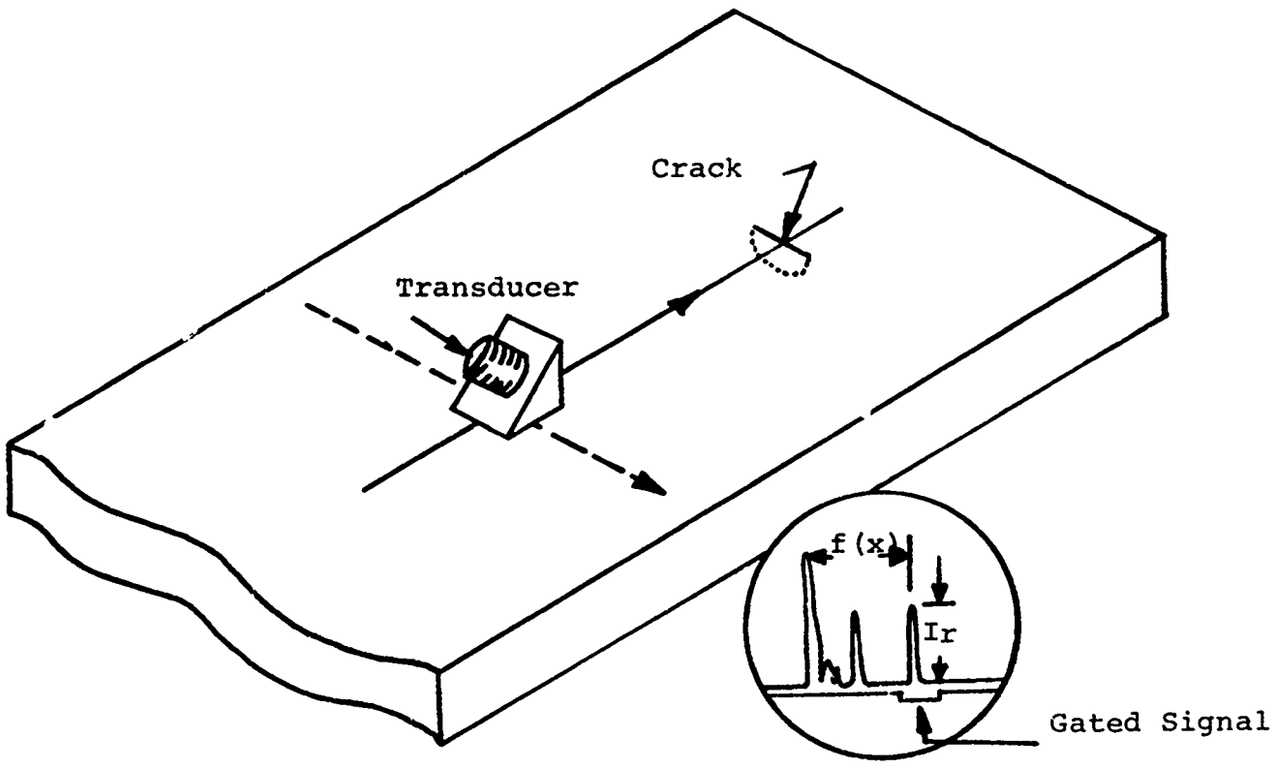

Figure 6

Typical Shear Wave Ultrasonic Setup
for Defect Detection

reflected indication must be at least twice the general interference signal, it can be seen that defects, EDM notches, less than 0.030 inches cannot be reliably found when the transducer indicia is focused on the top of the plate, and can be detected to approximately 0.023 inches when located on the bottom of the plate. Similar results were found for the aluminum specimens, i.e. the larger defects could be detected at the bottom of the plate due to the shorter ultrasonic path needed for the primary reflection. If one considers the presence of a defect at the center of the bolt hole, the approximate sensitivity is a defect on the order of 0.025 inches for signal to noise ratios of 2:1.

It should be noted that the AVG diagram[8] essentially predicts this behavior, i.e. a longer ultrasonic path would result in a smaller ultrasonic cross section, i.e. smaller signal reflections.

The signal response from selected fatigue cracks of varying length and depth are shown in Table VI. In this series, the depth and length are kept essentially in the same ratio, i.e. a = c. It should be noted that for this series, the crack length for reasonable flaw detection is approximately 0.035 inches. However, cracks of lengths less than 0.052 inches do not give signals consistantly above the signal noise values. It should also be noted that the ultrasonic response is only remotely connected to the length or depth of the crack. The signal response from cracks 0.015 inches in radial length is within the scatter of defects of 0.030 inches. In most cases the signal variations are due significantly to the orientation of the defect with respect to the location of the transducer.

This has been found too for simple part through cracks fatigued into plates. Table VII lists a series of part through fatigue cracks in aluminum with crack lengths ranging from 0.0438 inches to 0.3224 inches in surface length. The crack depth is approximately half of this value. It can be seen that for selected specimens there is a correlation between maximum signals reflected and the defect length, or defect area, assuming the depth to width ratio is approximately constant. However, it was found that the reflected intensity varies irregularily with the length.

In all cases the value of the ultrasonic indications when the defect was examined from the reverse side, i.e. shorter path length, were slightly higher than those with the single reflection path width. Hence, smaller defects would be detectable on the lower surface than on the upper surface if signal height readings are used as the primary sensitivity device.

If all specimens containing part through cracks are compared together and the signal height plotted as a function of the flaw size, one quickly sees that there does not appear to be any correlation between signal height and flaw size. The raw data shows no correlation between ultrasonic responses and surface crack lengths. This is similar to results obtained by Yee et all for Titanium specimens.[9] In Figure 7 all the responses from part through Aluminum specimens are plotted as a function of size. In Figure 8 Yee's data is replotted and both show the same general scatter.

Figure 7

Ultrasonic Reflected Amplitude as a Function of Surface Length for Part Through Cracks in Aluminum Blocks

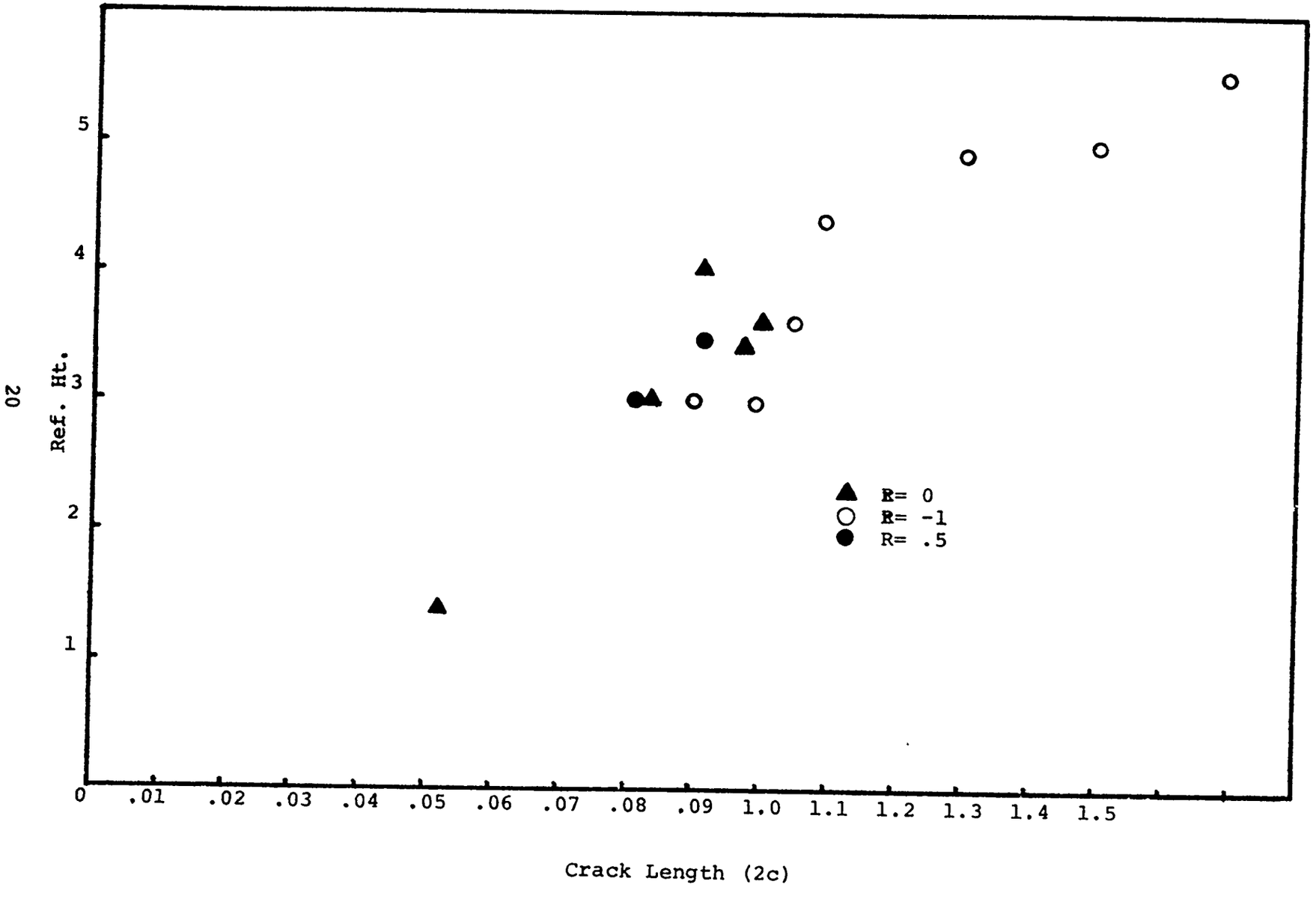

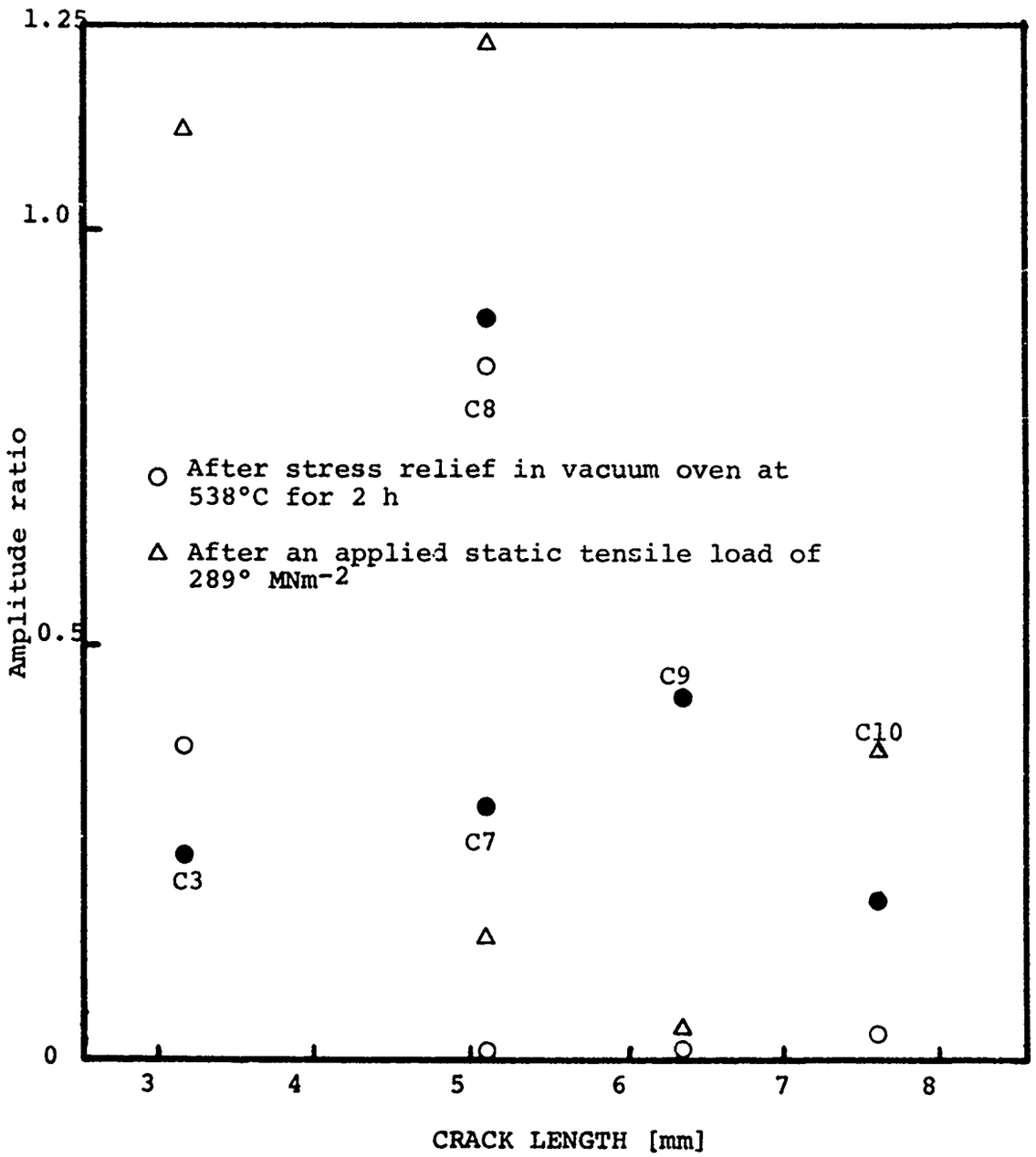

Figure 8 Stress relief affected the ultrasonic response of a deltascan at 5 MHz for cracks in the titanium alloy. Ref (9)

It is obvious that there are several parameters that significantly influence the flaw signal intensity, and if these can be separated, the signals would show a much greater degree of correlation.

Effect of Fatigue Stress Ratio

There are several irregularities in the reflected results obtained from the part through cracked specimens. In particular specimens A20, A22, A35 showed signal heights that were significantly lower than those of corresponding flawed specimens even though their measured sizes lie within those of A13, through A39, i.e .09 to .15 inches. These specimens were fatigued at R values different from those of the others. For these specimens, the R value was greater than zero, where the minimum stress was larger than zero. R = minimum stress/maximum stress. These results are illustrated in Figure 9 which shows the relative signal amplitudes associated with nearly the same flaw sizes as a function of the applied fatigue stress ratio. The values of signal reflection from the specimens fatigued at R = 0, or almost zero, since a small tensile load was always applied at the minimum stress level to prevent the specimen from moving so that there is a definate effect of the fatigue stress level on the amplitude of the reflected signal.

This is due to two effects, (1) the degree of crack closure[10] and (2) the distribution of residual stresses associated with the unloaded crack front in the part through crack due to changes in plastic zones.[11] It is well known that when a fatigue crack is produced in a material, there is associated

Figure 9

Ultrasonic Reflected Signal Intensity for Fatigue Cracks Grown at Differing Fatigue Stress Ratios, R

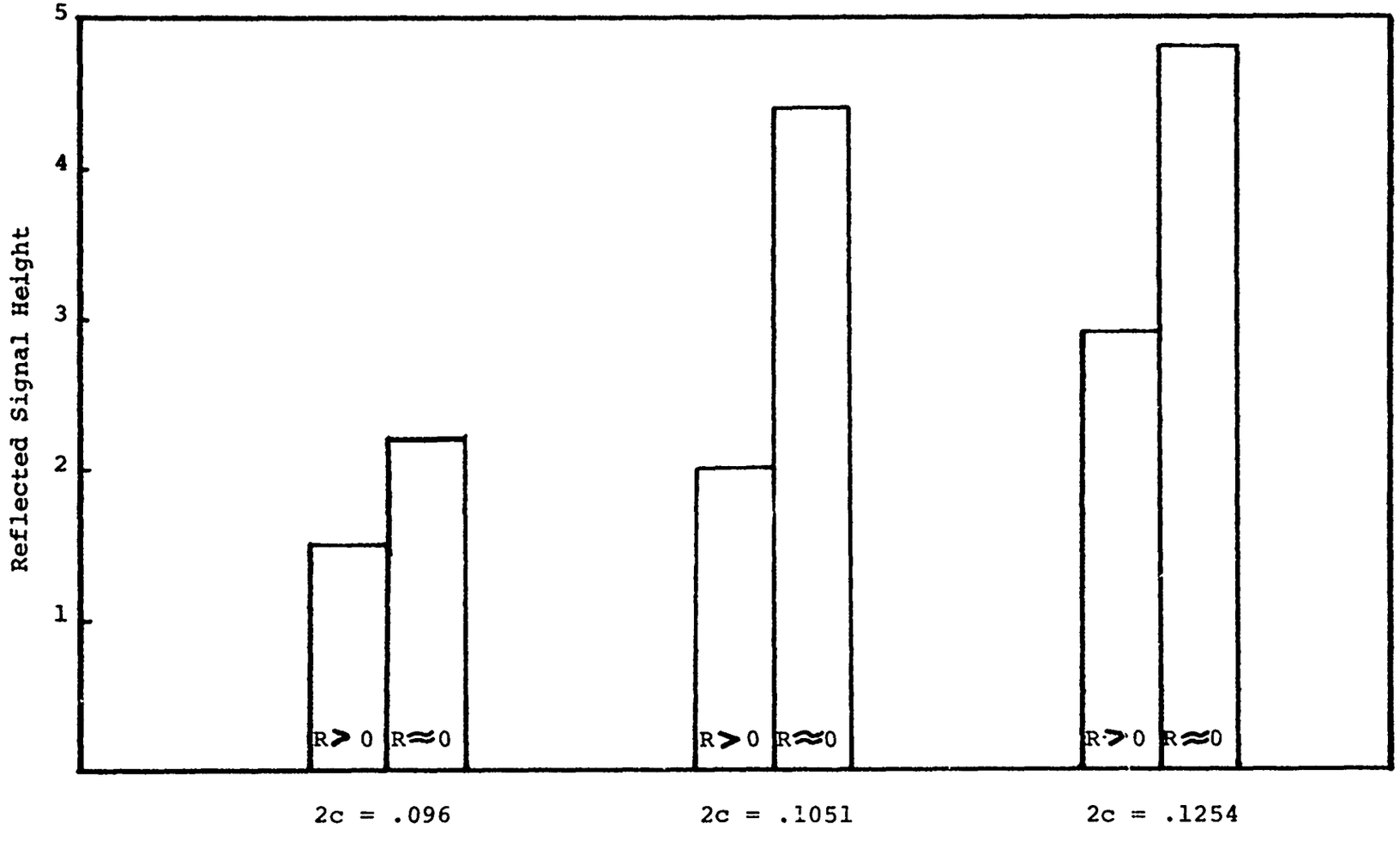

with the propagation of the crack, a plastic wake which represents the previous load cycling history of plastically deformed material associated with the plastic zones of the crack in prior crack front positions. Figure 10 illustrates this effect. This prior plastically deformed region results in a plastic enclave within the larger elastic material surrounding it. Thus, when the material is unloaded, there exists a residual stress pattern that tends to force the surfaces of the crack front together. Elber[10] refers to this as crack closure, where physical touching of the faces of the crack can be expected for positive applied stress levels. Thus, under zero external applied stresses, one would expect that a position of the crack were closed and ultrasonic energy would be able to pass through the crack interface and not be reflected back toward the receiver. The degree of closure is a function of the stress ratio used to produce the fatigue crack, and hence, there is a greater degree of closure for the specimens fatigued at R values greater than zero than there is for specimens fatigued at R=0. This is shown in Figure 11, where the two different R values have been sketched with the same maximum fatigue stress level. Hence, the difference in ultrasonic signals are due to differences in closure associated with the fatigue crack stress cycling.

Effect of Crack Closure

To evaluate the effect of crack tightness on the reflected signal intensity, a series of speciemns were examined under applied loads while on the testing machine. The objective

was to see if there was any loss of signal or signal enhancement due to a stress cycle. A loading fixture, was used to produce four point bending in contrast to the three point bending which was used to produce the fatigue crack. The 45° Lucite shoe was held down on the surface of the specimen with a spring loading attachment so that sufficient oil contact was maintained throughout the test. All loads were applied with the Instron testing machine. Measurements were taken at the same amplifier setting unless the signals exceeded the 4" height for peak saturation, at which time a change in sensitivity was needed to record further increases in signal intensity.

At least two runs were made for each specimen, one in tension, one in compression. For several specimens, additional load cycles were applied to determine the effect of intermediate loadings, and long hold times on the signals.

If the degree of closure, and hence, the residual stress pattern influences the transmittance of the ultrasonic signals across the defect interface one would expect that there would be a difference in reflected signal intensity as a function of the applied stress level. This implies that if external stresses were applied to the crack to open the crack faces, there would be an increase in the reflected signal intensity. This is shown in Figure 12, where the reflected signal intensity is plotted as a function of the external applied bending stress. This shows that the reflected signal intensity increases as the applied stress is increased, but rapidly saturates. Beyond a given applied stress, the rate of increase of signal height decreases, and slowly reaches a maximum value. In

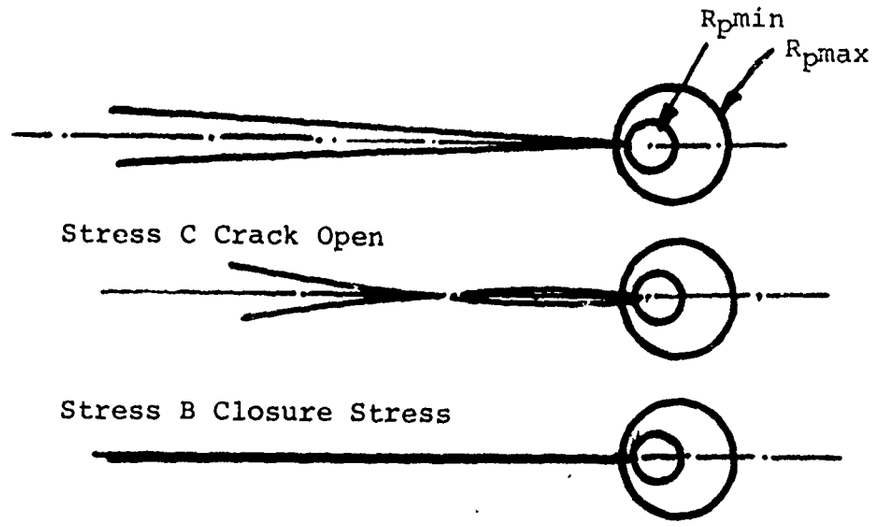

Stress C Crack Under Compressive Closure

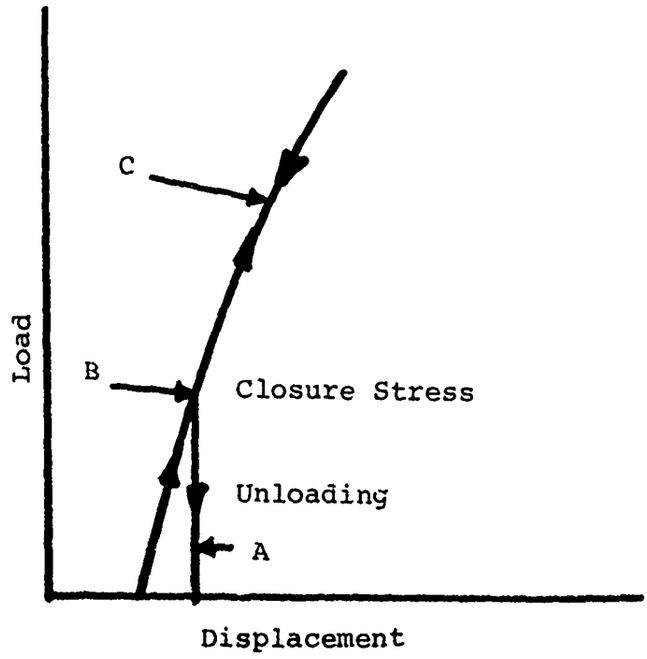

Figure 10

Schematic Illustrating Crack Closure
(After Elber(10))

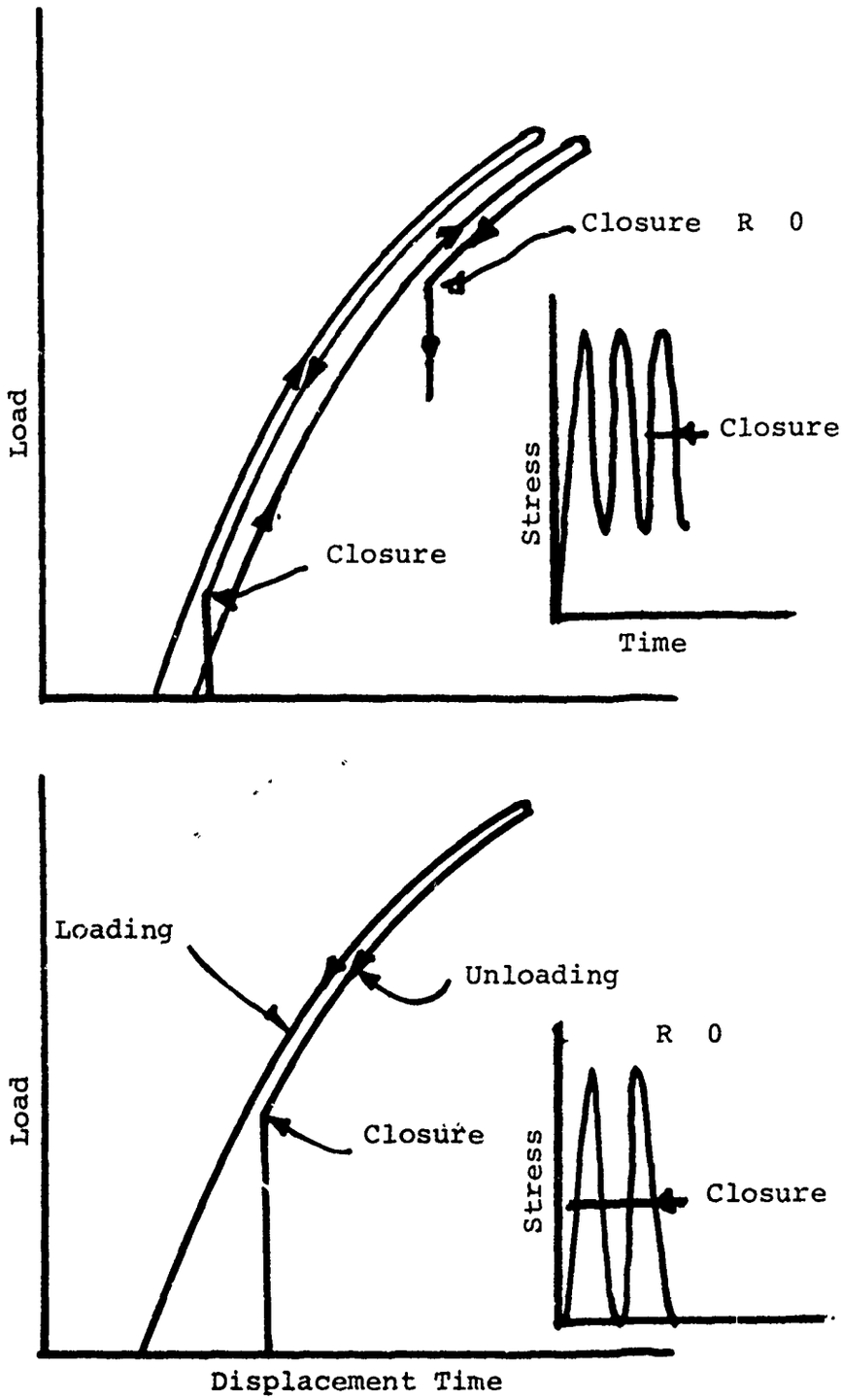

Figure 11

Effect of Stress Ratio (R) on Closure Stress

all cases the saturation stress level is approximately 18ksi. Of particular interest is the reflected signal-applied stress curves for the cracks of length 0.1526 and 0.1560 inches long. For the low stress levels, the 0.1560 inch crack gives a signal height significantly below that for the 0.1526 inch crack. The magnitude of this reflected signal rapidly increases until at approximately 12 ksi the signal heights are almost identical. This implies that the residual stress-closure stress on the 0.1560 inch crack were greater than those on the 0.1526 inch crack, and when the stresses are removed, the reflected signals are almost identical.

Hence, one may conclude that the external stress state exerts a significant influence on the reflected signal intensity, and hence the detectability.

Figure 13 shows similar data obtained by Yee, for Titanium 6Al-4V, and Figure 14 shows similar data found by Prichett, Ratz and Woodmansee for 2024 Aluminum.[9,6]

Figure 15 shows the influence of external applied stress on signals reflected from EDM slots in Aluminum as a function of applied stress. In this case there is essentially no influence of the external stress level.

Figure 16 shows the effect of external applied stress on the reflected signal intensity for fatigue cracks in the vicinity of the fastener holes. These are 0.5 inch fastener holes with part through cracks eminating from one side. The maximum value of reflected peak height is plotted which is the signal associated with the small secondary peak aside from the major peak. The major peak is obviously the reflection from the bolt

Figure 12

Effect of External Applied Stress on Ultrasonic Reflected Signal for Part Through Cracks

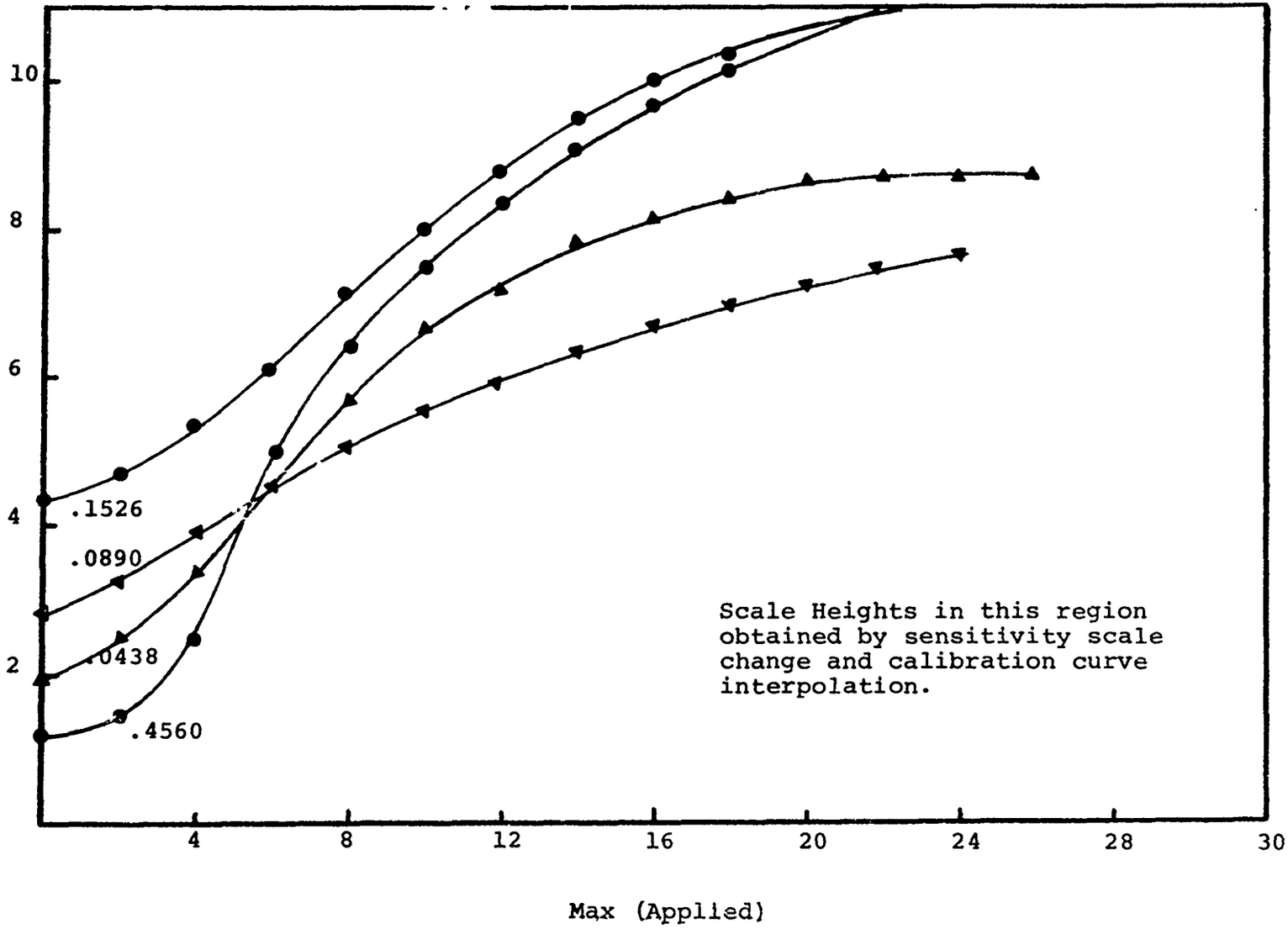

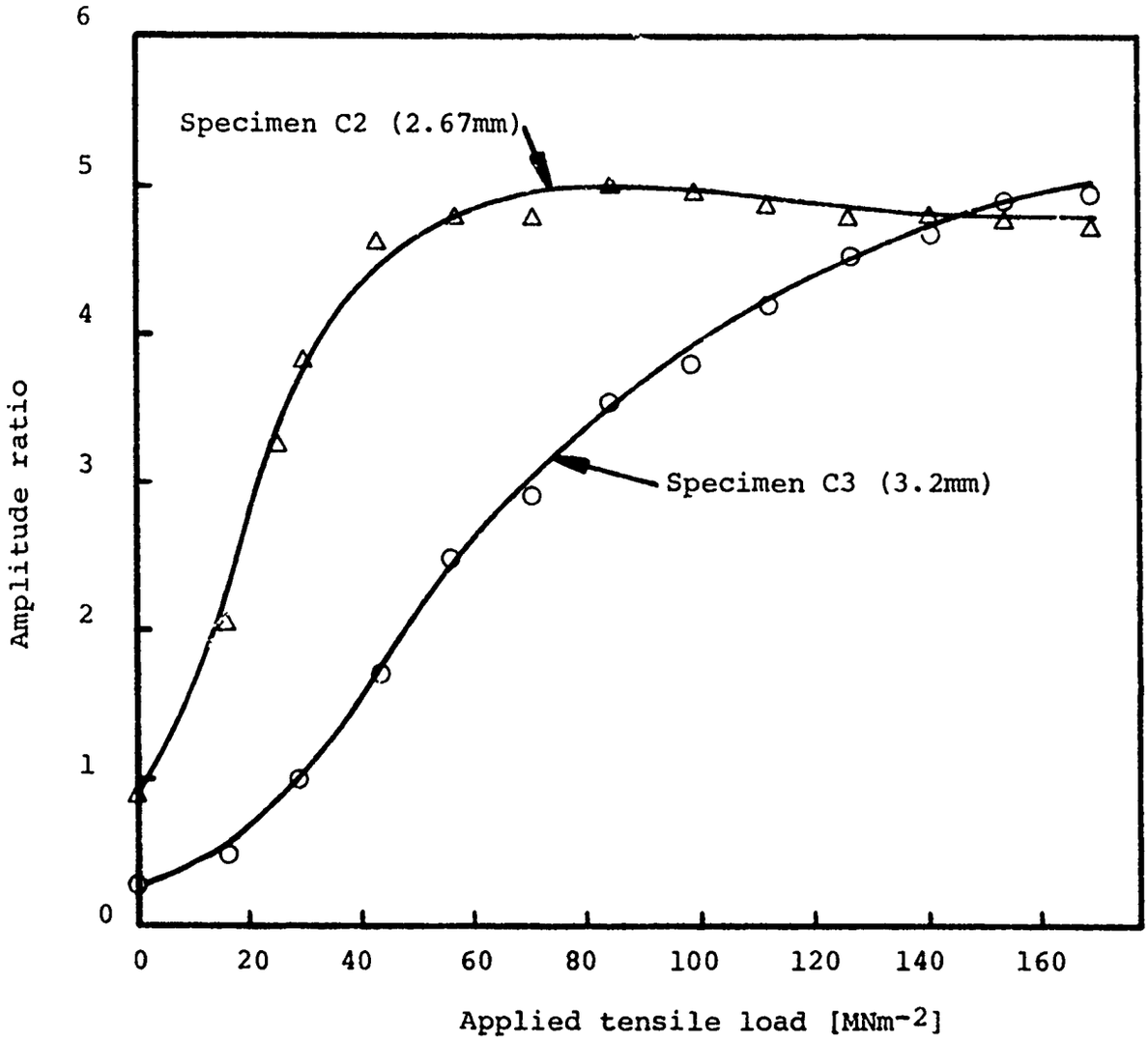

Figure 13 The titanium alloy specimens C2 and C3 were loaded under tension and the ultrasonic response for shear waves at 5 MHz compared to the Elox slot reference standard . Reference (9)

Figure 14

Effect of External Stress on Ultrasonic Signals From Cracks Growing Out of Fastener Holes

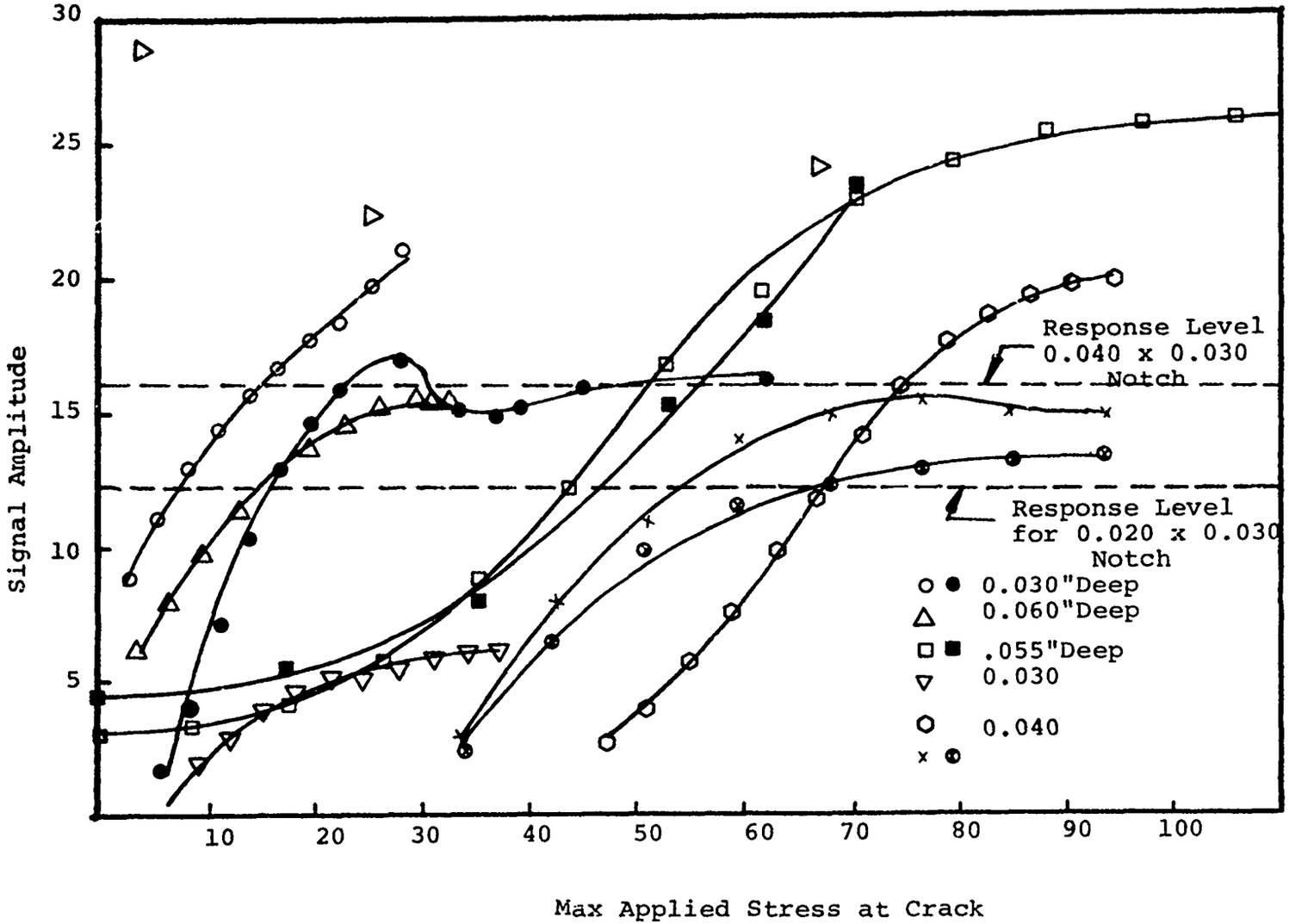

Figure 15

Effect of External Stress on Reflected Signals
From EDM Notches in Aluminum

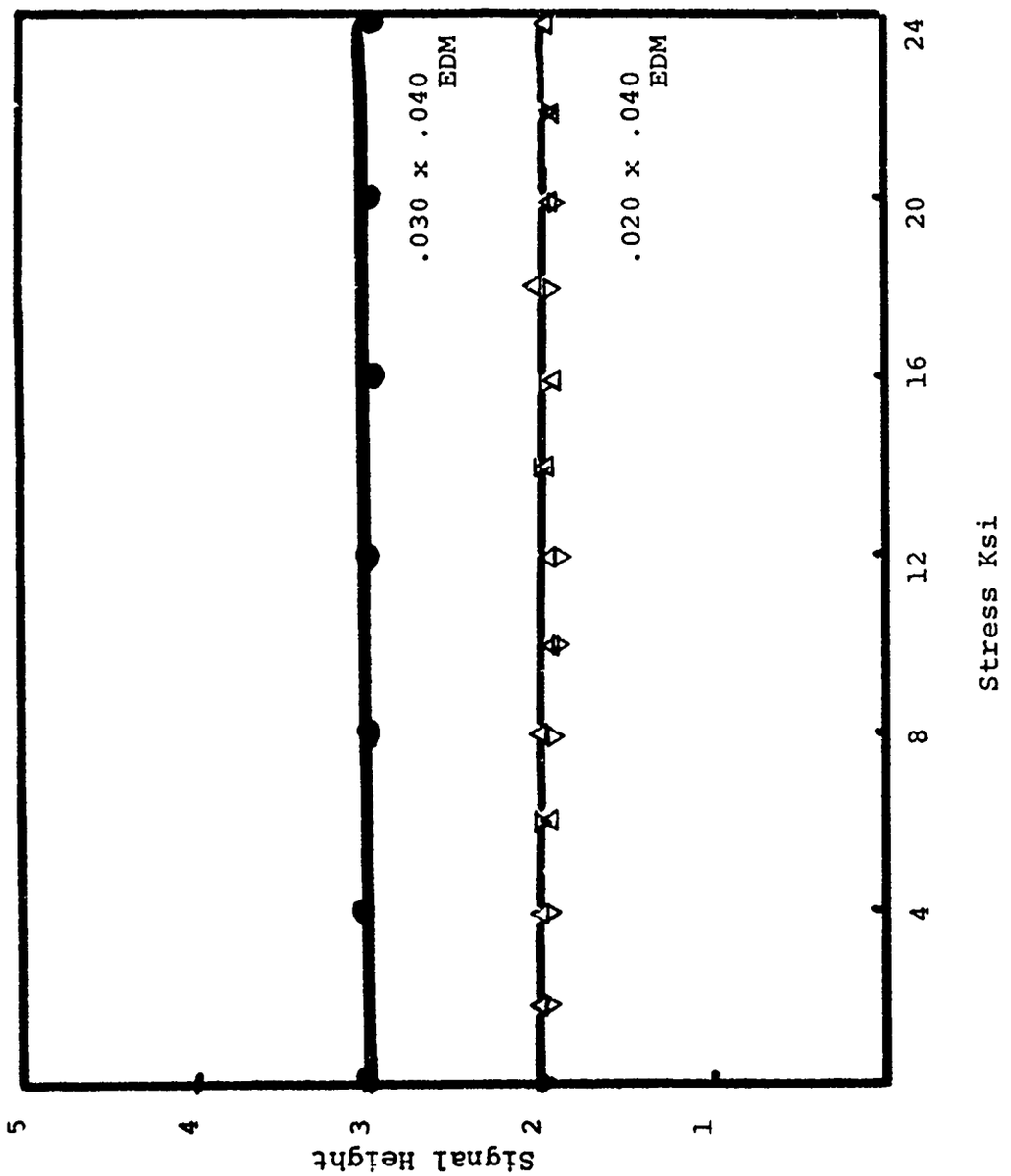

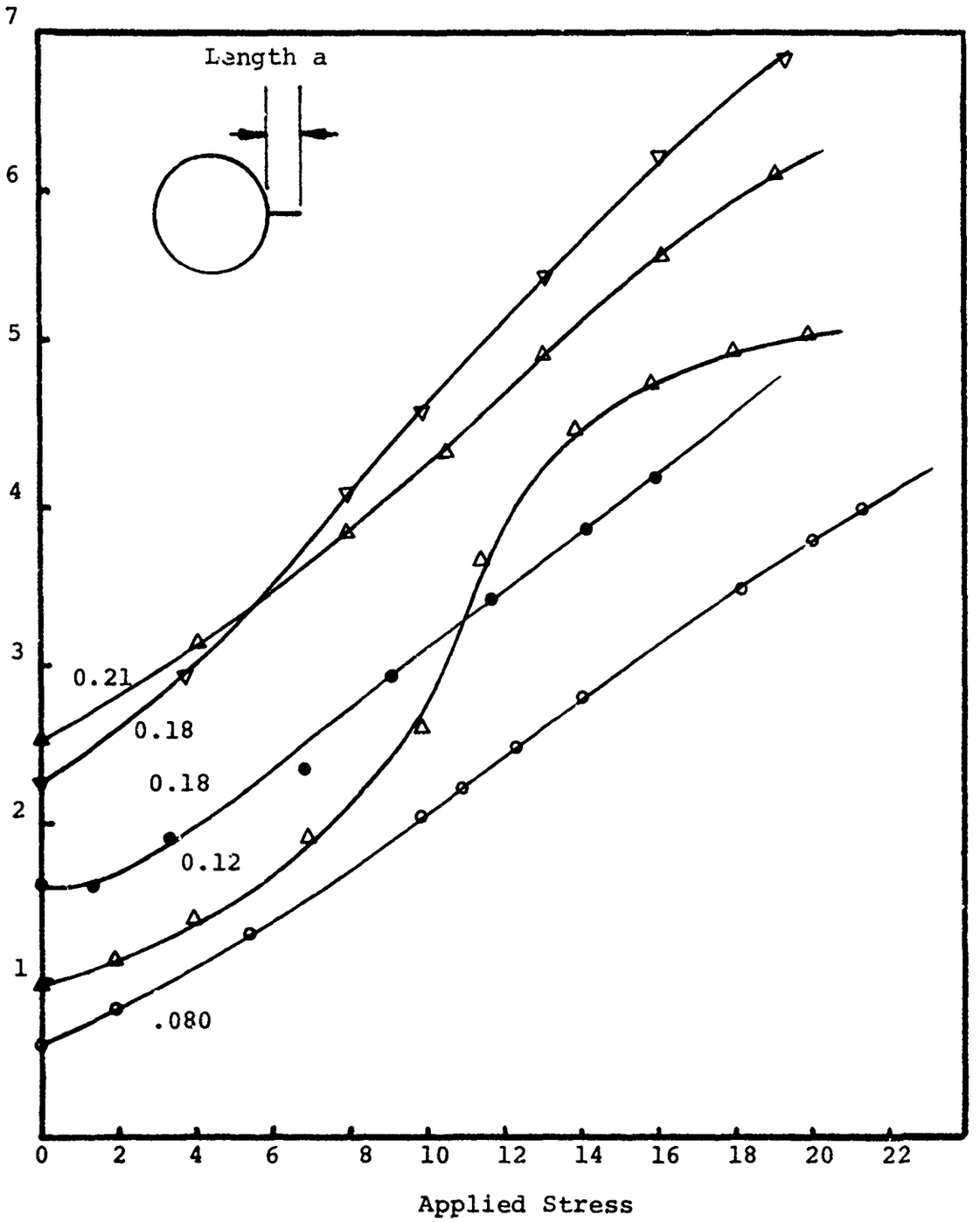

Figure 16

Effect of External Stress on Reflected Signals from Fatigue Cracks Growing Out of Fastener Holes in 7075-T6

hole itself. As would be expected, there was no change in reflected signal intensity from the bolt hole as function of the applied stress, but there was a change in the signal from the fatigue cracks.

Effect of Load Cycling

If the fatigue cracked specimen were loaded until the saturation signals were obtained and unloaded, in many cases the reflected signals did not return along the same path back to zero applied external load. This is shown typically in Figure 17. The increasing applied stresses have been applied to a part through fatigue crack of length 0.0438 inches. Upon saturation of the ultrasonic signal, the stresses were reduced, and measurements taken during the unloading. At about 14 ksi, the unloading signal heights fell below those of the loading, and remained below those of loading until zero applied load. This was repeated for a series of specimens, and indicated that the ultrasonic response from a fatigue crack of given length need not be a single valued function but depends strongly on the external applied loads. When the maximum external stress was applied, a plastic zone associated with the stress was formed which upon unloading results in a residual closure stress, approximately half of the maximum applied stress. If this stress level is then exceeded by an additional applied external load, the degree of closure (tightness of the crack) changes, and becomes greater for a given value of applied stress. Hence, the unloading curve ultrasonic response is

Figure 17

Effect of Loading and Unloading on Ultrasonic Signals from Part Through Cracks in Aluminum 7075-T6

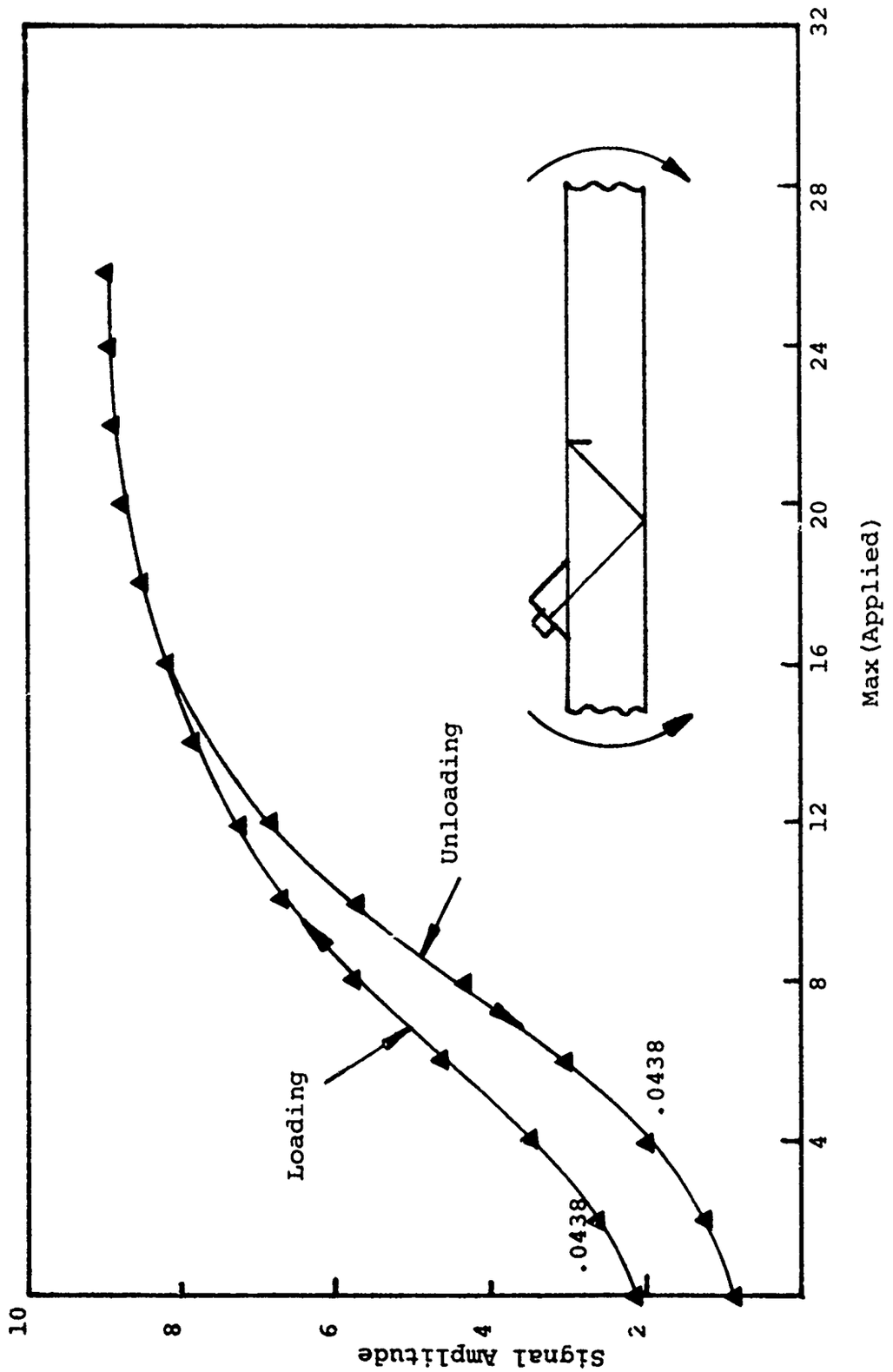

below that of the loading curve if the maximum applied stress level is exceeded. If however, additional stress cycles are applied that do not produce a saturation of the ultrasonic signal, indicating that the crack is completely open, then the hysterysis loop does not occur, and the loading and unloading signals are essentially on top of each other. This is seen in Figure 18 where the same speciemn has been loaded initially to 26ksi, but for the second cycle only loaded to 10ksi. The curve now lies essentially on top of the original unloading curve.

If now the specimen is loaded in compression, the ultrasonic signal decreases as shown in Figure 19 due to decreasing crack displacement. When the gap between the adjacent faces of the crack is small, the degree of transmission across the interface decreases. This is in agreement with the general equation for transmission across a narrow air gap.[8] In this reference the sound reflection from a thin layer is given by:

$$R = \sqrt{\frac{\frac{1}{4}\left(m - \frac{1}{m}\right)^2 \sin^2 \frac{2\pi d}{\lambda}}{1 + \frac{1}{4}\left(m - \frac{1}{m}\right)^2 \sin^2 \frac{2\pi d}{\lambda}}}$$

Where R is reflected energy

m is acoustic mismatch $= (c\rho)_1 / (c\rho)_2$

d is layer thichness

λ wavelength in air

$c\rho_1$ density times velocity of sound in materials across interface 1.

The general shape of these curves for a 5mhz wave is shown in

Figure 20. This indicates that for 5mhz wave in Aluminum-air-Aluminum one would expect complete reflection from the gap when the gap distance exceeds 10^{-5}mm. This implies that for crack displacements greater than 0.008 inches one would expect complete reflection. Examination of Figures 12, 13, and 14 clearly shows that this is not the case. Hence, one can conclude that considerable sound transmission is occuring across the gap in the fatigue crack due to intermittant contact between adjacent protions of the fatigue crack.

This occurs because of the topography of the fatigue crack. In each application of load, there occurs a corresponding amount of subcritical crack growth. There is therefore, a one to one correspondance between the applied stress excursion and the amount of crack propagation.[12] This produces fatigue crack striations which are microscopic marking indicating the intermittant propagation of the fatigue crack front. The topography of the surface produces intermittant areas of contact. When these areas of contact are under a compression loading, local deformation increases the area of contact, and the gap between the surfaces decreases, both effects increasing the transmission of the ultrasonic energy across the interface. Thus, when a compressive load is applied the reflected signal decreases as shown in Figure 19.

When the part is further compressed, the signal decreases considerably, being approximately 25% of the original value at 20 ksi compression. However, when the compressive load is removed, the return to the zero load also produces a hysteresis effect. When the load is removed to zero, the

Figure 18

Effect of Low External Stresses on Ultrasonic Signals from Part Through Crack

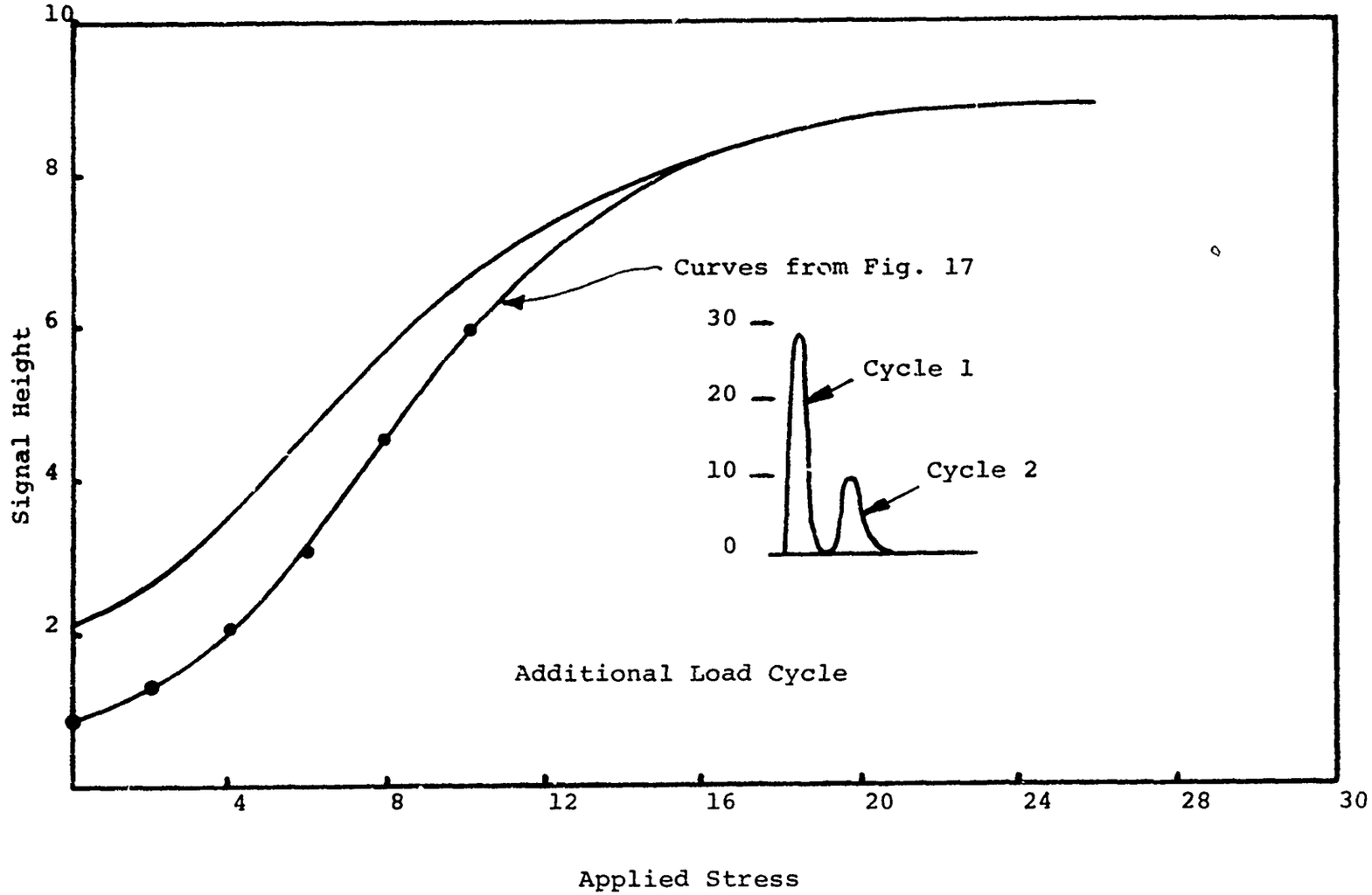

Figure 19

Effect of Compressive Stresses on Ultrasonic Signals from Part Through Cracks in Aluminum 7075-T6

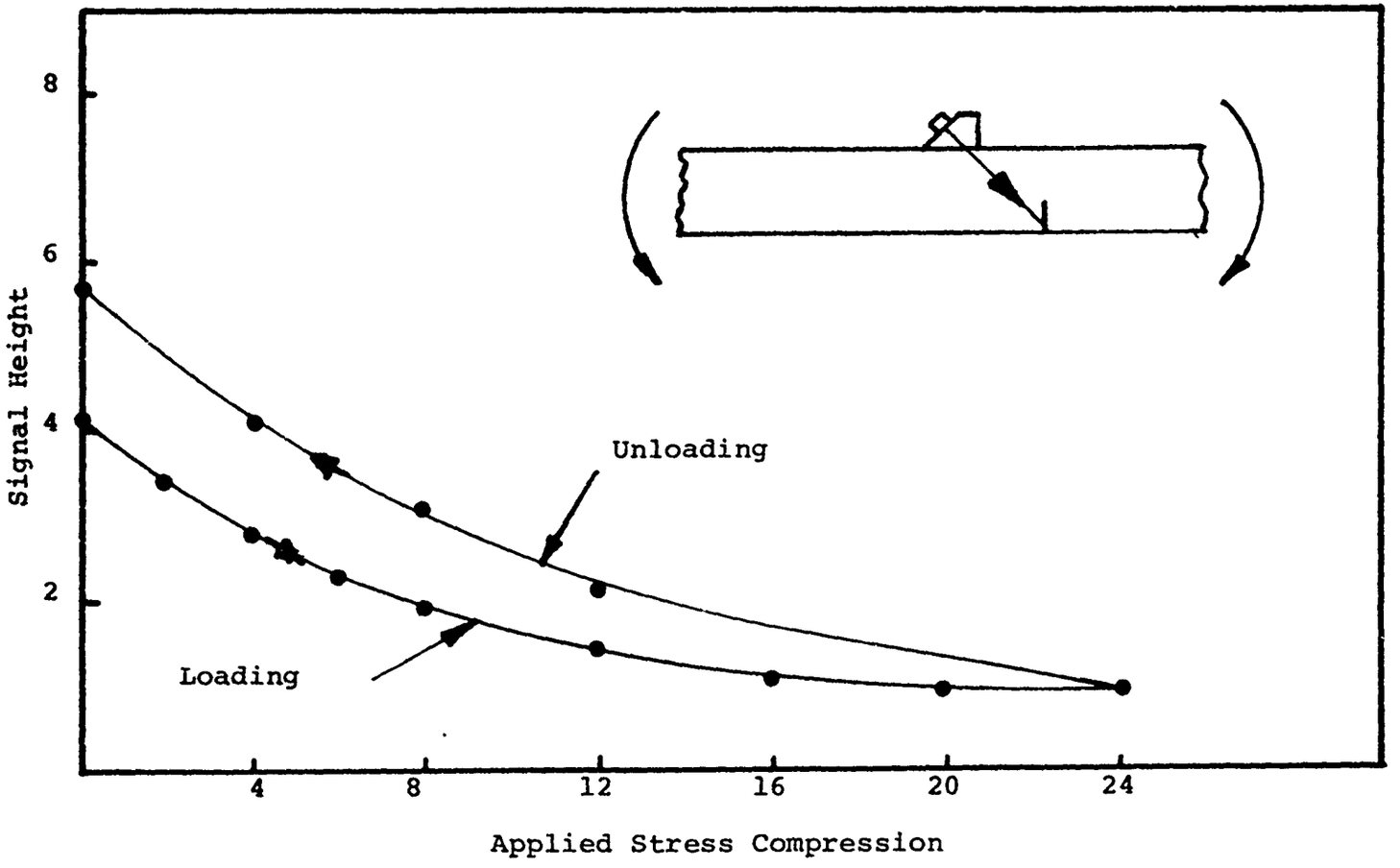

Figure 20

Theoretical Curves for Percent Reflection and Transmittance Across Air Gap in Aluminum and Steel

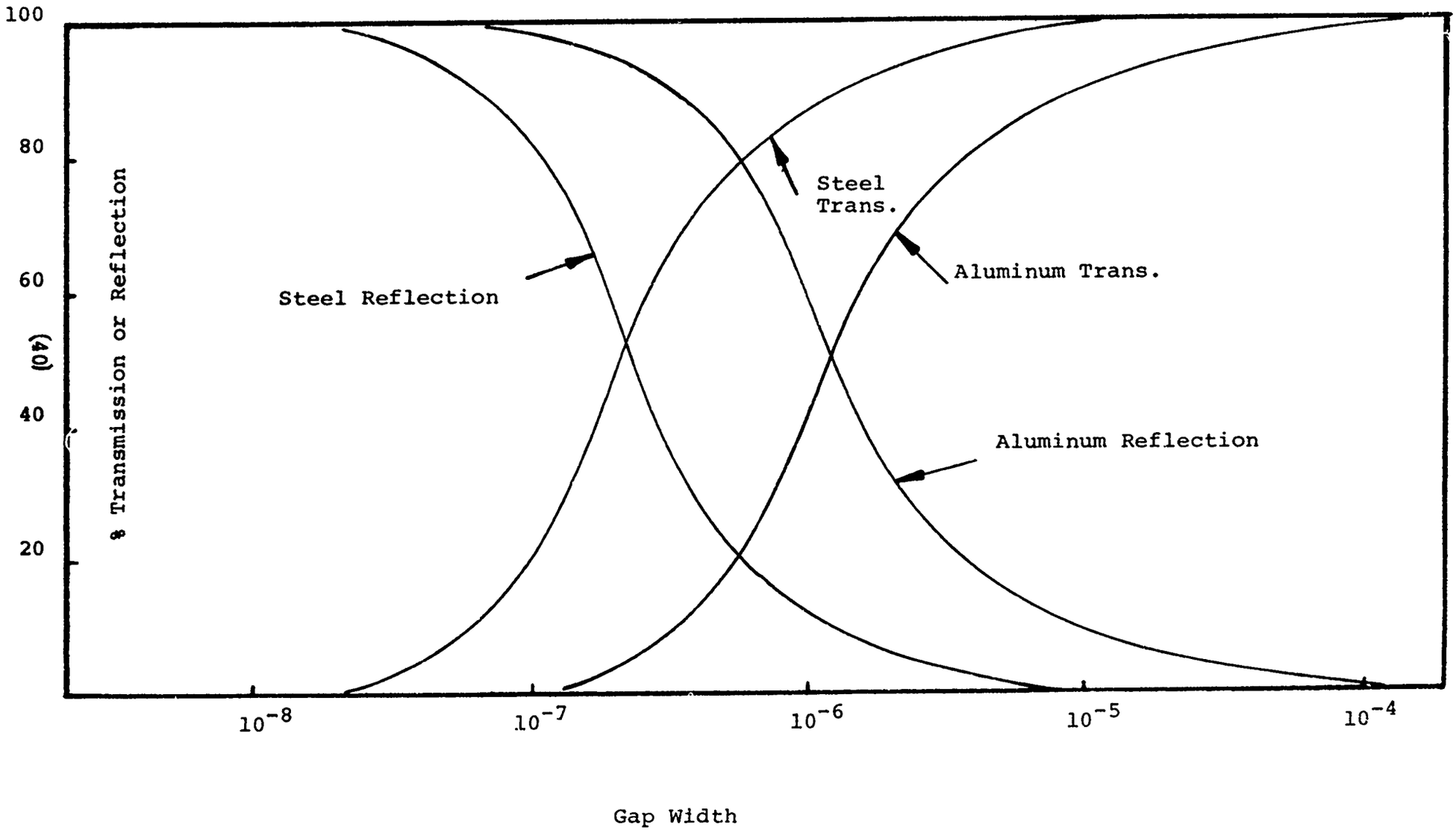

ultrasonic signal is greater than would have been if the compression load had not been applied. This appears due to the fact that when the compression was removed, the original areas in contact were flattened, and upon removal of the load, now produce an increase in the air gap, resulting in more complete reflection. Figure 21 shows a schematic of the series of events that might be expected to occur upon tension and compression loading of a fatigue crack and the changes in ultrasonic signals.

Effect of Hold Time

A series of experiments designed to study the influence of hold time on the ultrasonic response was also conducted. The specimens were initially loaded in tension to saturation of the ultrasonic signal. After that time they were unloaded and examined at periods for up to four days by the normal shear wave technique at no load. Figure 22 shows the effect obtained. The signals appear to show a moderate decrease in intensity after the first 12 hours, after which the loss in signal strength is considerably less. Specimen A48 showed a much larger drop in signal intensity for the first 24 hours after which no significant loss in strength was seen.

It appears that this may be associated with a "tightening" of the crack due to gradual loss of the residual stresses associated with the crack tip plastic zone. There is associated with the loaded crack a degree of closure due to its having been formed by fatigue cycling. This closure results in a touching of some adjacent portions of the crack face, particularly at the free surfaces of the specimen, i.e. the semi-major axis positions. As the crack stress field relaxes, this

Figure 21

Schematic Showing Effect of Tension-Compression Cycle on Ultrasonic Signal

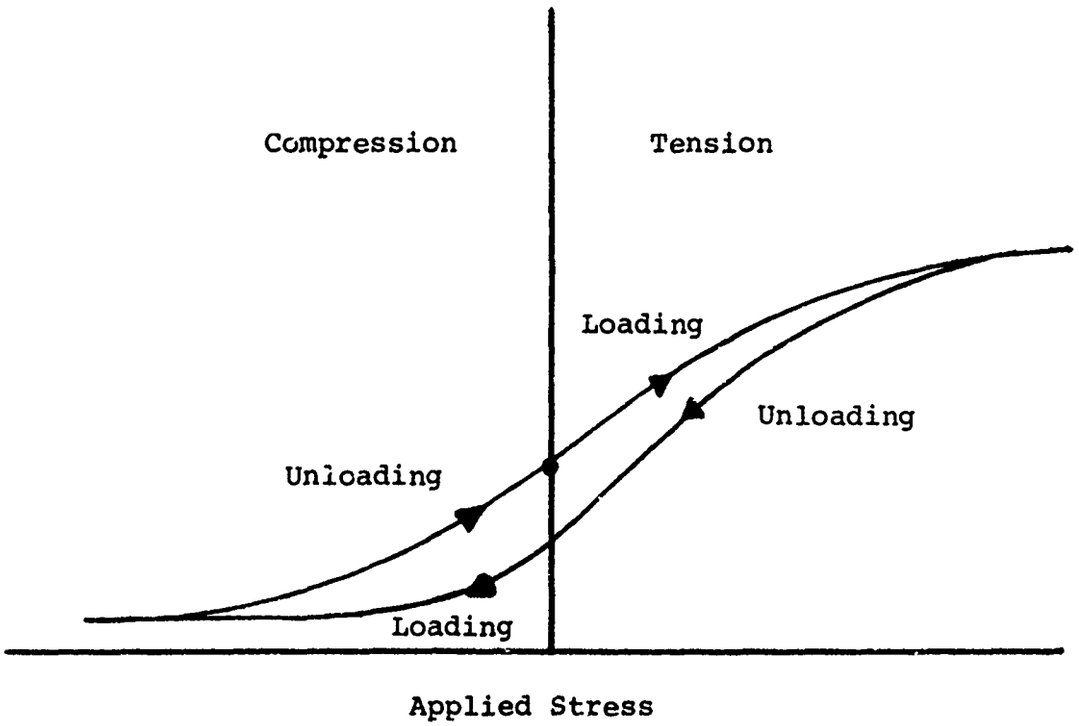

Figure 22

Effect of Hold Time After Unloading on Ultrasonic Signals from Part Through Cracks

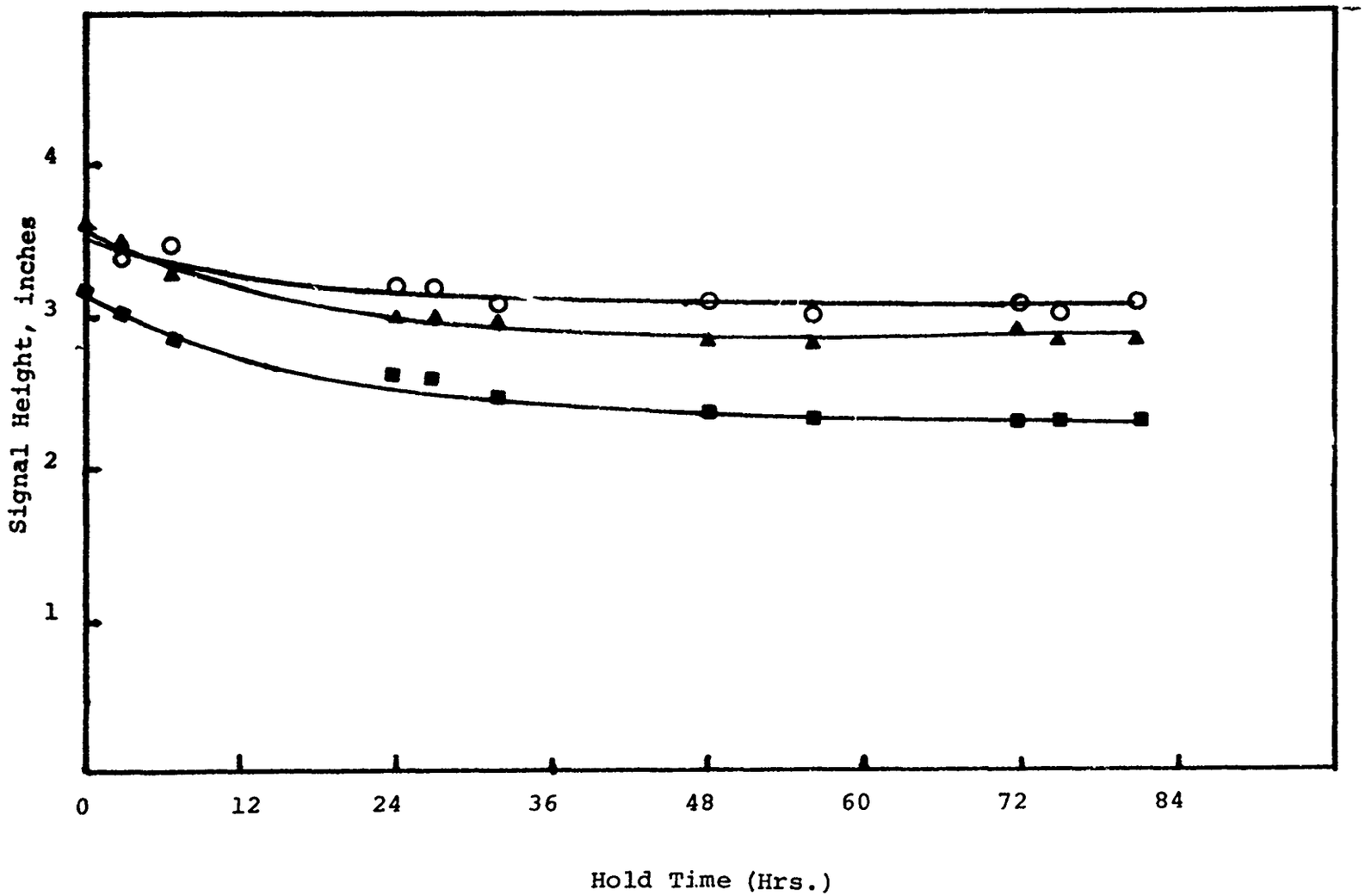

results in a "tighter crack". This is in contrast to fatigue experiments conducted by others which indicates that sufficient hold time effectively reduce the degree of closure on the specimen.[13]

The influence of hold time at the applied stress level is shown in Figure 23 . Here the specimens have been loaded to a given stress level and the reflected signal intensity measured as a function of the time at load. At the time the loads were measured, and relaxation load loss was made up by adjusting the position of the crosshead by hand so that the load reading remained the same independent of the degree of relaxation of the specimen.

For specimens that were loaded to loading stresses less than those required to cause saturation of the applied signals, the load relaxation and subsequent change in deflection of the specimen needed to compensate for relaxation caused the ultrasonic signals to increase slowly but continually during the test period. These increases appeared to be due to a creep relaxation of the tightness of the crack faces resulting in an increased reflection from the interface. The degree of relaxation, as was expected, increased with increasing applied stress, and hence, there was a greater increase in signal reflection for the more highly loaded cracked specimens.

For specimens loaded to within the saturation level of stress, i.e. 20 ksi, increased time and loading crosshead compensation did not result in an increase in the reflected signal. The crack faces appear to be as reflective as they are going to be due to the initial opening of the crack by the applied stress and further time at stress serves no purpose

Figure 23

Effect of Load Time at Applied Load on Reflected Ultrasonic Signals in Part Through Cracks

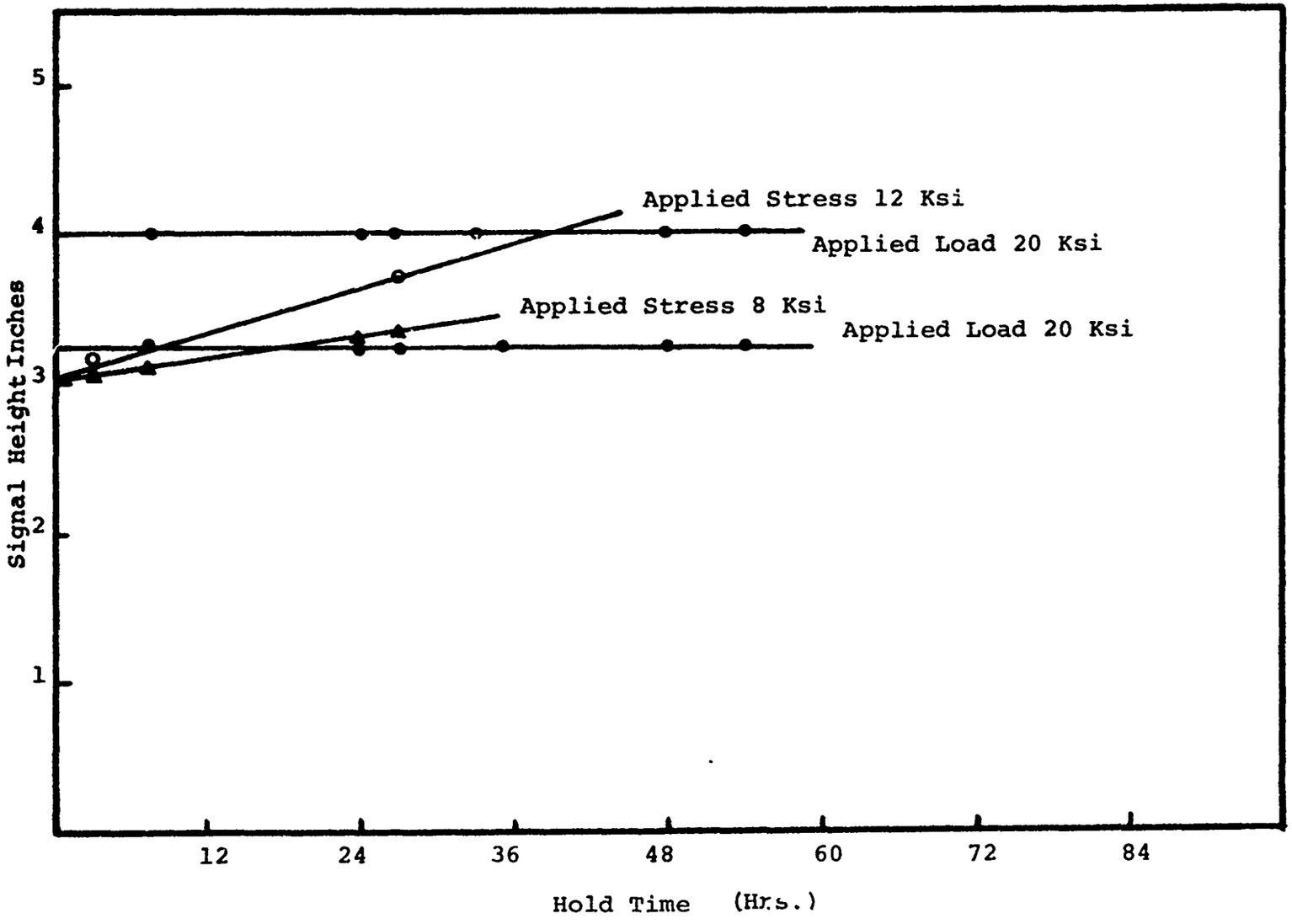

with regard to increases in the reflected signals.

Effect of Corrosion

The effect of corrosion on the ultrasonic detection of fatigue cracks was investigated as well as the influence of corrosion on the detection of EDM notches. Several fatigue part through cracks were subjected to 24, 48 and 72 hour exposion to a 5% NaCl salt solution, and three others were subjected to a salt spray of NaCl for several days. The salt spray and dipping in the salt solution resulted in a relatively severe surface pitting and corrosion.

Ultrasonic inspection of the fatigue cracks was conducted in the normal manner using a 5 mhz transducer with a 45° Lucite shoe. The maximum value of the signal reflection was used.

Table VIII shows the results of the corrosion. It was found that the corrosion had no effect on the signals received from the EDM notches. This agrees with the results found by Boeing[6] where there were no significant effects of corrosion on the reflected signal, as shown. This indicates that the corrosive effect significantly opens the surface of the fatigue crack to produce high reflection.

A similar series of fatigue cracked specimens containing both the bolt hole and fatigue crack were corroded in the same salt solutions. The specimens were examined by 45° shear wave ultrasonics. This indicated that significant improvements in the ultrasonic signals are obtained when the surface of the fatigue crack is subjected to mild corrosive environments.

Several specimens containing fatigue cracks eminating from the bolt holes indicated that unless the specimen was cleaned

sufficiently, there remained sufficient material within the crack that would reduce the ultrasonic signals.

SECTION V

INDICIA ANALYSIS

Introduction

When the size of the defec nder investigation by ultrasound is larger than the diameter of the transducer, such as a long delamination within a weld, measurements of the length of the defect are relatively simple and straightforward. The position of the transducer at which the initial defect signal is received is noted, and the transducer moved along the direction for which the greatest length of the defect is indicated. The position at which the signal reflection drops is also noted, and the difference between the two positions of the transducer are noted and measured. This is the approximate length of the defect. Krautkramer[8] recommends using the position of the transducer for which the ultrasonic response is 50% of the peak response, but this amounts to only a small correction for large flaws.

Giacomo, Crisci and Goldspiel[14] describe an ultrasonic method for measuring the crack depth in large structural weldments of high strength steels and titanium. They use the motion of the transducer, essentially perpendicular to the plane of the defect as a measure. To perform a crack size measurement, the transducer is moved slowly until the reflected signal reaches a lower threshold level, passes through a maximum when impinging fully on the flaw, and diminishes when passing over the crack plane. The crack size-transducer-geometry is then used to estimate the size of the flaw. The basic

equation is given by:

$$D' = 2d - \left\{1 + \left(\frac{\Delta(\varphi+\gamma) - \Delta'(\varphi+\gamma)}{2\Delta(\varphi+\gamma) - \Delta(\varphi+\gamma)}\right)\right\}\Delta\cos(\varphi-\gamma)$$

Where the geometric parameters are given in Figure 24. Typical results are shown in Figure 24. In almost all cases the technique underestimates the size of the flaw due to (1) tightness of the crack, (2) crack branching and (3) multiple reflections from the surface of the crack.[14] The influence of crack tightness, stress level and roughness on the measure of the crack length has been discussed in a previous section.

Considerable Soviet work exists on measurement of defects in welds by ultrasonic techniques. Gurvich and Ermolov[15] have published a treatise on ultrasonic flaw detection in welded joints, and numerous other Soviet scientists have contributed to the understanding of the factors influencing weld defect detection by ultrasonics. Gurvich and Ermolov introduced the concept of a scattering "indicatrix", or "indicium" as a measure of the size and configuration of imbedded defects. The indicia is a normalized function describing the total field of an ultrasonic wave reflected toward the probe.

Geometric Concept of Indicium

Consider the ultrasonic setup pictured in Figure 25. Here the bolt hole is in the process of being scanned by a transducer with a shoe converting the normal wave to shear mode. The transducer is positioned so that it is at the correct distance $t/\cos\varphi$ to obtain a reflection associated with the hole after

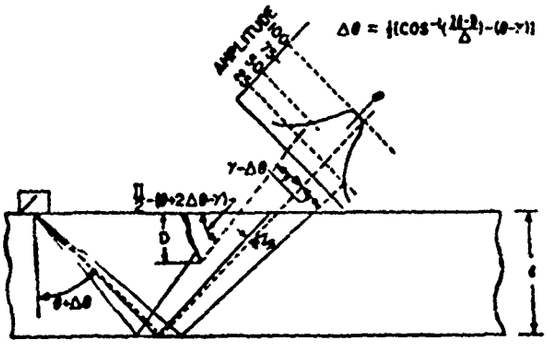

Reflection from the bottom of a crack at an angle $[(\theta - \gamma) + 2\Delta\theta]$.

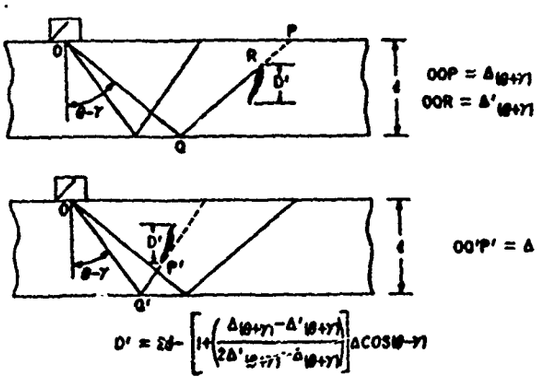

Schematic diagram for estimating defects which do not come to the surface.

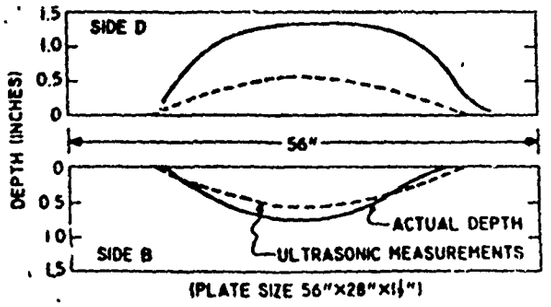

Crack-depth results for first tee-welded plate specimen.

Figure 24

Crack Depth Measurements of Large Defects in Welded Structures (14)

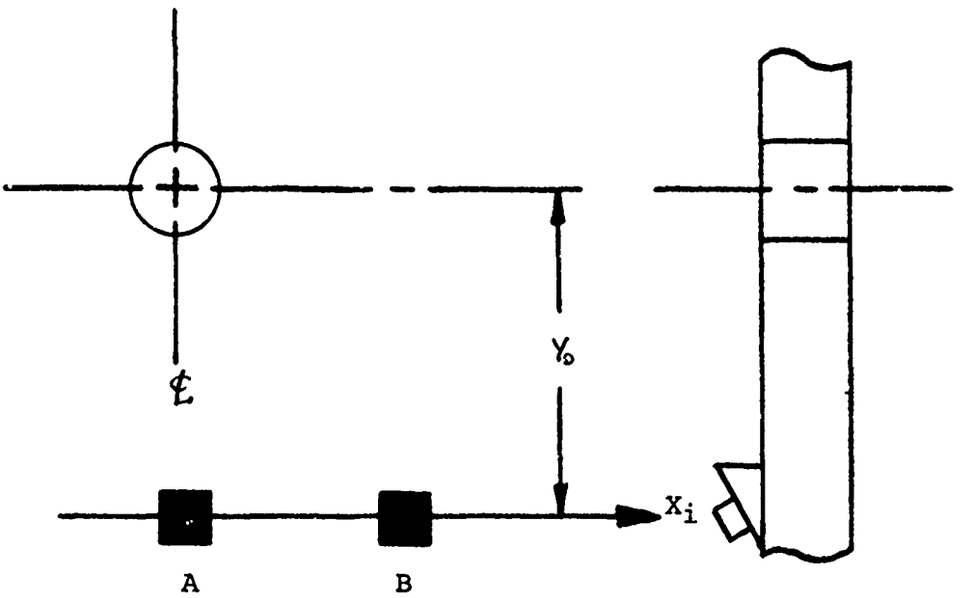

TRANSDUCER POSITIONS

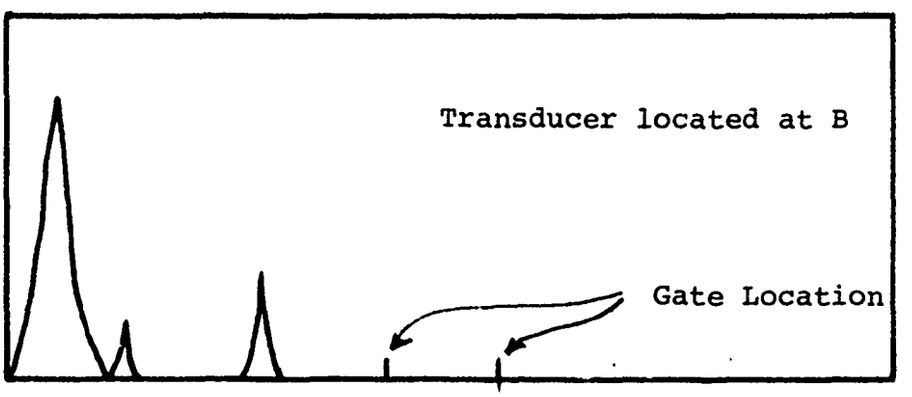

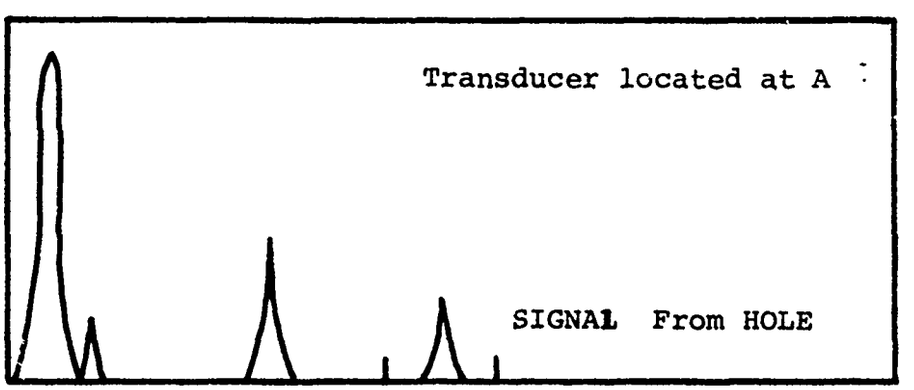

Time Base

Figure 25 Shear Wave Ultrasonic Scan of Bolt Hole for Indicia Measurements

reflection from the lower surface of the plate. There would be a second reflection located at $2t/\cos\phi$, which is associated with the second reflection from the top surface of the plate. These two reflections are shown in Figure 26. There are additional reflections associated with higher order interactions of the beam with the top and bottom surface of the plate, but these need not enter into the discussion.

When the transducer is located directly in front of the hole, there is an additional reflection due to the hole with partial or complete supression of the second reflection. This is shown as the lower half of Figure 26. Here the hole reflection signal is shown located between the first and second reflections resulting from the position of the transducer and bolt hole. (If the distance from the transducer to the bolt hole were different, the reflection from the bolt hole may appear in a different position) Thus, it is important to understand the particular geometry of bolt hole-transducer reflections to be able to identify and locate the particular signal associated with the bolt hole. There appear to be several other reflections such as A' and A'' which can also be associated with the bolt hole. For the sake of simplicity, however, only the first reflection from the bolt hole is used in this analysis. However, it should be recognized that in some indicia studies reflections other than the first may be used.

If the dc signal from the defect is gated and plotted as a function of the position of the transducer and indicia of the bolt hole is developed as shown in Figure 27 for a good hole. This indicia represents all of the reflections associated with

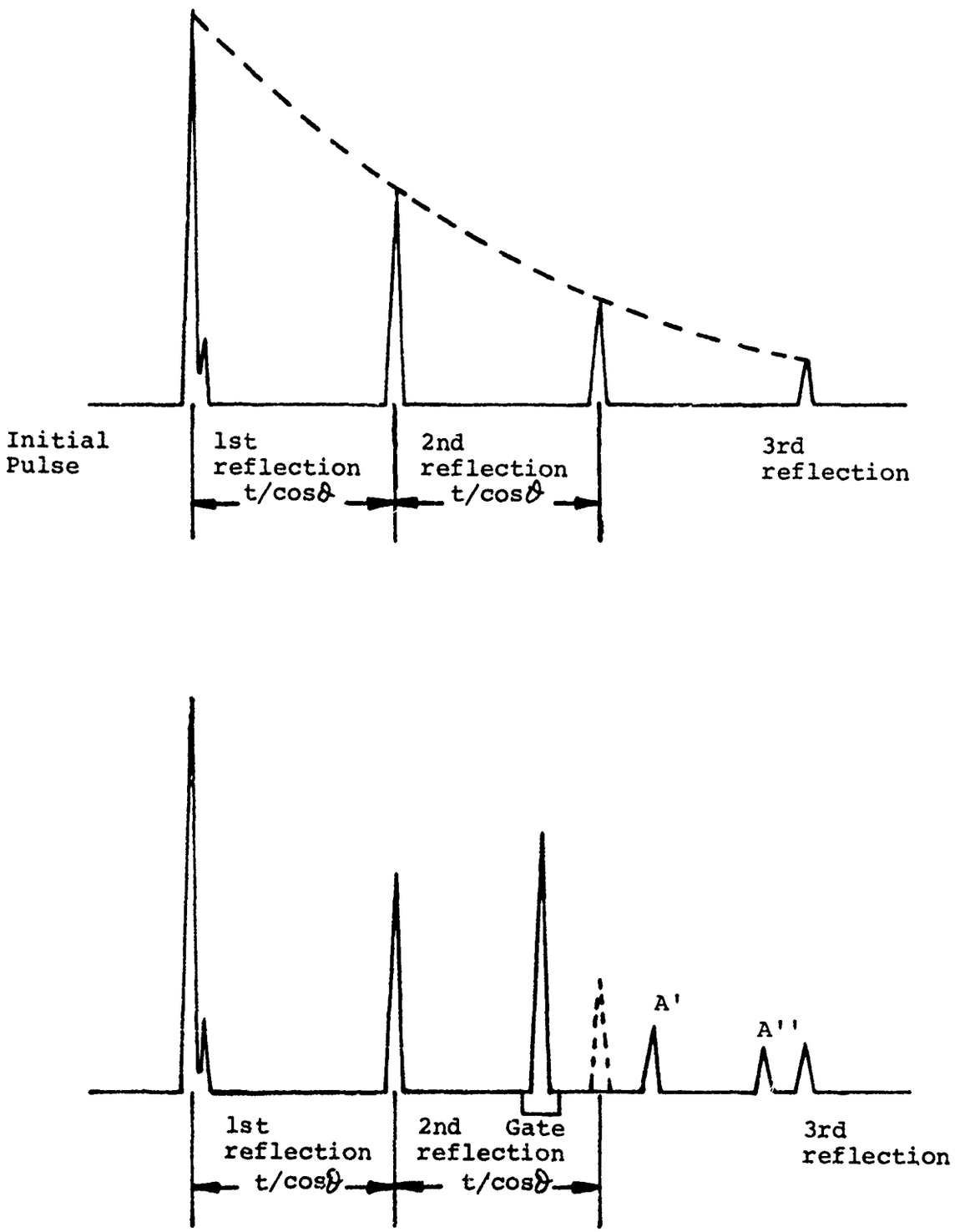

Figure 26

A Scan Showing Multiple Reflections From Shear Wave in Flat Plate Containing a Defect

the bolt hole in the particular configuration shown.

If the defect were now considered to be a bolt hole containing a crack, the configuration would be as shown in Figure 28. Here we assume the scan to be approximately perpendicular to the plane of the crack. It can be seen that if the transducer scan starts on the left side of the hole, the indicia would be identical to that of the hole without the defect. As the transducer beam approaches the right portion of the bolt hole, there are additional reflections from the crack. These reflections pertubate the original indicia of the bolt hole as shown in the Figure. A typical indicia from a crack in the lower surface of a bolt hole is shown in Figure 29. This crack is approximately 0.030 inches long.

Thus, it can be readily seen that the pertubation of the signal of reflection from the bolt hole is a clear indication of the presence of a defect within the bolt hole area.

Several geometric and metallurgical factors can influence the signals associated with the detection of the defect as they influence the shape and interpretation of the indicia. These are discussed in the following sections.

Transducer Characteristics Influencing Indicia Analysis

The influence of transducer characteristics on the sensitivity, reproducability and reliability of the ultrasonic signal has long been recognized. The choice of transducer diameter, central frequency and pressure pattern can significantly influence the shape of the indicia, and hence, the degree of characterization possible from the indicia analysis. The initial

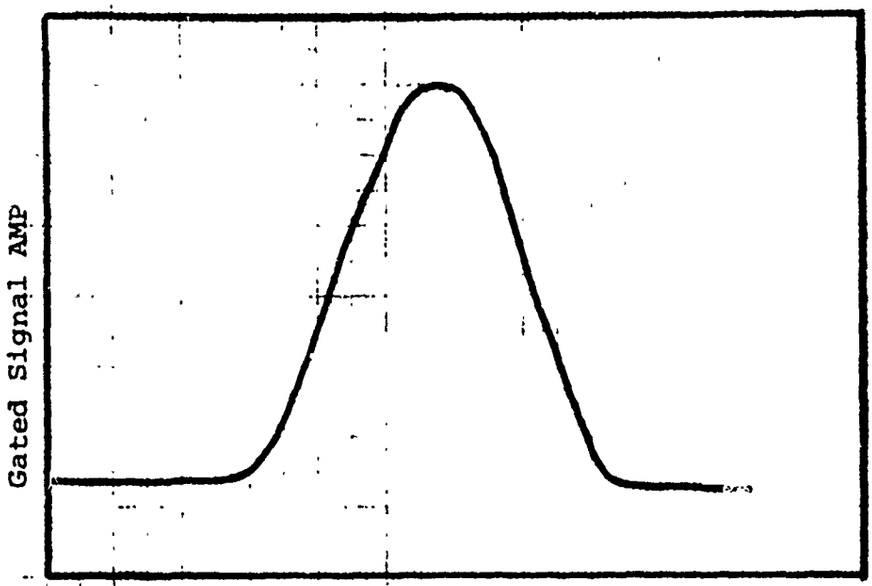

Figure 27

Shear Wave Indicia for Bolt Hole in 0.5 Inch Plate Without Defects

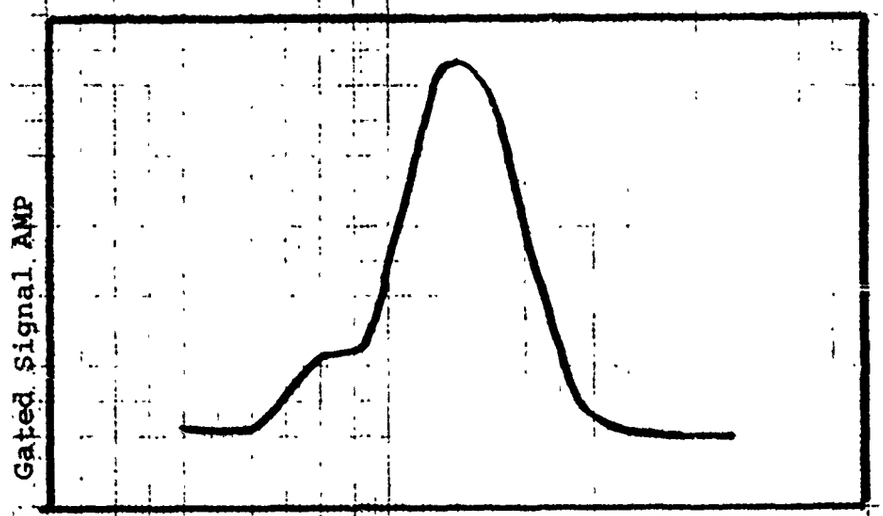

Figure 28

Indicia Scan From Shear Wave Investigation of Bolt Hole Containing Defect in Immediate Vicinity of Plate

Figure 29

Indicia Scan From Shear Wave Investigation of
0.5 Inch Diameter Hole With 0.030 Inch Defect
In Lower Surface of Plate

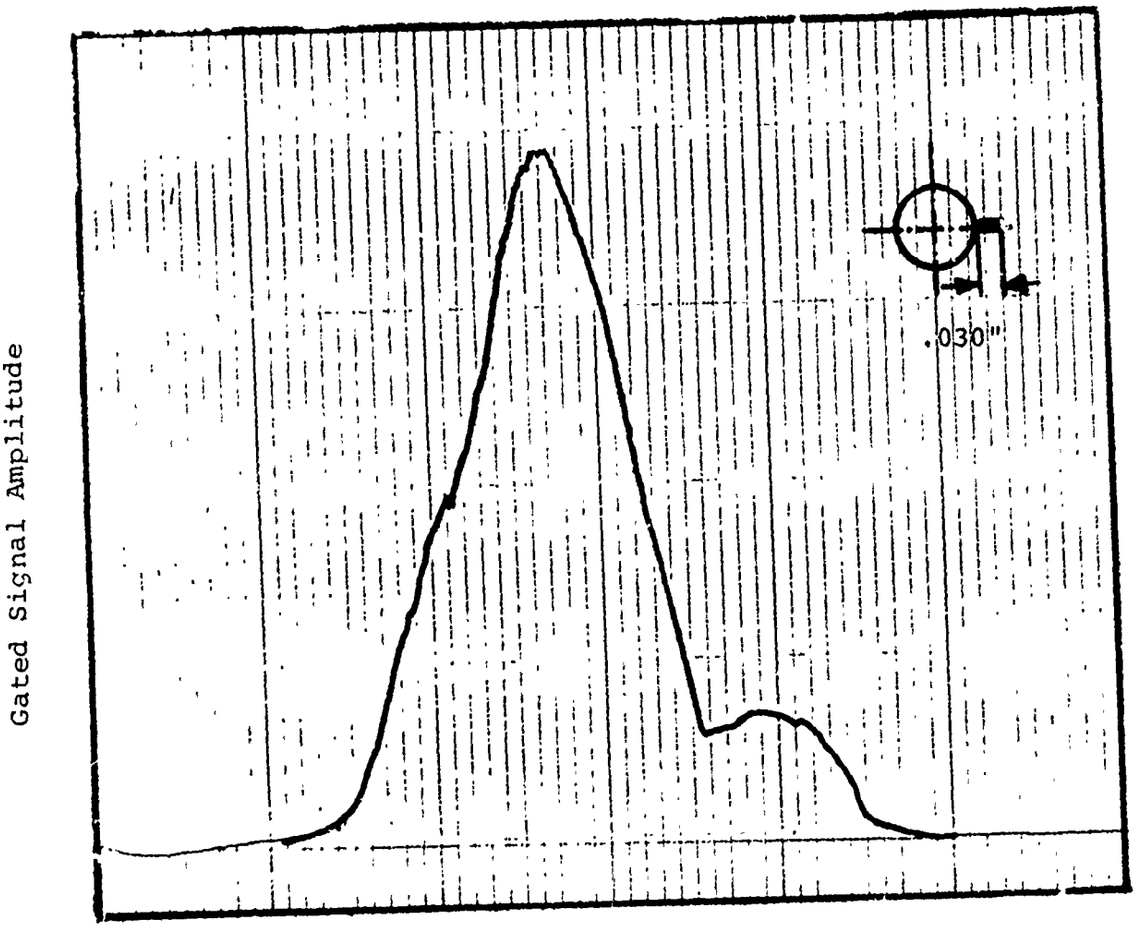

choice of transducers was made based on the ability of the shear wave configuration to find small part through cracks as discussed in the previous sections.

Two methods of evaluating transducer characteristics are available; (1) frequency spectrum analysis, and (2) sound beam profile. Because the indicium analysis is essentially a position analysis as opposed to a frequency analysis, it was felt that the exact frequency characteristics of the particular transducers, while of interest, would not be necessary in this program. It is questionable whether frequency content of the ultrasonic transducer obtained by continious wave analysis is accurate for a pulse pattern.

Transducer frequency and diameter influence the sound beam patterns because the diameter and central frequency relate to the location of the end of the near field of the transducer. The near field is the area where interference effect due to interaction of edge effect and the plane wave of the sound pressure pulse. (8) Beyond the near field distance, well into the far field, the pressure pattern is relatively continuous. For a circular transducer whose wavelength is small compared to the diameter of the transducer, the location of the near field end is given by: (8)

$$Y = D^2/4\lambda$$

Where Y is the location along the axis of propagation of the end of the near field

λ is the wavelength of the ultrasonics $=V/f$

V is sound velocity

f is frequency

Thus, the location of the gated reflection for the indicium should be beyond the near field. If the gated reflection were still within the near field, the presence of a small reflection or no reflection in the indicium need not be indicative of the shape of the reflecting flaw but would be a characteristic of the transducer pressure pattern.

Figure 30 shows the effect of transducer frequency on single transducer shear wave detection of the crack associated with a bolt hole. It can be seen that the 2.25Mhz transducer gives the lowest peak to peak indicium, while the 5 and 10 Mhz units give approximately the same signal from the crack. All three signals were adjusted so that the maximum reflection from the hole were approximately the same. It is important to recognize that particularly noisy signals can be produced by a slight change in the positioning of the gate. For example Figure 31 shows another crack eminating from a hole on the lower surface with a straight shank but with the gate narrowed down to only produce a signal within an extremely small portion of the reflected space. The indication of the crack is present, but is extremely noisy.

The divergence of the transducer beam also influences the shape of the indicia. This can be significant if the divergence of the beam is such that small defects within the beam pressure pattern do not receive sufficient ultrasonic energy to produce strong reflections. If the divergence of the beam is such that the sound pressure pattern is broadly dispersed, this will occur. A measure of the angle of divergence of the pressure pattern is given by:[8]

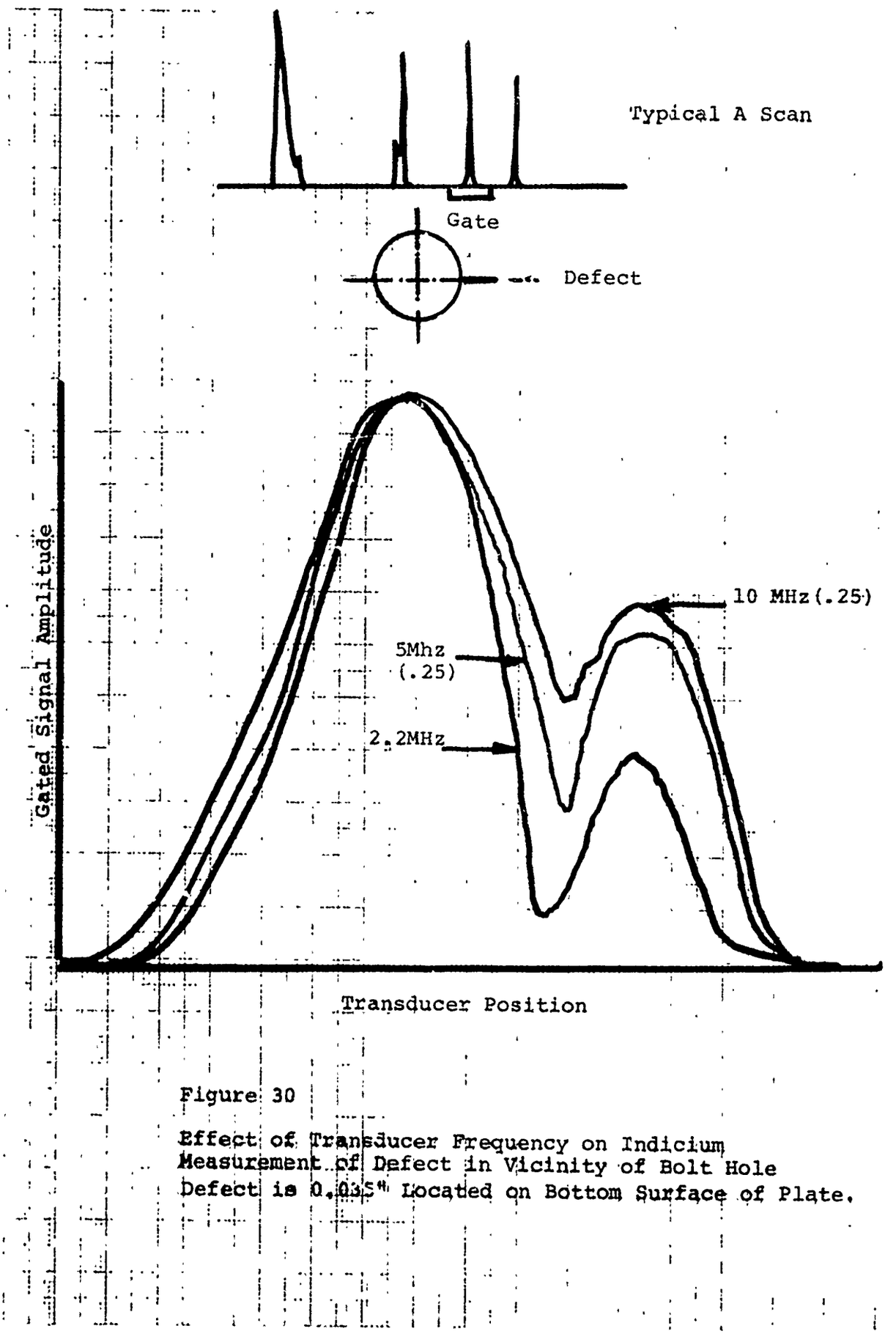

Figure 30

Effect of Transducer Frequency on Indicium Measurement of Defect in Vicinity of Bolt Hole Defect is 0.035" Located on Bottom Surface of Plate.

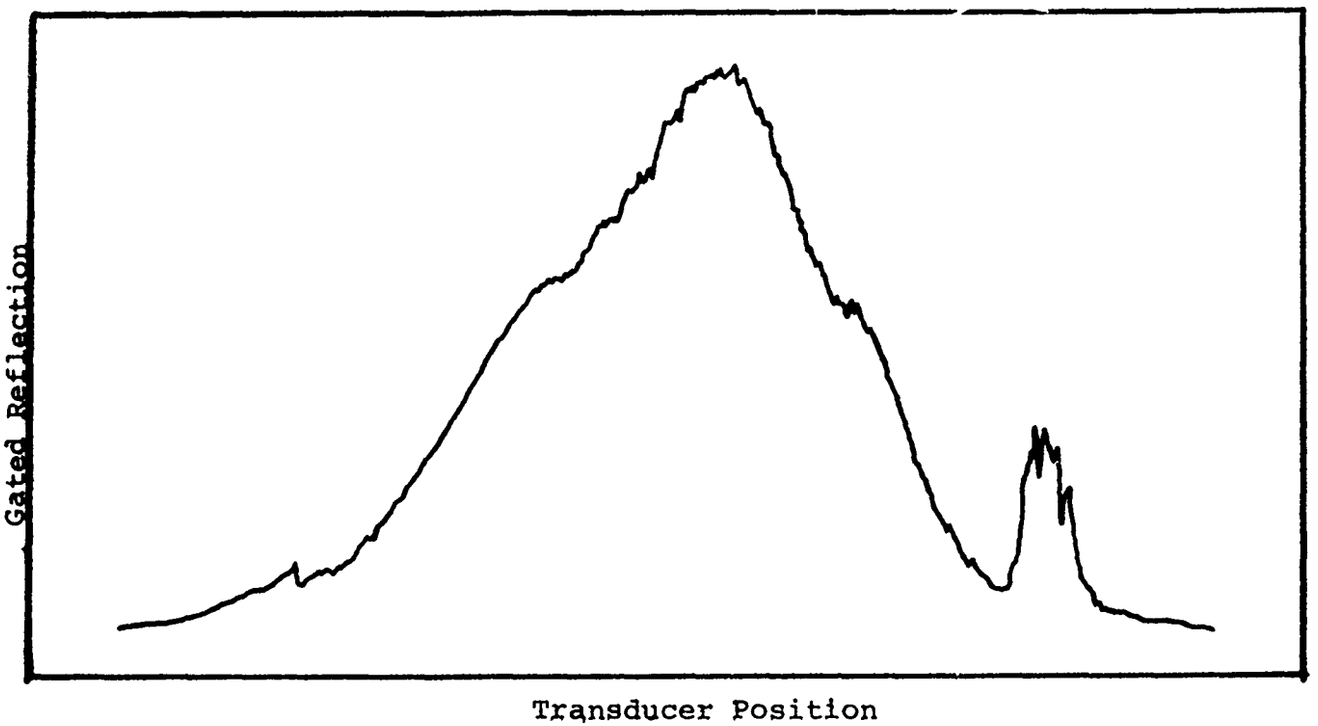

Figure 31

Influence of Gating on Indicium of Bolt Hole
Containing 0.035 inch Defect on Bottom of Plate

$$\sin \gamma_o = 1.2\lambda/D$$

Where $\sin \gamma_o$ is the half angle of divergence of the pressure probe measured along the probe axis

λ is the wavelength = V/f with V the sound velocity, f the frequency

D is the diameter of the transducer

The calculated half angle divergences for 10, 5 and 2.5 Mhz transducers of 0.25 and .375 inch diameter are shown in Figure 32. Also shown is a schematic illustrating the polar divergence of the sound pattern. For this program six transducers were evaluated.

It would be most effective to chose the transducer with the smallest beam diameter. This would supposedly produce the most sensitive indicia. However, the angle of divergence only considers the pattern and not the magnitude of the pressure pattern. To obtain a good reflection from the defect one must not only have a good pressure pattern, but must also have sufficient magnitude of acoustic pressure at the point in question. Since the magnitude of the acoustic pressure depends upon the ratio of the area of the transducer to wave length, a larger area of transducer would give a higher acoustic pressure. Hence, it was decided to select the 5 MHz, .375 inch diameter transducer for the balance of the indicia studies. Additional studies have also been conducted with other transducers.

Closed Form Solution for Indicia

Gurvich and Ermolov have calculated the normalized shape of the indicia that would be expected for reflection from

Figure 32

Influence of Frequency and Transducer Diameter on Beam Spread Angle

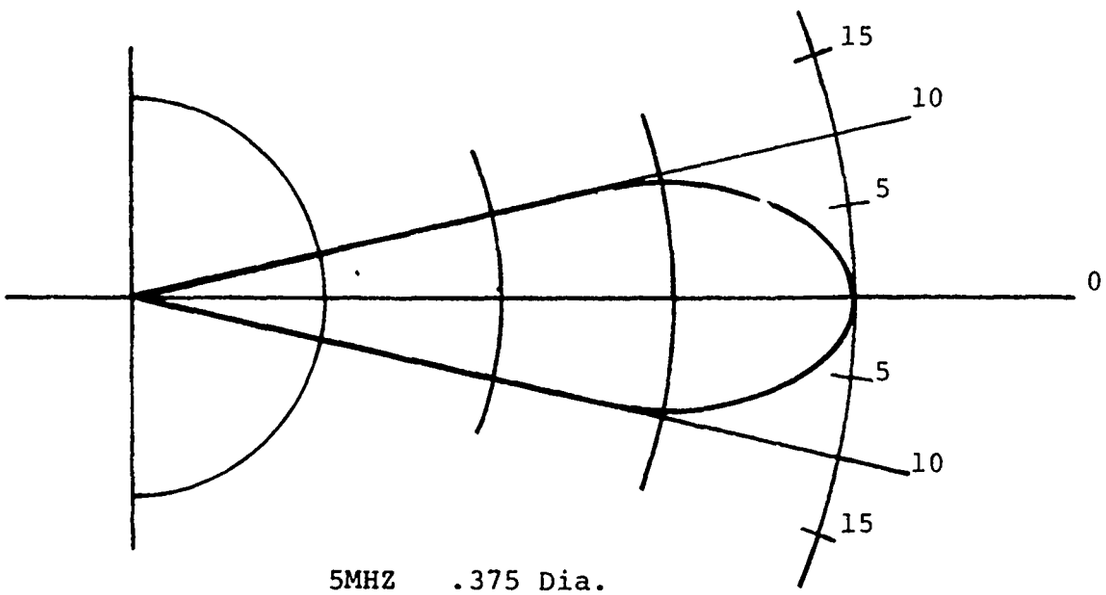

5MHZ .375 Dia.

HALF ANGLE OF DIVERGENCE

	10MHZ		5MHZ		2.5MHZ	
	.250	.375	.250	.375	.250	.375
Aluminum	6.84°	4.55°	13.79°	9.14°	28.4°	26.41°
Steel	6.38°	4.25°	12.85°	8.55°	18.50°	17.24°

a spherical or disc like defect within a material when examined by the shear wave technique. The normalized equation has the form:[15]

$$F(x) = \frac{\phi_0\left(\operatorname{arctg}\left(\frac{x_i}{H}\right)\right)\cos^2\left[\frac{\pi}{5\varphi_0}\left(\operatorname{arctg}\frac{x_i}{H}-\alpha_0\right)\right] \times (x_i^2+H^2)^{-n/2}\exp\left[-2\delta(x_i^2+H^2)^{\frac{1}{2}}\right]}{\phi_0\left(\operatorname{arctg}\left(\frac{x_1}{H}\right)\right)\cos^2\left[\frac{\pi}{5\varphi_0}\left(\operatorname{arctg}\frac{x_1}{H}-\alpha_0\right)\right]\left[(x_1^2+H^2)^{-\frac{n}{2}}\exp\left[-2\delta(x_i^2+H^2)^{\frac{1}{2}}\right]\right]}$$

Where F(x) is the indicia function

Xi the position of the transducer

H the depth of the defect

ϕ_0 the scattering coefficient of the defect

φ_0 the angle relating the pressure pattern of the transducer

δ attenuation coefficient

n 2 for spheres, 1 for discs

X_1 position of the transducer at the maximum signal.

The experimental configuration for Gurvich and Ermelov analysis is different from that used in the scan for the cracks eminating from the bolt hole. Their scan in <u>toward</u> the defect (Y variable, X constant) while the particular scan used for defects in bolt holes is <u>parallel</u> with the defect (Y constant, X variable).

Figure 33 plots a series of calculated indicia for varying angles of beam divergence φ_0. If a scan is made in the direction analyzed by the indicia equation, a plot such as Figure 34 is obtained.[5] This is a plot of the indicia of the same type as the equations for Gurvich and Ermelov. The indicia shows a two maxima and a drop intermediate in a manner similar

FIGURE 33 EFFECT OF PROBE PRESSURE PATTERN ANGLE ON INDICIA OF SPHERE

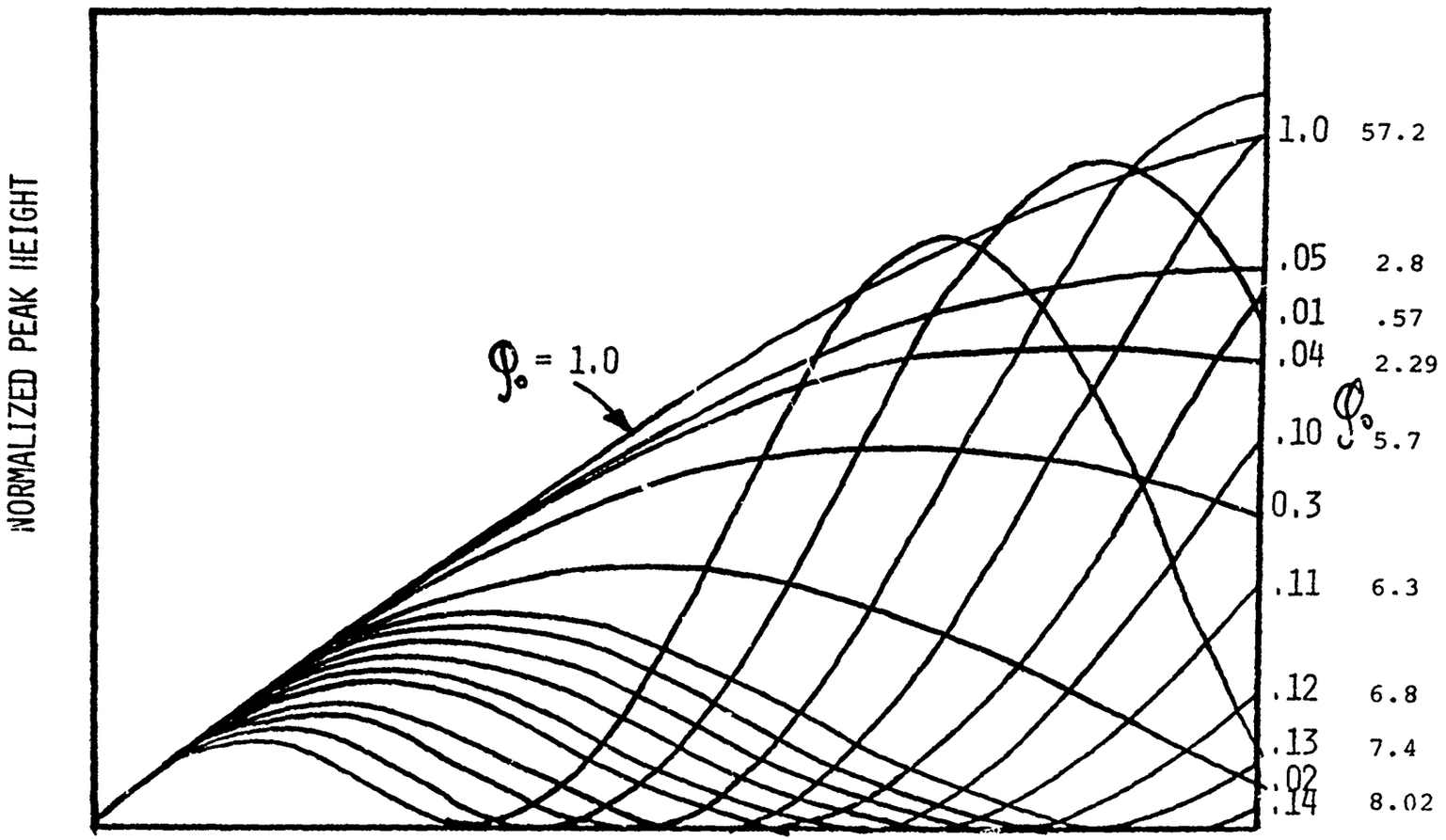

Figure 34

Experimental Form of Indicia for Equivalent Scan of Figure 33 = 8° = 9.14

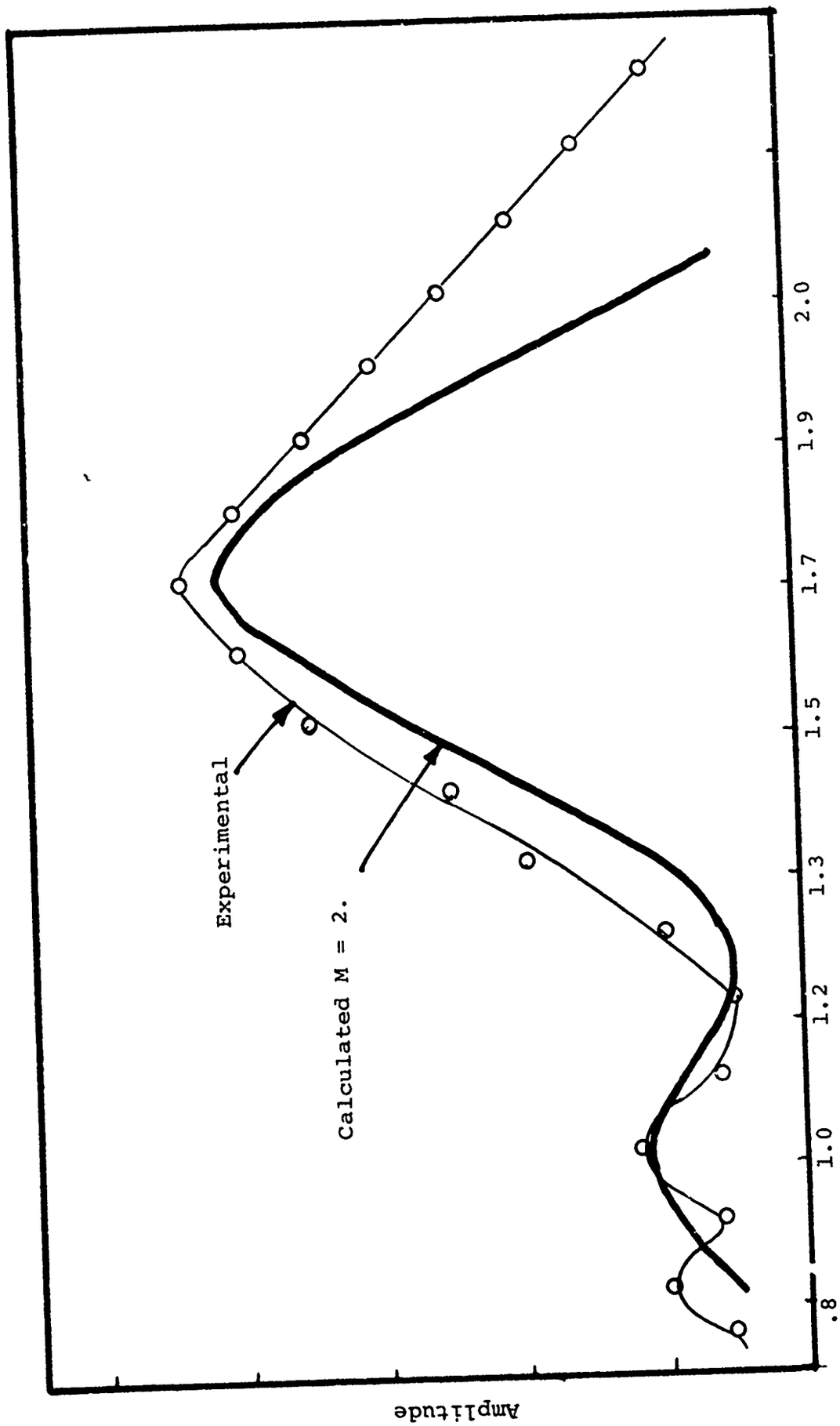

to Figure 33, however, the form of the curve is not identical to that of the calculations since they are for a sphere or disc, and the reflector in this case is a circular cutout. The fit would not be expected to be too good, but follows the same general pattern as expected.

If a series of traverses are now made with the Y value constant and the transducer moving in an X direction, the series of gated signals would appear as shown in Figure 35. Here there are two sets of peaks, one of which corresponds to the bolt hole the other of which corresponds to the defect signal. In each case the location of the centerline of the bolt hole appears strongly, but the intervening reflection from the glancing sides of the bolt hole reflect away from the reciever, and are not contained within the indicia. This can be considered to be a form of "focusing" in which the relative reflections associated with the defect and bolt hole can be tuned in such a manner as to magnify the presence of the defect.

If the system is defocused by positioning the gate that the reflections from a majority of the bolt hole are outside the gated region, while the reflections associated with the defect are within the gated region, a sequence such as shown in Figure 36 results. The series indicates that the indications of the crack presence can be greatly exaggerated by the local combination of focusing and gating.

When two defects are present on both sides of the bolt hole one would expect the Indicia to be trimodel, with the major lobe indication of the bolt hole flanked by two side patterns. This is illustrated in Figure 37, where two defects,

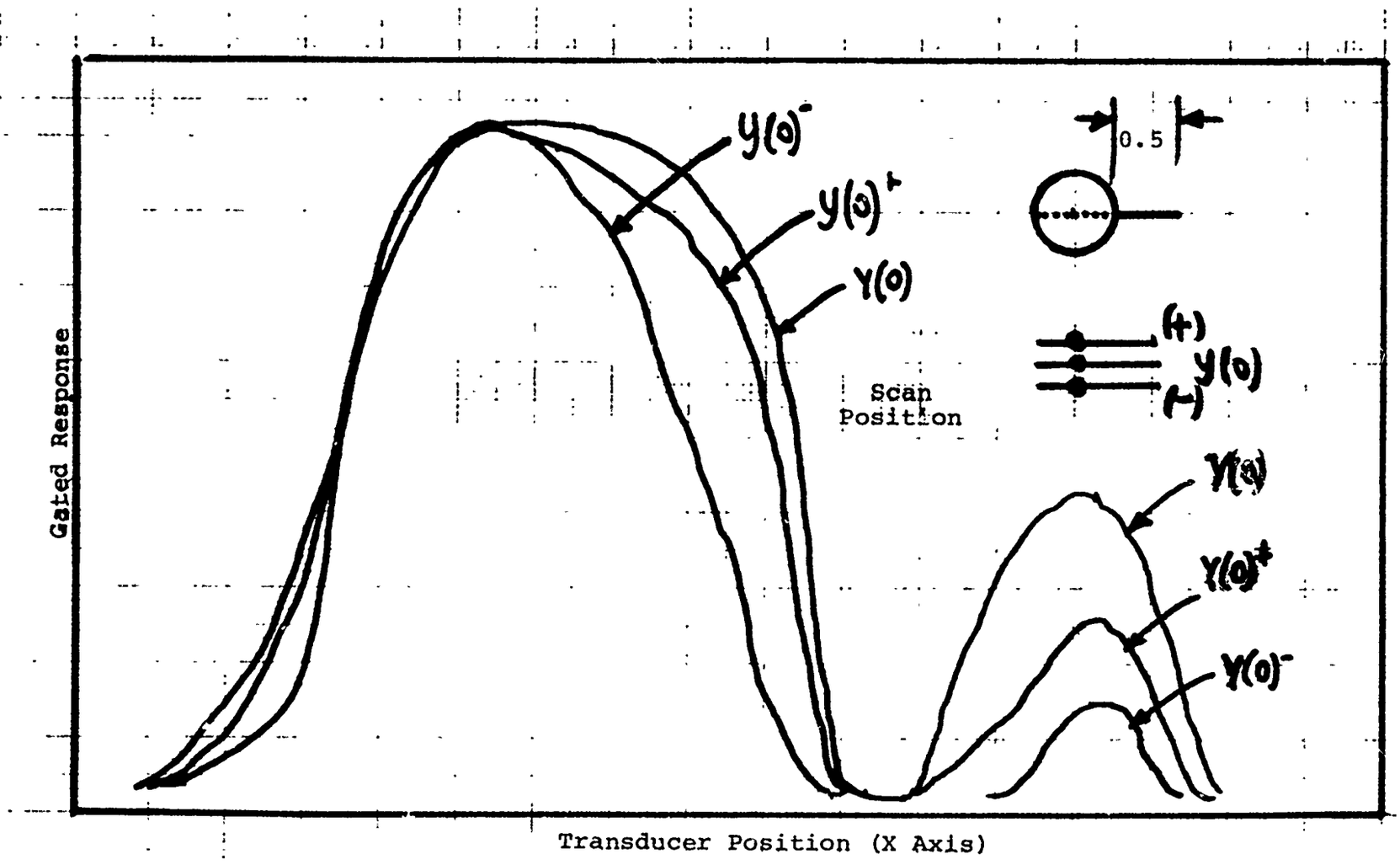

Figure 35

Effect of Transducer Position on Scan on Indicia of Bolt Hole Containing 0.030 In. Defect

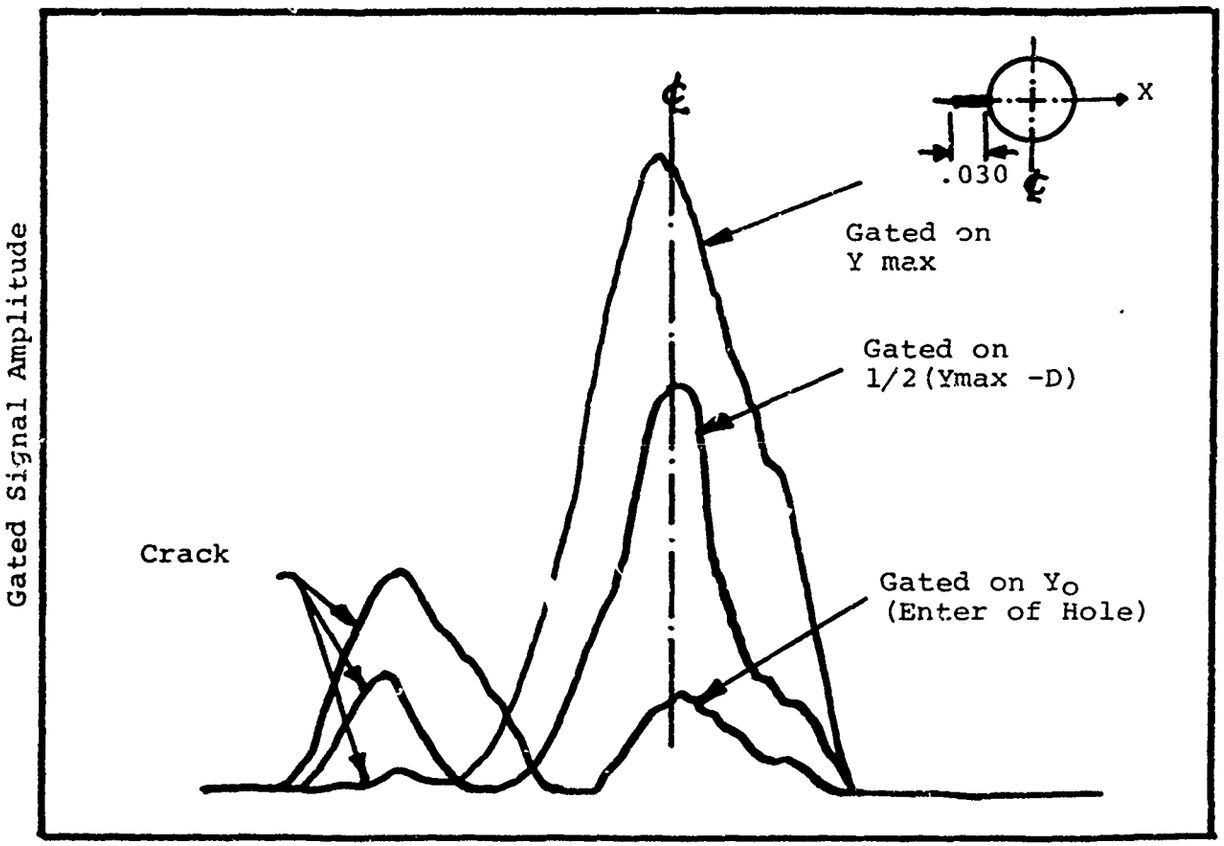

Figure 36

Effect of Gating on Indicia of Defect and Bolt Hole

Figure 37

Indicia of Bolt Hole Containing Two Defects 180° Apart. Defects are 0.025 Inches Long and 0.040 Inches Long

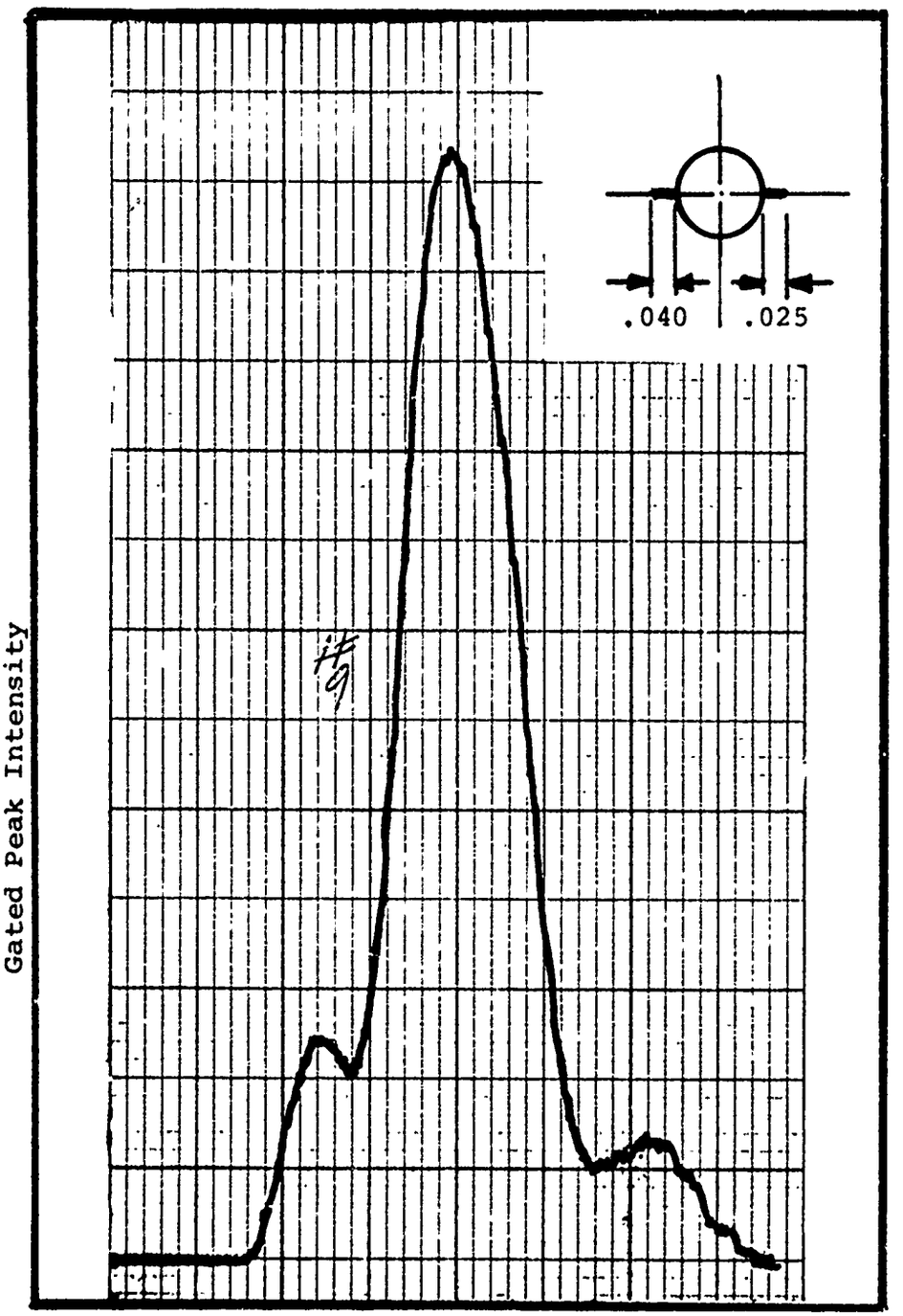

one 0.040 inches (left) and one 0.025 inches (right) are growing out of the fastener hole. The identification of the presence of both defects is easily seen for this configuration.

Effect of Defect Orientation in Bolt Holes

If the transducer scan direction is not parallel to the orientation of the crack, the indications of the defect within the bolt hole are obviously not as clear as shown. The pertubation of the bolt hole indicia does not occur as a bimodel indicium within the bolt hole scan, but occurs as a secondary peak or bump on the rising or falling face of the original indicia. This is shown in Figure 38, where three different scans have been made at 90°, 45° and at 20° to the orientation of the crack. The position of the defect along the bolt hole indicia is shown.

A simple proportion can be made relating the percent of the distance along the bolt hole indicia to the orientation angle of the normal to the crack. Hence, if the location of the pertubation on the bolt hole indicia is midway between that of the bolt hole maximum indicial point and the lowest point of the scan, one may relate this to a 45° angle between the defect and probe axis. This proportion is shown in Figure 39. It can be seen that the experimental results agree with this simple proportion analysis.

One closing point should be made. The point at which the defect would be the most difficult to identify by the indicia would be when it is located perpendicular to the sound beam. Here the beam would encounter the smallest cross section of the

fatigue crack. If the defect were an EDM slot, which had sufficient thickness the indicia would be pertubated sufficiently within the gated area to register as a defect. However, for tight cracks "head on" the resolution is extremely poor.

If the ultrasonic beam is parallel to the plane of the crack, the only reflections that can occur are due to (1) the plastic zone associated with the tip of the crack, and (2) the small equivalent reflector of the thickness of the defect. It is apparent that cracks grown at low stress levels, i.e. those with small plastic zones would be difficult to detect. A study of detection of defects "head on" was made by Throop et all[16] in examining the detection of fatigue cracks grown in a thick walled pressure vessel cylinder. In their analysis they found that the defects could easily be detected, but their loading situation was such as to resemble the low cycle high stress fatigue of a gun barrel, and it is doubtful that the cracks were as tight as would be encountered in aircraft fatigue stressing. The small reflector that comprises the tip of the defect would easily be missed unless prior knowledge was available as to the orientation of the defect. In most aircraft situations there is some knowledge as to the orientation of the principle stress, and hence, it would be important to perform at least two separate scans to minimize the possibility of encountering a fatigue defect head on.

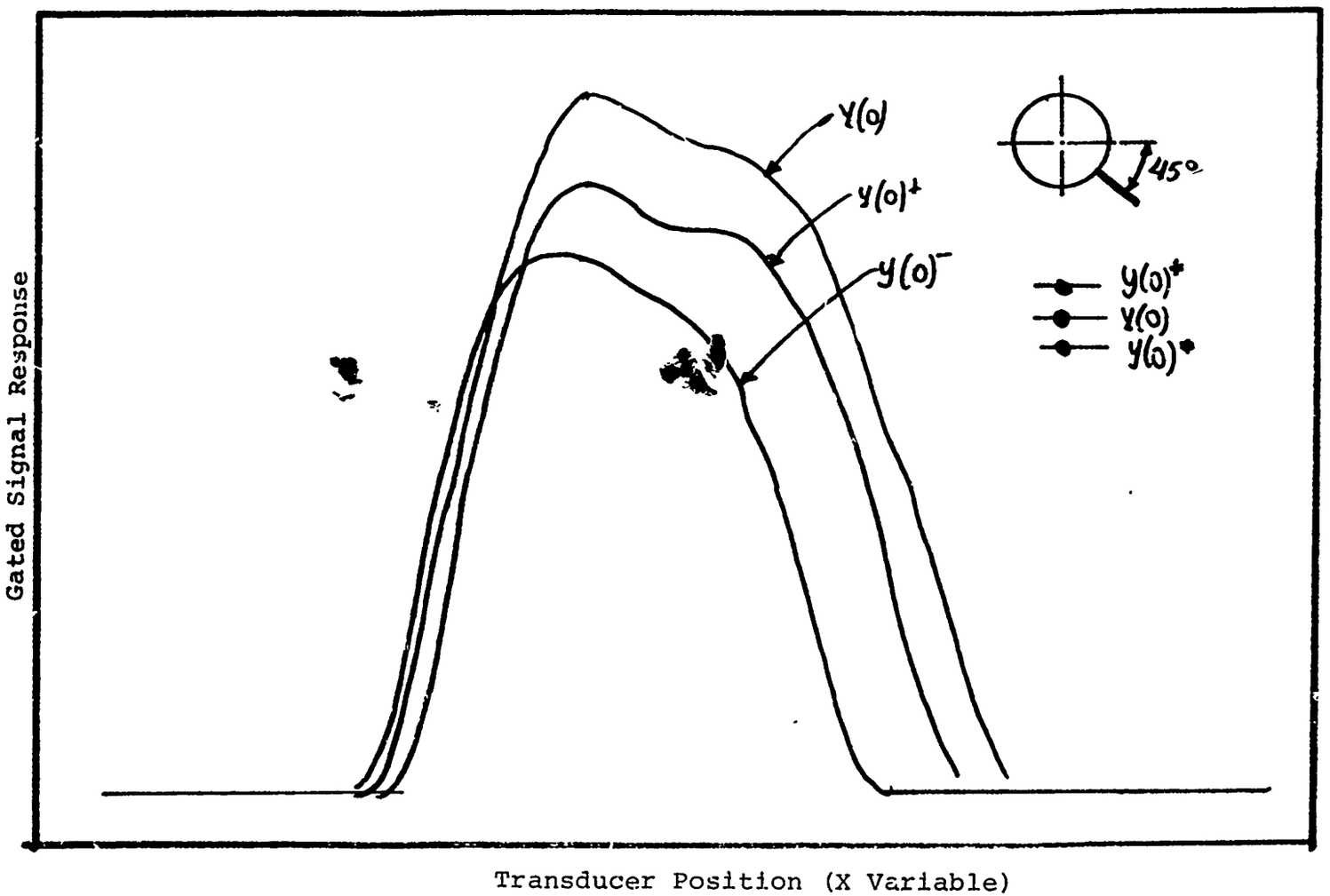

Figure 38

Effect of Orientation of Defect to Direction of Transducer Scan on Indicia

Figure 39

Plot of Percent of Distance Across Indicia of Defect Indication as a Function of Angle of Orientation of Defect with Respect to Transducer Scan

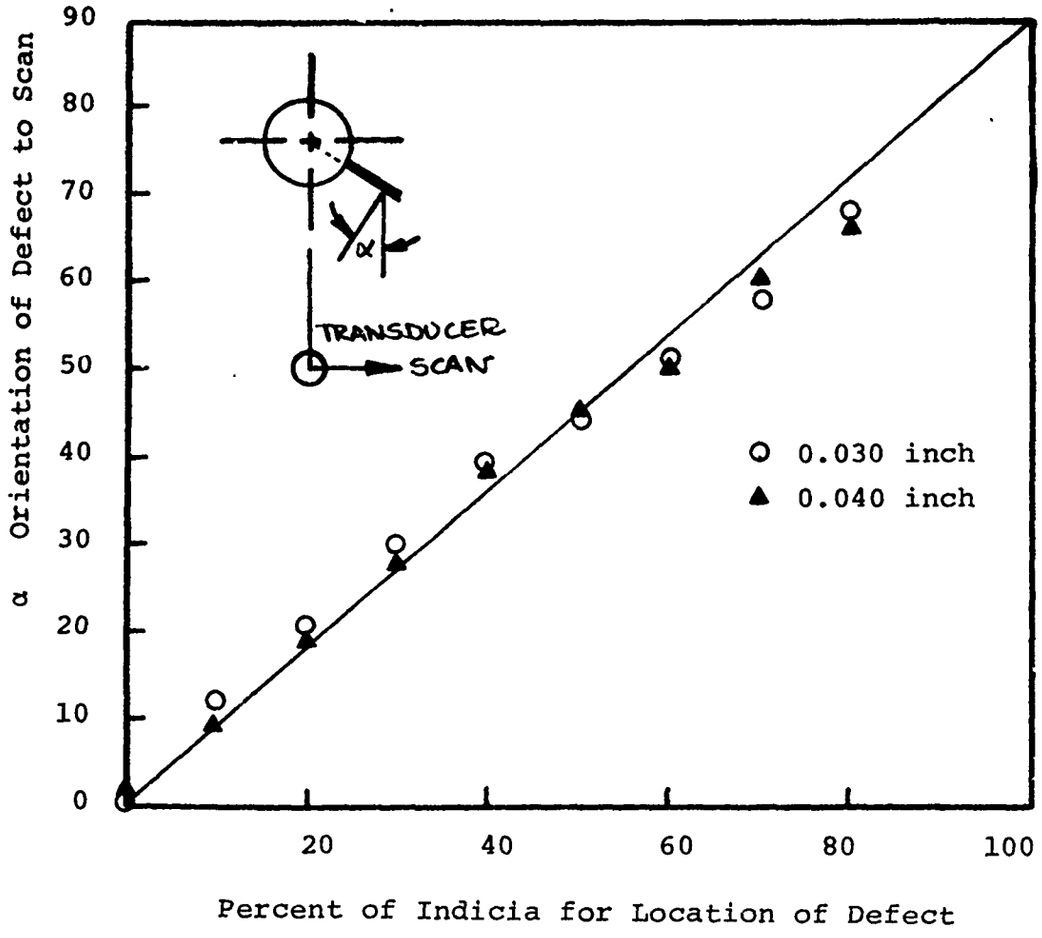

SECTION VI

TRANSFER FUNCTION ANALYSIS

Introduction

If the pertubation of the indicia by the presence of the defect is small, as would be with cracks on the order of 0.020 inches eminating from the bolt hole, the identification of the presence of the defect by direct examination of the indicia becomes difficult. When there is roughness within the hole, or the exact position of the gating is such as to produce noisy signals, the random variations of the reflected signals, and the noise within the indicia may hide the larger pertubation that is the crack indication.

In the use of an indicia technique, it would be impractical for an x-y plotter to be present in the field to draw the indicia and have it examined visually for verification of the presence of the defect. For this purpose it was decided that some form of pattern recognition technique should be used to enable on-line, real-time interpretation of digitized indicia information to be made. Hence, recognition of the presence of the defect could be made without recourse to visual examination of the indicia.

It was suggested that we examine Fourier analysis techniques, as well as transfer function and Bode techniques to see if these would produce sufficient characterization of the defect as distinct from the bolt hole. In this section, the impulse

analysis techniques used for signal recognition are discussed and presented.

Impulse Analysis

Impulse analysis may be considered as an "input-response" method where the response of a system to some forcing function is measured. It is usually desired to deduce from such a a test the most likely form of the system transfer function, $Tr(s)$. (17)

Let $I(t)$ be the process input function, with the input defined as a pulse where at $t = 0$, $I(t) = 0$, and let $0(t)$ be the process output function. Then

$$Tr(s) = 0(s)/I(s) = L[0(t)]/L[I(t)]$$

Where the transfer function is defined as "The ratio of the Laplace transform of the output function $0(s)$ = Laplace $0(t)$ to the Laplace transform of the Imput function $I(s)$ = Laplace $I(t)$". The Laplace transform is defined as:

$$L[f(t)] = f(s) = \int_{-\infty}^{+\infty} f(t)\ \exp(-st)dt$$

Where s is a complex variable defined by $s = \sigma + jW$, with $j = \sqrt{-1}$

The Laplace transform is a linear transformation between functions defined in the t domain and functions defined in the s domain. Knowledge of the form of the transfer function implies knowledge of the processes differential equation, and therefore, of the process mechanism. For example, the driving differential equation for a first order process may be:

$$T\,dy(t)/dt + y(t) = Kx(t)$$

Whose transfer function is given by:

$$Tr(s) = K/Ts + 1$$

Since the Laplace transform of this equation is:

$$(Ts + 1)\ Y\ (s) = Kx(s)$$

If the impulse equations I(t) is a dirac impulse function, as shown in Figure 40, the Laplace transform of the input function is L(d(t)) = 1, since the Laplace transform of a unit impulse is always unity. The response function of the first order de is given by:[17]

$$X0(t) = \frac{AK}{T} \exp - t/T$$ which is graphically shown in Figure 41. This equation can be rearranged and plotted on semilog coordinates as:

$$\ln\ [0(t)] = \ln\ (\frac{AK}{T}) - \frac{t}{T}$$

Thus, one may see that the impulse response of a first order differential equation is a straight line. In a like manner, the differential equation for a second order process has a transfer function of the form

$$Tr(s) = \frac{K}{T^2s^2 + 2T\mu s + 1}$$

and the response can be overdamped, critically damped or underdamped for different cases of the damping ratio μ , being greater

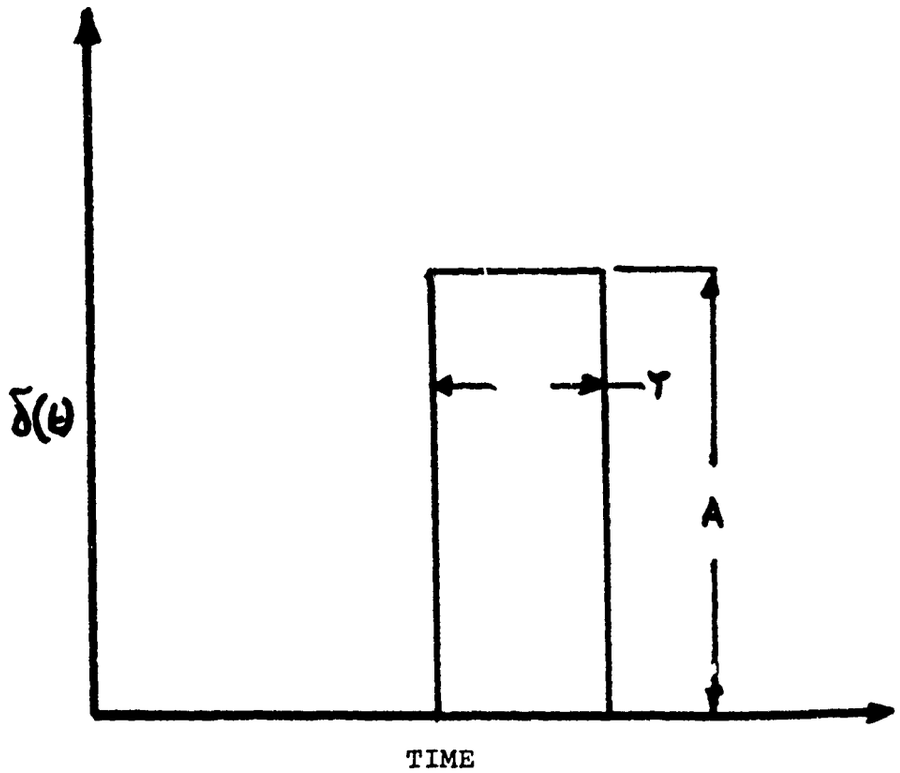

Figure 40

Dirac Impulse Function Whose Laplace Transform is Unity

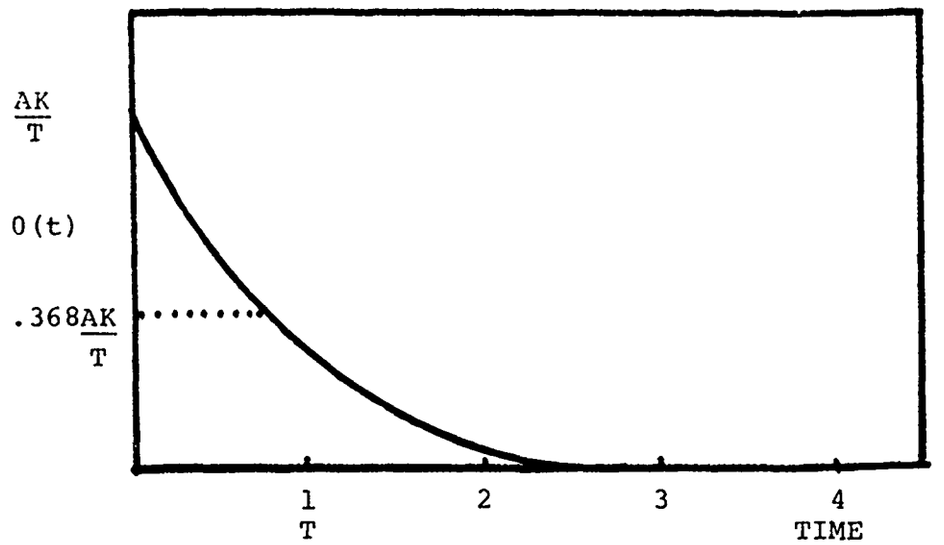

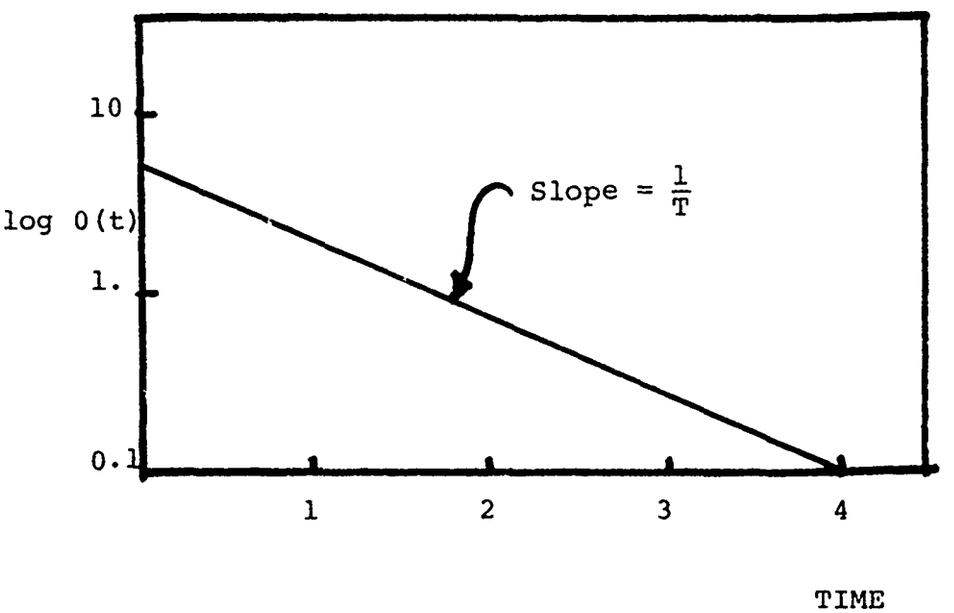

Figure 41

Response Function for First Order Differential Equation

than one, equal to one or less than one. The transfer function plot for an underdamped case consists of a damped sinusoid, while for the over damped are peaking decay functions as shown in Figure 42.[18]

The relative stability of the transfer system is illustrated by the use of a Bode plot.[18] Logarithmic scales are used for Bode plots because they are considerably simpler than linear plots in their construction, manipulation and interpretation. The Bode plot relates the logarithm of the magnitude of the response to the logarithm of the frequency. Consider a single pole transfer function

$$Tr(s) = \frac{P}{S + P} \qquad P > 0$$

The Bode plot for this frequency response function $\frac{1}{1 + jW/P}$ is given in Figure 43. The Bode plots for second order transfer functions with complex poles

$$\frac{1}{1 + 2j\mu\omega/\omega_n - \left(\frac{\omega}{\omega_n}\right)^2} \qquad 0 \leq \mu \leq 1$$

are shown in Figures 44. Note that the damping ratio μ is the variable parameter on these curves.

Thus, the form of the curve on the Bode plot clearly indicates whether the transfer function, and hence the differential equation governing the transformation of the imput function to an output function is of first, second order (and variable damping) or of higher order.

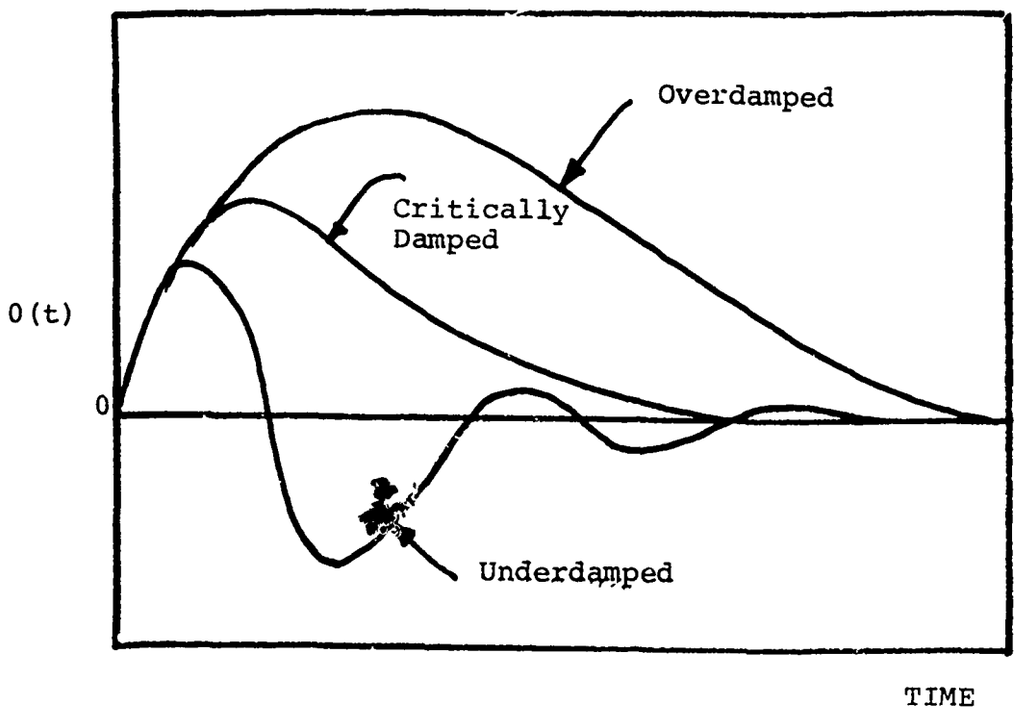

Figure 42

Transfer Function for Second Order Differential Equation, Variable is the Damping Ratio

Figure 43

Bode Plot for Single Pole Transfer Function

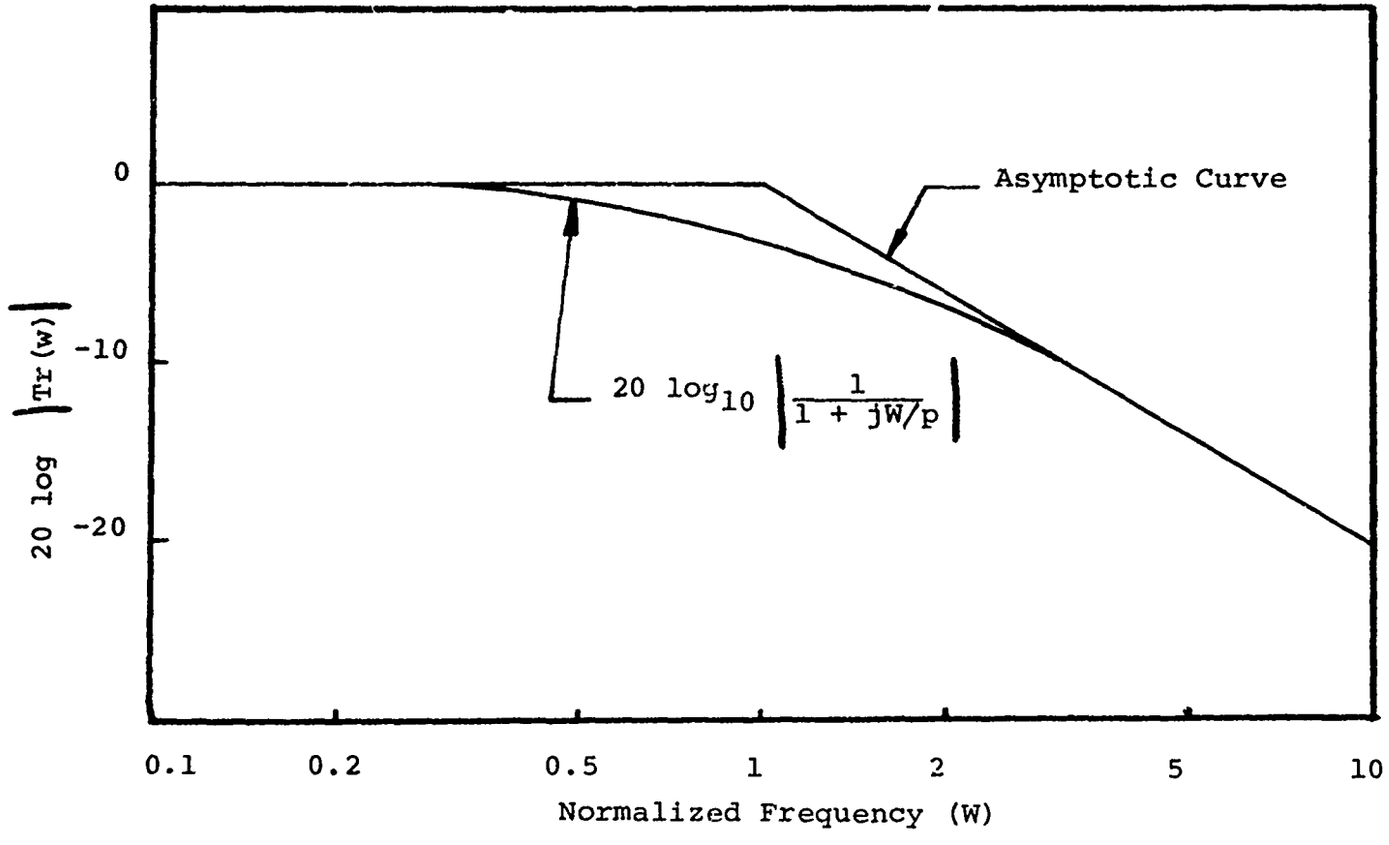

Figure 44

Bode Plot for Second Order Transfer Function

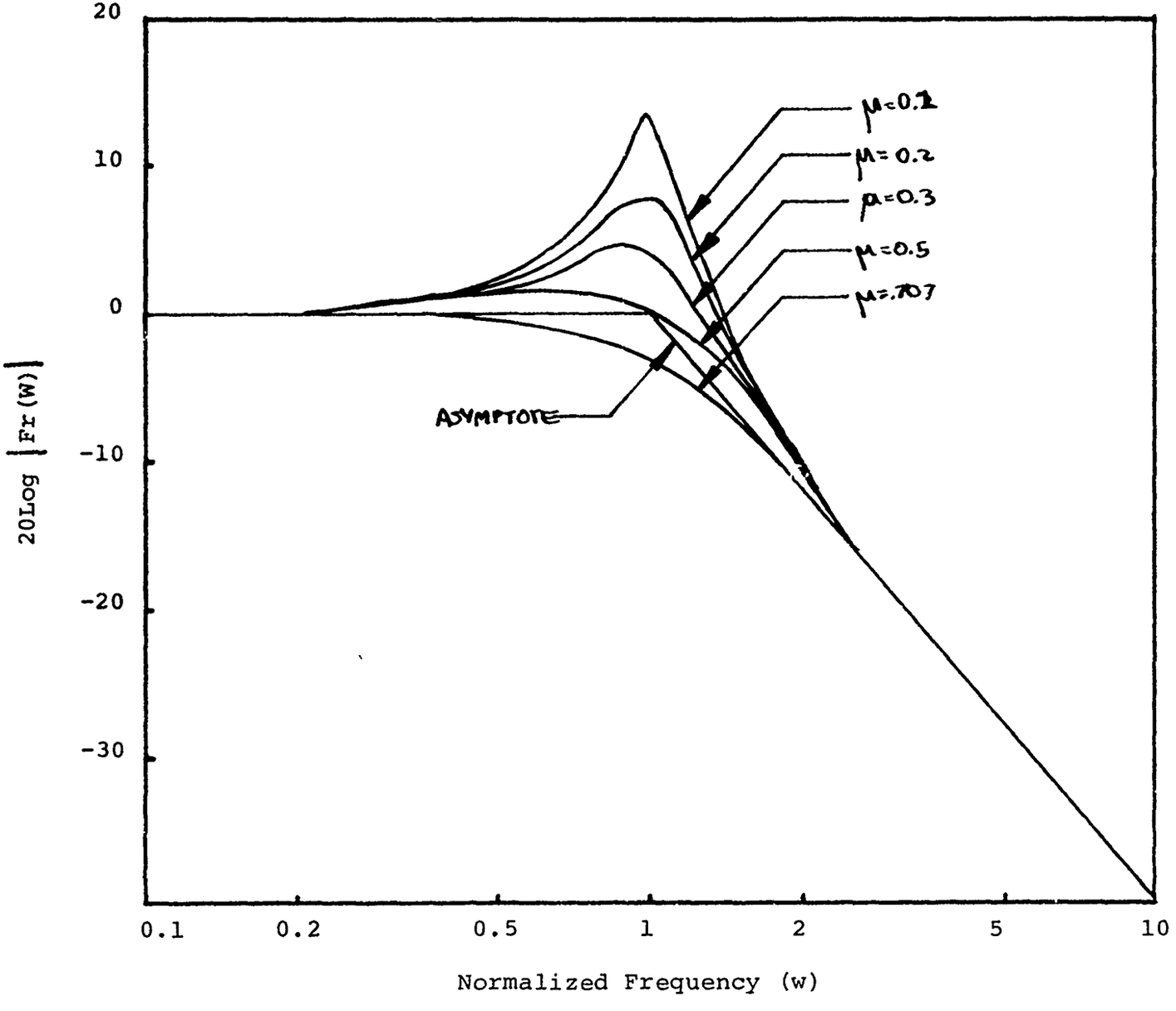

In most analysis techniques using this type of transfer function approach, the form of the forcing function is known, and the problem is to determine the form of the response. In this manner the Bode plot finds many uses primarily in feedback and control system analysis.(19) However, for our purposes we will use this analysis as a method of characterizing the ultrasonic response indicium for the identification of the presence of a defect.

Impulse Analysis of the Indicium

In the previous section, the impulse functions were all time like, one must then reevaluate the indicium to be a "pseudo" timelike impulse. To do this one simply transforms the space like pulse of ultrasonic gated amplitude vs position of the transducer into a curve of gated amplitude vs time. This is not totally unreasonable since one could consider the linear velocity of a transducer and plot the amplitude of the reflection as a function of time for a slowly moving constant speed transducer scan.

The impulse indicia is now considered to the the OUTPUT function. For simplification the INPUT function is considered to be the Unit impulse.

Consider the scan indicium output of the x-y recorder system to be a pulse in time rather than a pulse in space. This is accomplished by a simple exchange of x coordinate to time coordinate. The space pulse can now be transformed to a Laplace time like pulse. The transfer function for the Laplace transform is given by:

$$|Tr_2(S)| = \sqrt{Re^2(S) + Im^2(S)}$$

$$Re(S) = \frac{AC+BD}{C^2+D^2}$$

$$Im(S) = \frac{AC-BD}{C^2-D^2}$$

$$\omega = 2\pi S$$

The magnitudes of A.B.C.D. are given by:

$$A = \int_0^\tau O(t)\cos\omega t\,dt$$

$$B = \int_0^\tau O(t)\sin\omega t\,dt$$

$$C = \int_0^\tau I(t)\cos\omega t\,dt$$

$$D = \int_0^\tau I(t)\sin\omega t\,dt$$

Where I(t) is the input pulse and O(t) the output pulse of the x-y recorder.

Typical Bode plots of the transfer function for the clean hole output with Dirac inputs are given in Figure 45. The figure shows the Bode plot for a clean hole. One can see that there is a first order differential equation that governs the transform of the Dirac pulse into the symmetrical output function. The Bode plot shows a horizontal line which then slopes negatively toward the x axis. This is typical of a plot for a first order differential equation governing the transfer process. The point for the change in slope is related to

FIGURE45: Bode Diagram of typical specimen for ultrasonic indicium of straight shank fastener hole.

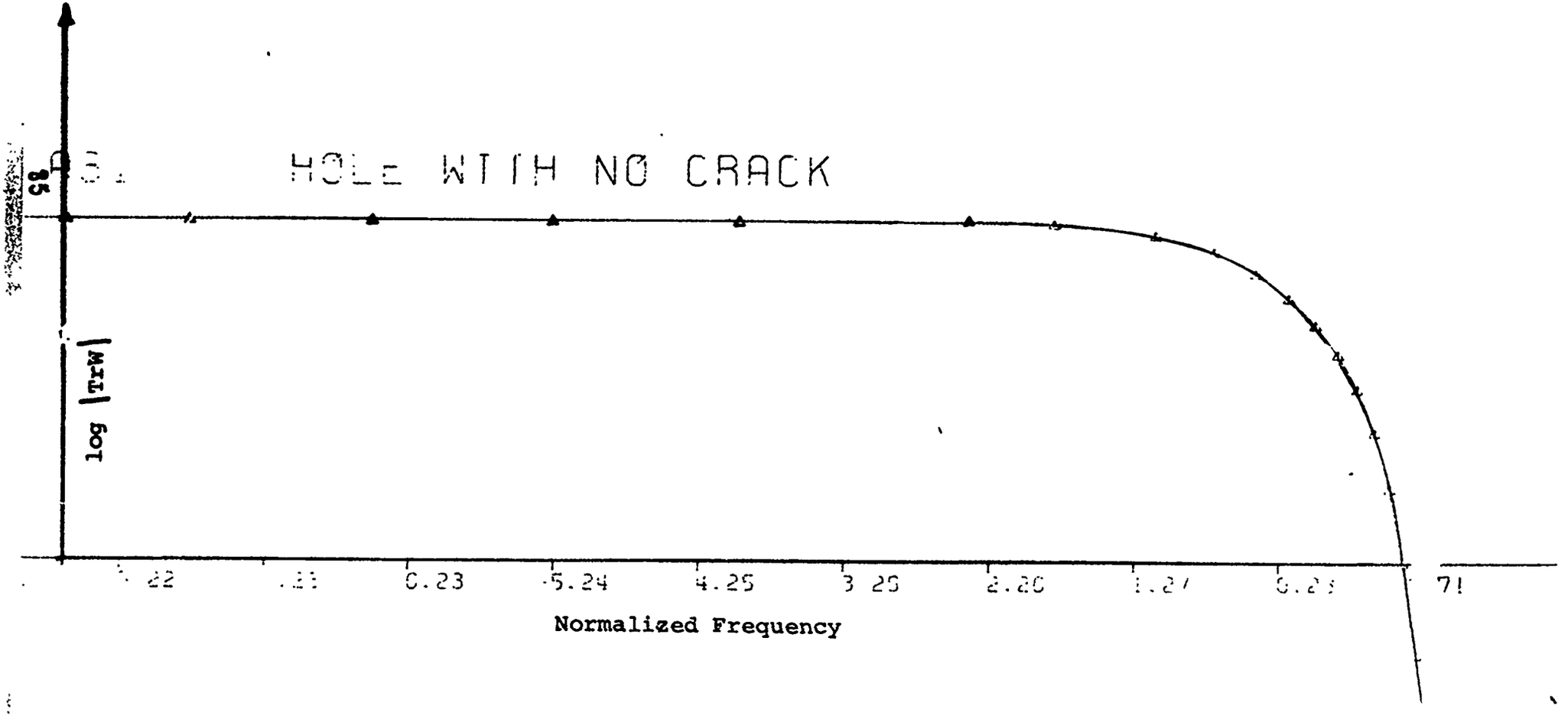

the characteristic or natural frequency of the transfer system.

In contrast Figure 46a shows the Bode plot for a transfer function that was obtained from a hole containing a crack. The Bode plot for a bolt hole containing a defect shows a pertubation at the higher frequencies that indicates higher order transfer processes are occurring. This means that the simple first order imput-response function that converts the unit impulse Dirac function into the indicium for the clean hole is pertubated. The pertubation in this case indicates that there is a defect present. The logical assumption would be that the size of the indicia pertubation, i.e. the size of the defect, would influence the form of the Bode plot in a simple manner. This is not the case as is seen in Figure 46b. Here a series of indicia typical of that shown in Figure 35, with different positions of the transducer scan are plotted. It can be seen that all of the indicia transform into a Bode plot and indicate that there is a defect present. However, there is no consistant shift in the shape of the Bode plot.

The transfer function concept, and the Bode representation is a form of autocorrelation, in that the difference between the theoretical input function and the experimental output function is examined over the total time span for the impulse. A single small pertubation on the output function will cause a shift in the form of the Bode plot, indicating that the input and output functions are not identical. This would be extremely useful if the input function were not a theoretically derived Dirac unit impulse, but consisted of an indicia of a good bolt hole without the presence of the defect. In this latter

case, the Bode plot would indicate that there was a difference between the overall indicia for a good hole and that of a hole containing a defect.

This is particularly useful in scans of bolt hole with defects with the fastener still in place. In this case the input function is the left hand side of the bolt hole (presumably without a defect) and the output function is the right hand side of the bolt hole (presumable containing a defect). The side for which the defect is present is immaterial, since the transfer function divided the indicia of one side of the scan by the transfer function of the indicia of the other side. If there was a difference, the Bode plot would deviate from unity. This is illustrated in Figure 46c, where an interference fastener containing a 0.035 inch defect has been scanned, and the Bode plot made of the transform of the left side divided by the right side. The presence of the defect is seen in this case by the shape of the Bode plot in a manner similar to Figure 46a, and b but not as pronounced.

The major advantage of the transfer function analysis is that minor pertubations within the indicia are smoothed out, i.e. high frequency noise that is random in nature due to random reflections within the interference fit of the bolt hole and surrounding material are "averaged" by the Laplace intergal transform. Only the pertubation that is not random in nature, i.e. the defect,is identified. If the "typical" clean interference fastener is used, the system is essentially self standardizing, since it uses each particular bolt hole as its own standard rather than relying on an external calibration as would be with

other simple amplitude methods.

It,therefore, appears that the indicia, when combined with the transfer function impulse technique, provides a rapid-self standardizing technique for identification of defects within the area of the bolt hole.

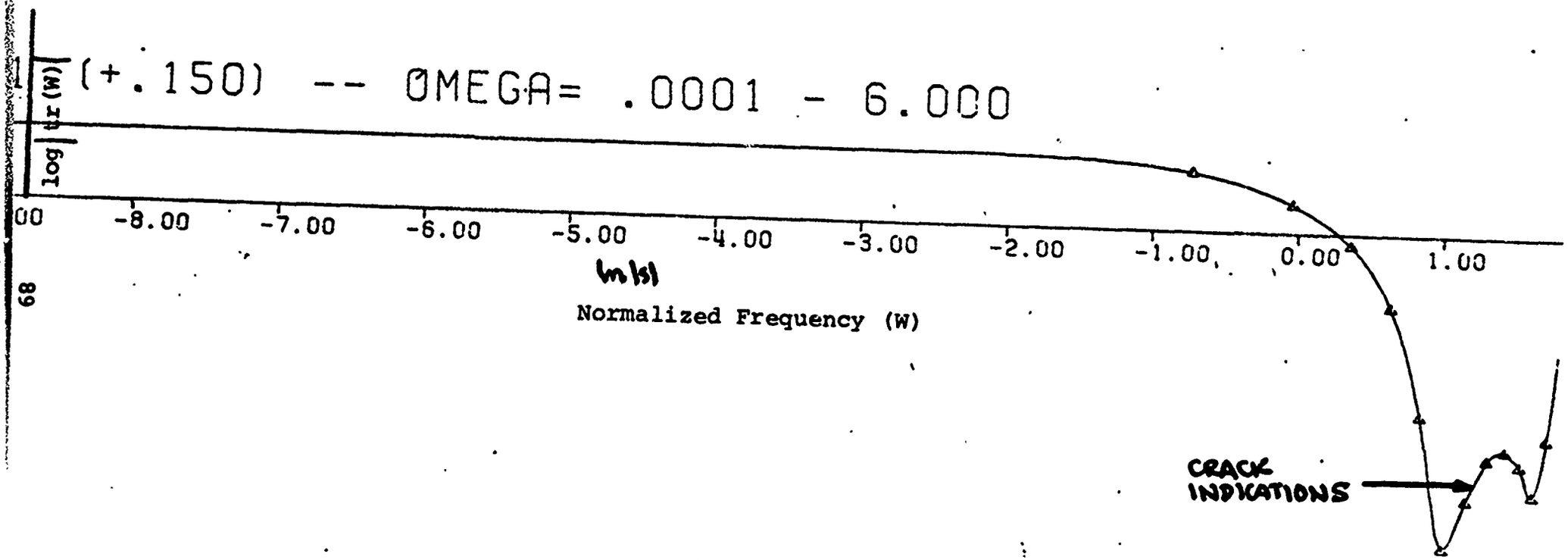

Figure 46a

Bode Plot for Transfer Function for Bolt Hole Containing Small Defect

Figure 46b

Bode Plots for Transfer Function for Bolt Hole Containing Small Defects as a Function of the Position of the Transducer Scan

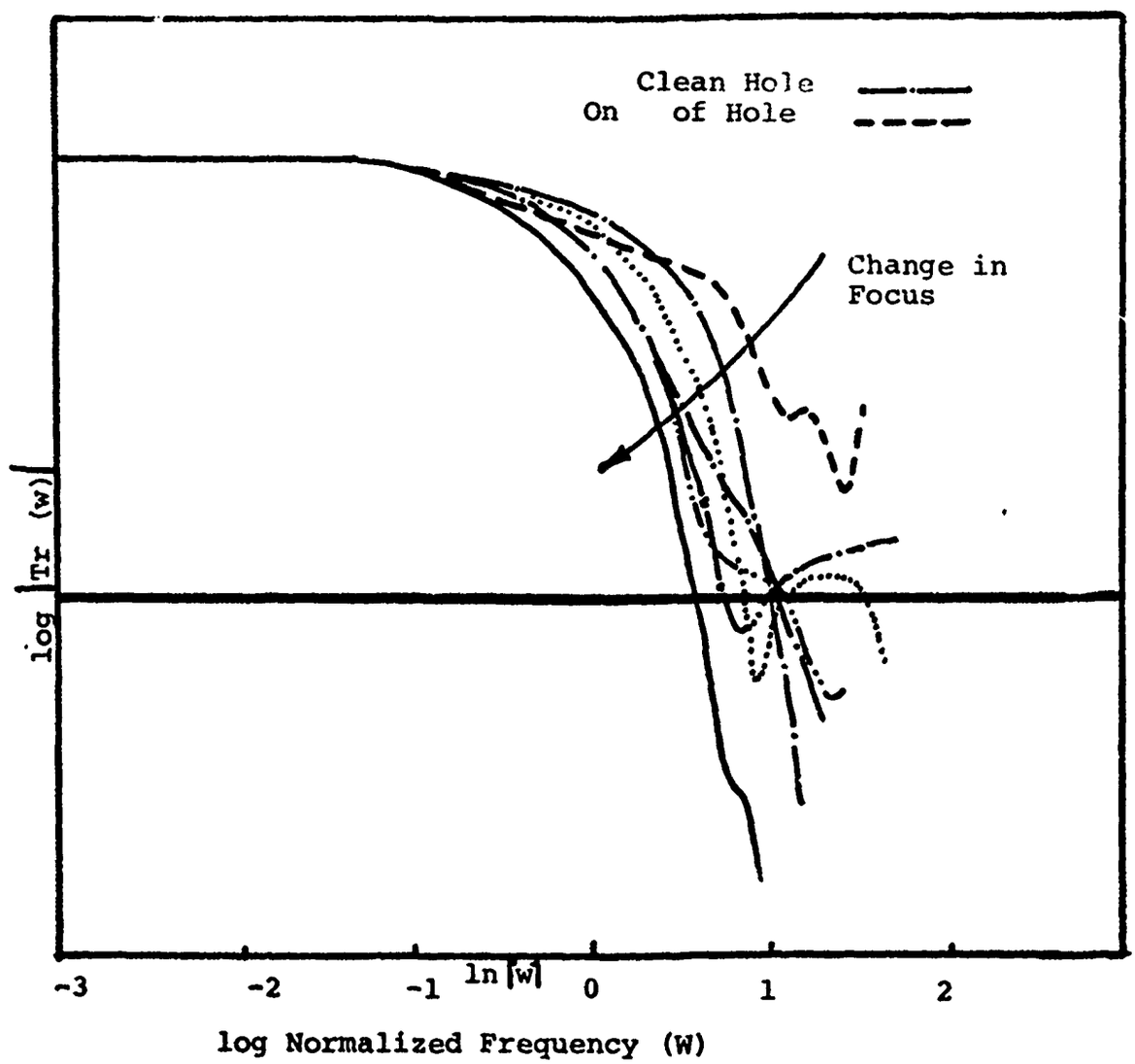

Figure 46c

Bode Plots for Transfer Function for Bolt Hole Interference Fastener Containing Defect in Vicinity of Fastener Hole With Fastener Still In Place

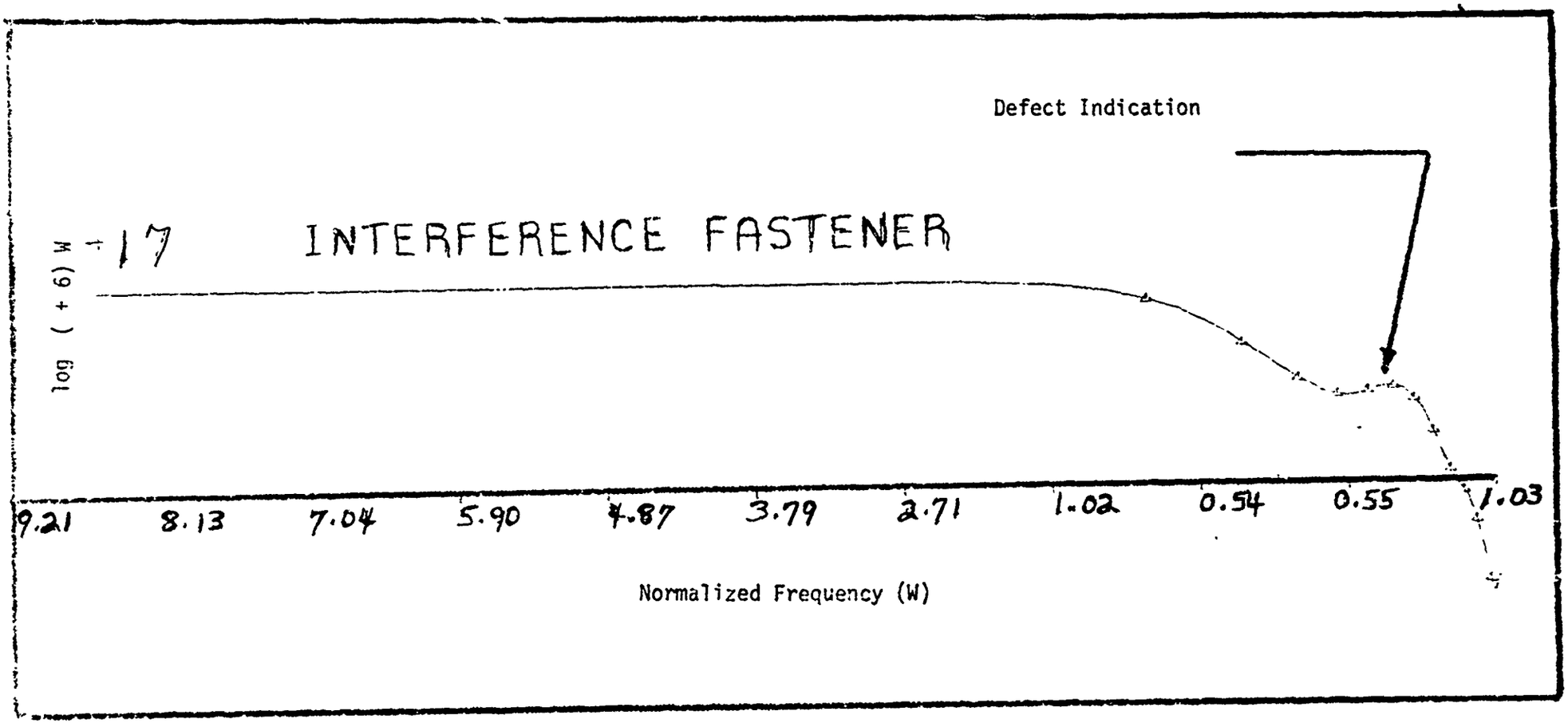

THIS PAGE INTENTIONALLY LEFT BLANK.

SECTION VII

EDDY CURRENT BOLT HOLE PROBE

Fundamental Eddy Current Concepts

Faraday's Law of Induction states that the electromotive force induced in a circuit is equal to the negative time rate of change of the magnetic flux through it. When applied to eddy current testing, the application of a changing magnetic field on an electrically conducting material result in a pulsating, circular current flow in the conductor; hence the name eddy current. (20) It is the resistance to the production of eddy currents in a test material which gives rise to the value of this technique for use in nondestructive testing. Using the proper analysis technique , this inspection method can yield information about flaws, dimensions, hardness, alloy composition, strength, crystal orientation, foil or wall thickness, plating thickness, porosity, grain size, heat treatment, and any other property which is related to magnetic permeability and electrical conductivity.(21)

The basic equipment needed in order to generate eddy currents in a specimen is shown in Figure 47. The components are (1) a source of alternating current, (2) a primary coil which generates the magnetic field, (3) a secondary coil which continuously monitors the magnetic field strength, and (4) an instrument to analyze the signal from the secondary coil.

The source may produce a frequency of electrical pulses, but more commonly an alternating current is used. The frequency should be variable since the depth of penetration, sensitivity, and resolution are all frequency dependent. The source

Figure 47

Schematic Showing, Generation of Eddy Currents

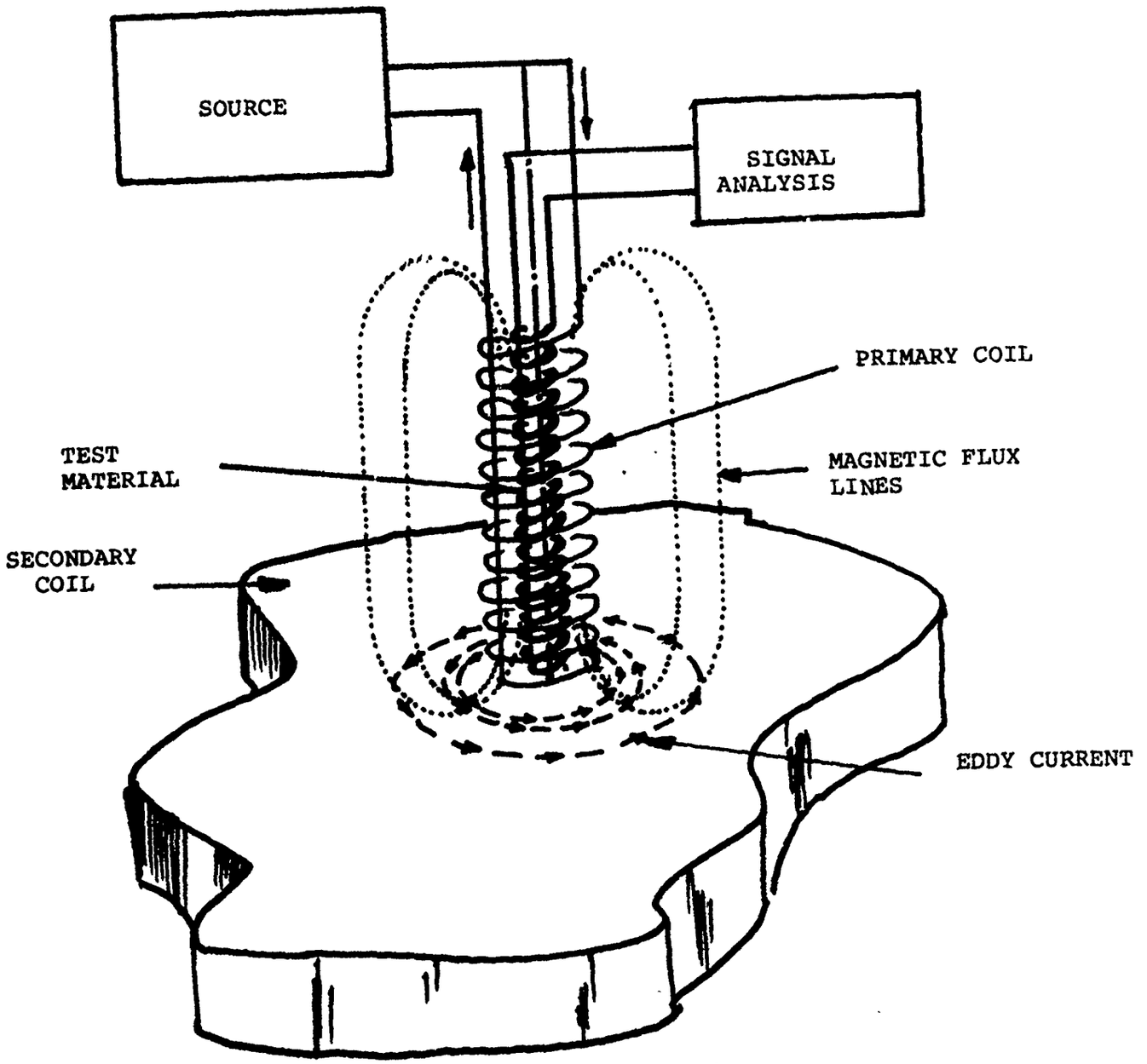

induces an alternating current in the secondary coil, producing a magnetic field shown by the flux lines in the diagram. The secondary coil is generally composed of enameled copper wire wound on a ferrite core. As shown in the drawing, the changing magnetic field surrounding the primary coil extends into the surface of the test specimen. The action of this field is to produce eddy currents which move circularly in the material immediately beneath the inspection probe in a direction opposite to that of the current in the coil. The effect of these currents is to produce a magnetic field in the test specimen which opposes the existing field of the primary coil. As a result, the total field strength of the primary coil is reduced. Thus, any material property or configuration which tends to change the density of eddy currents produced also changes the magnetic flux density, and this change may be monitored to produce an output voltage representative of the variations encountered in the test specimen.

Monitoring of the flux density is handled by the secondary coil. This is commonly wound within the primary coil, and the changing flux of the primary coil produces a current flow in this monitoring coil. This output current is fed into a unit for either impedance analysis or impedance plane analysis. In impedance analysis only the magnitude of the impedance $Z = \sqrt{R^2 + X_L^2}$ where R is the resistive component and X_L is the inductive. The resistive component evolves as a result of heat lost due to eddy currents in the test specimen and thus is related to the material electrical conductivity (22). The inductive reactance results from the inductance of the coil which is affected by the

permeability (23) of the material. Thus, all material properties that can be related to changes in these two variables can be detected with the use of eddy current inspection.

In cases where the number of the various discontinuities and/or compositional changes exist simultaneously, it may be necessary to use a more complex signal processing method of impednace plane analysis - also known as phase analysis. Here the phase angle of the impedance is also measured and one may calculate the individual components of impedance. Usually, however, it is more convenient to graph the data on an impedance plane. Examples of such curves are shown in Figures In order to generalize such curves for various coils, they have been normalized. The normalized inductive reactance is plotted as the ordinant (wL/wL_o = inductive component in the presence of test specimen/self - inductive reactance), and the normalized resistance (R/wL_o = resistance/self inductive reactance) is plotted as the abscissa.

Figure 48a is a plot of impedance values as a function of f/fg where f = frequency of the current in the primary coil and fg is a frequency which is characteristic of the material and the configuration of the inspection coil. Most of the theoretical work done in the field of eddy current testing has been applied to the feed-through coil. This is a coil used for inspecting rods and tubes, and is designed such that its inside diameter provided minimum clearance for the outside diameter of the cylinder being tested.

There are two general classes of coils,feed through coil and a probe coil. The feed through coil is generally circumferential

in nature and has an open center through which the material to be inspected passes. This is most commonly used for inspection of tubes, barstock, or rods. The probe coil is a small coil that is placed on the surface of the part to be tested so that its axis is perpendicular to the surface. Theoretical treatment of the field strength has been developed for the feed through coils, but is not available for the general case of the probe coil, and must be developed empirically.

The differential encircling coil (for the tube inspection) should be thought of as part of the instrument. Each inspection coil is balanced and matched to a specific flaw detector, and coils are not interchangeable with other flaw detectors even though they are believed to be of identical design. For this case, $fg = 5060/\sigma\mu d^2$ where d is the diameter of the rod.

Figure 48b shows the variance in impedance as a function of permeability and conductivity. Impedance changes due to these two variables will generally be shown to move in directions oriented perpendicularly to each other on the impedance plane. The various structural conditions capable of being detected by the eddy current method give rise to still more characteristic curves for the composite changes in permeability and conductivity which identify the flaw type or property. Figure 48c is an example of the impedance plane curves for various cracks as a function of f/fg. Thus, the impedance plane approach to signal analysis can be used to detect and differentiate among several defect conditions.

In actual practice it is often necessary to make calibration blocks from the material to be tested, containing the flaw

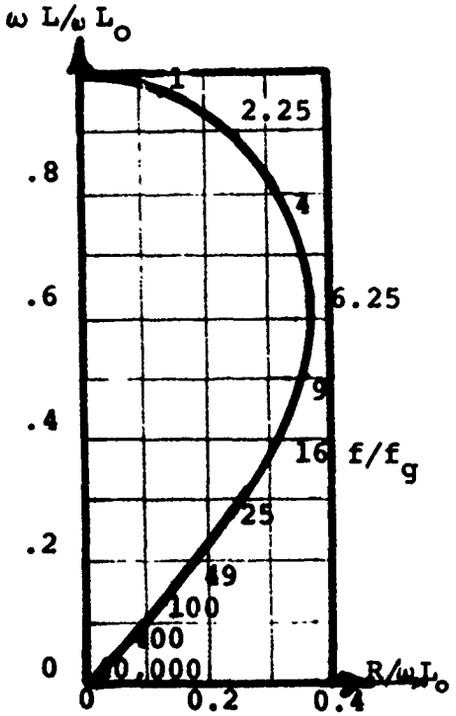

Figure 48a

Impedance as a Function of f/fg

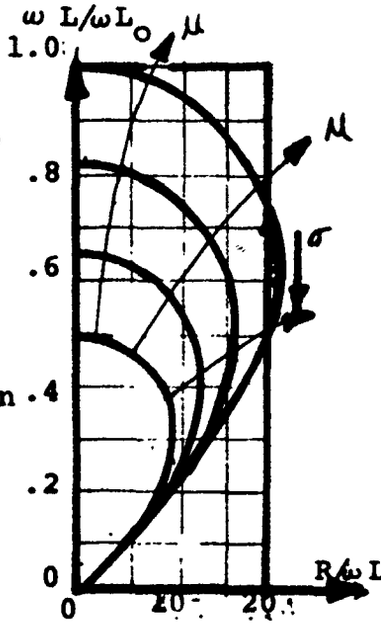

Figure 48b

Impedance as a Function of Permeability and Conductivity

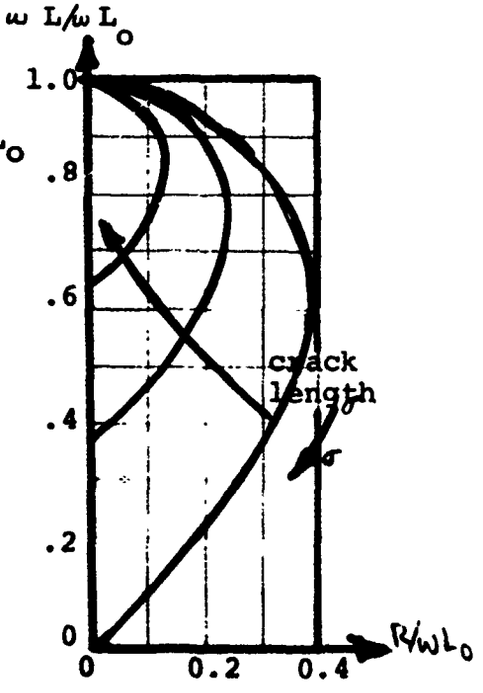

Figure 48c

Impedance as a Function of Crack Length

types expected to be found in the inspected parts. The practice of eddy current testing is advanced such that theory can assurately predict behavior only in the most rudimentary cases.

One of the major shortcomings of the eddy current inspection is its inability to penetrate significantly within the test material. Figure 49 shows current density (J_x) as a function of x/S where x = actual depth and S = depth of penetration which is defined as the depth at which the current density is reduced to i/e or 36.8 percent of the surface value.[21] The parameter varies inversely as a function of the frequency of the primary coil.

The sensitivity also varies as a function of frequency. For a nonmagnetic material sensitivity is greatest when the resistive component of impedance is a max. mum. This occurs when at the knee of the curve pictured in Figure and thus defines a characteristic value of f/fg for a particular material and eddy current probe.[23] However, sensitivity may not dictate the optimum frequency. In many cases it may be possible to attain a better signal to noise ratio at a less than maximum sensitivity because this signal can easily be amplified to the desired strength. Therefore, the selection of a working frequency for an inspection test should be determined by a trade off between depth of penetration needed and signal to noise ratio.[21]

Eddy Current Sensitivity

A standard eddy current coil tube inspection procedure requires detection of flaws whose size is greater than 10% of wall thickness.[24] By virtue of the inherent design characteristics of a differential coil, flaws of considerable depth can pass

Figure 49

Current Density (J_x) as a Function of Reduced Surface Depth of Penetrant (21)

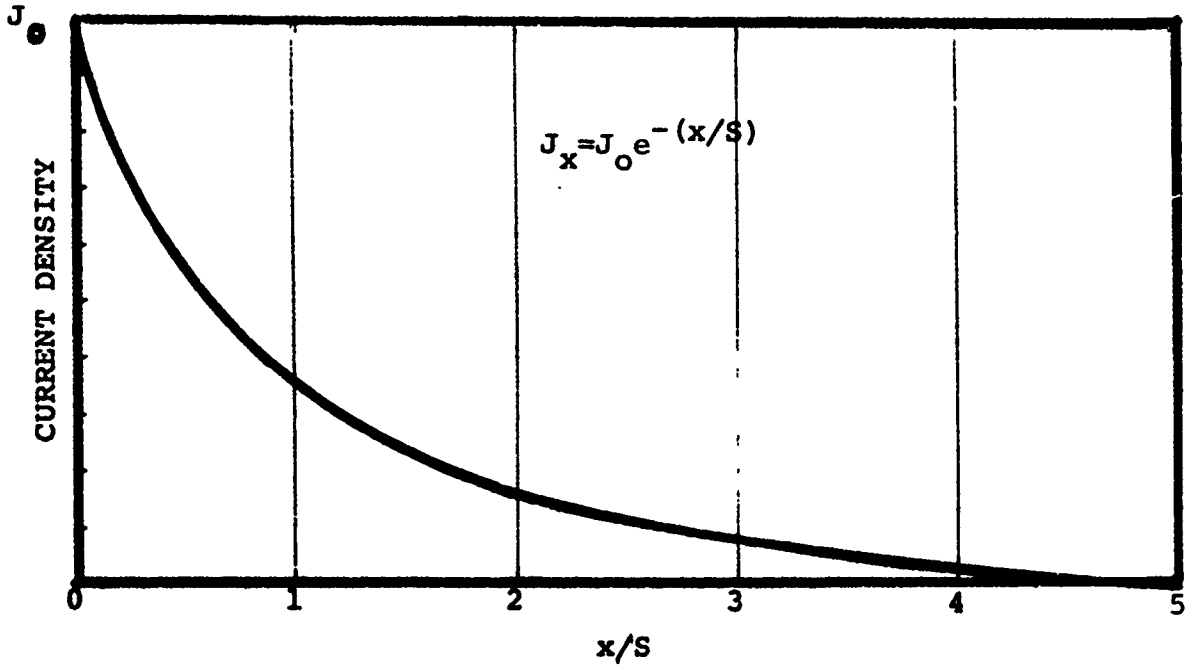

through the coil and not be detected. For example, in a tube which produces a low noise background, a void 26% of the wall thickness, the deflection for this defect was only equal to the average peak-to-peak signal. If the background noise had been higher the signal would be missed.

The most prevalent problem associated with increasing the sensitivity of the eddy current system is that the linear amplification of signals results in a great number of rejections that have little bearing on the actual flaws present. For example, Lloyd[25] has determined the ratio of rejections found by eddy current signals divided by the number of defects found by visual/tactile methods as a function of the signal level as shown in Table IX.

Thus, while the inspection procedure is effective in finding most of the flaws at the larger size levels, it finds 11 times more "benign" flaws when the signal level is much lower. Therefore, in establishing the rejection level for defects, it becomes necessary to set a definite inspection level. This level is set so that the eddy current technique is at least as effective as the current level it is planned to replace, preferably somewhat better. Lloyd concludes that the eddy current coil inspection of copper tubing does not reject at reasonable inspection levels local surface flaws, but is more effective in detecting surface porosity and is not entirely equivalent to visual inspection.

Flaws can be defined as any discontinuity that produces a signal above the noise. The theoretical number of maximum probability for passing flaws of a certain size is the ratio of

the number of signals passed to the length of tube passed.

A plot of the probability of accepting flaws as a function of the discrimination level shows that the confidence in the inspection falls off rapidly as the discriminator level is raised above the noise level. Tube noise is largely responsible for the ultimate confidence level that might be achieved. Tube noise is the result of many factors, including a combination of minute nicks, scratches, dents, and other surface irregularities. Singularly these might be of little or no consequence, but when occurring in clusters may often be detected as single large flaws.

There were many factors to consider in the design of a unit for fastener hole inspection. The factor of greatest consideration was the type of information which was sought concerning the cracks which might emanate from these holes. Since it was important to precisely describe the crack location and geometry, it was necessary to use a probe which would inspect only a small area of the hole bore at any one time. This was most easily done using a small surface probe which would rotate against the hole surface, scanning its entire area. Such devices are commercially available, described simply as a bolt hole probe. However, a device which would rotate the probe in the proper manner with an allowable noise level was not available on the commercial market and it was necessary to design and fabricate the scanner.

Helical Scan Bolt Hole Probe Design

A helical scan eddy current unit was constructed in the initial portion of this program. This is shown in Figure 50. It consists of a constant speed motor driving a slender tube

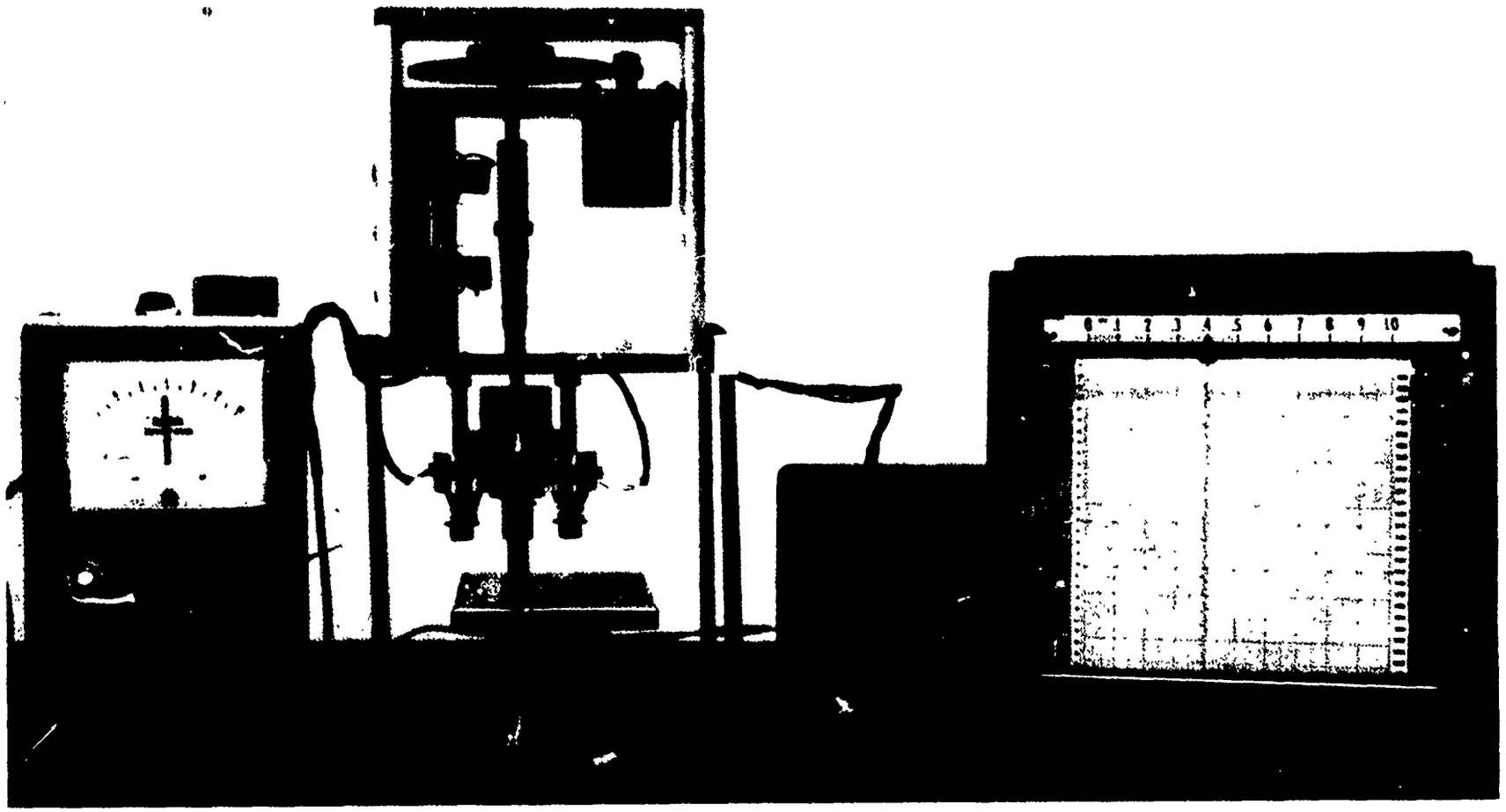

Figure 50

Helical Scan Eddy Current Unit

mechanism connected to a micrometer. Attached to the anvil of the micrometer is the eddy current probe assembly. The motor system drives the eddy current probe at about 10 rpm and advances 0.025 inches per revolution. Thus, the probe scans a helical path within the bolt hole as it enters and leaves the bolt hole. Limit switches are used to reverse the scanning direction; these are adjustable to allow different plate thicknesses to be scanned.

A close up of the eddy current probe is shown in Figure 51. This consists of the probe coil mounted in a bakelite split tube and signal pickup coils. The pickup coils and feeds are mounted on external spring mounts so that positive signals can be obtained for all positions of the eddy current probe. The coil is an absolute coil with a ferrite core and two layers of windings. The total diameter is approximately 0.040 to 0.050 inches. The inductance of the circuit is 4 milihenrys and has a variable capacitor that is used to tune the the resonance frequency to about 4Mhz.

Typical operation of the unit entails simply setting up over a selected bolt hole and allowing the unit to scan in both the inward and outward rotational modes. Proper selection of coil, external balancing, and damping are essential to obtaining significant information.

The probe selection was made between two basic types - an absolute probe and a differential probe. An absolute probe measures a gross impedance value and changes from the norm of this value. The differential arrangement requires two secondary coils, wired in series, but wound in opposite

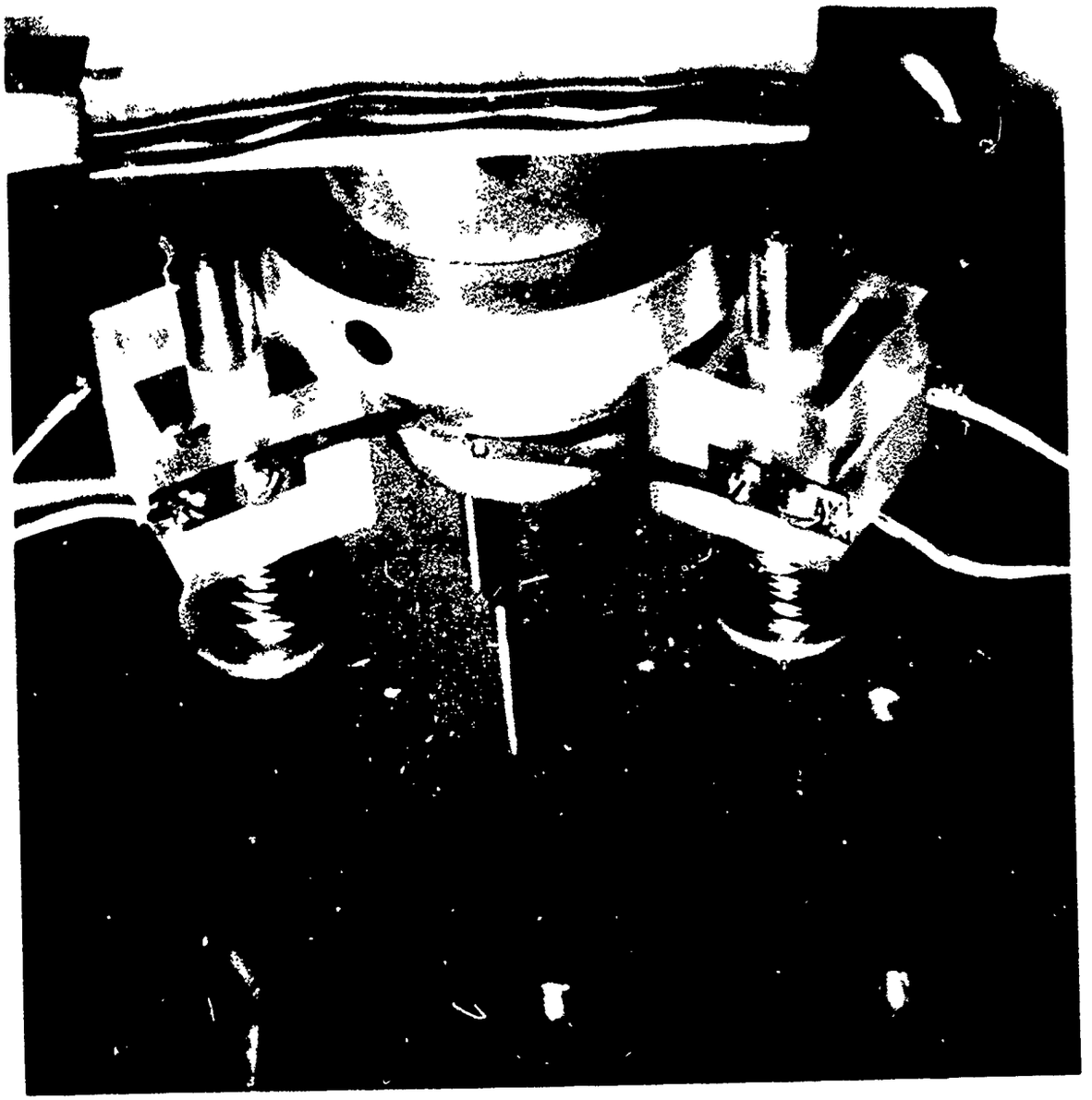

Figure 51

Close up of Eddy Current Probe
Entering Bolt Hole

directions such that they oppose each other and the voltage output is zero when the same flux density is monitored in each coil. The effect is to test one part of a test specimen against another part under the assumption that any discontinuities or structural changes are local and thus will be detected by only one coil at a time resulting in a relative voltage drop across the two terminals. If a long flaw should exist in such a manner that it is scanned simultaneously by the two secondary coils, the field effects will be equal and a flaw signal will be output only at each end of the flaw. Due to difficulties encountered with a differential coil arrangement for a bolt hole probe, the most common type commercially available was of the absolute variety. This was quite satisfactory for the specialized inspection for fatigue cracks emanating from fastener holes in aircraft structural members.

Since the expected flaws were very precisely defined as fatigue cracks, it was found desireable to combine the data availal le from the components of impedance into the single variable of impedance magnitude. By thus doing, much unnecessary labor involved in impedance plane analysis was avoided, with very little apparent loss in detectibility of the flaw. The specific unit used was the Defectometer Type 2.154 manufactured in Germany by the institute of Dr. Forster and distributed in the United States by Automation Industries, Inc., Danbury, Connecticut. It was designed to operate at the constant frequency of 4 Mhz. This frequency was satisfactory since it provided good resolution and sufficient penetration for use in surface crack inspection. It came equiped with a number of

ferrous bolt hole probes, but it was necessary to have some non ferrous probes built. This was done by the Ideal Specialty Company of Tulsa, Oklahoma.

As a means of permanently recording the signal output from the Defectometer a Hewlett Packard 7004B x-y strip chart recorder was obtained. This unit was capable of following the output signal with only slight variations due to the rapid nature of the voltage changes.

Specimen Configuration

Three defect bolt hole configurations were produced. These are shown schematically in Figure 52 and Tables X, XI, and XII. They are (1) a constant depth slot, (2) a part through varying depth slot, and (3) internal varying depth slot. Table X is specimens with essentially constant depth and widths varying from 0.007 to 0.015 inches in width. All depths and widths were measured using a Zeiss metallograph at 100x, and were checked using the vernier microscope of a Tucon microhardness tester. Table XI contains some of the part through varying depth cracks. This series was intended to confine the crack to the near surface. Table XII is a mixture of varying depth, through and internal slots.

A detail of a typical test block is shown in Figure 52. It should be noted that in some holes the condition of the interior is typical of what would be expected for a hole with the bolt removed, and contains both horizontal and veritcal cuts and scratches in addition to the elox slots. Additional specimens have been produced using pre-cracked fatigue test specimens. These are made from 0.5 inch thick aluminum and steel blocks fatigued in a three point bending unit on

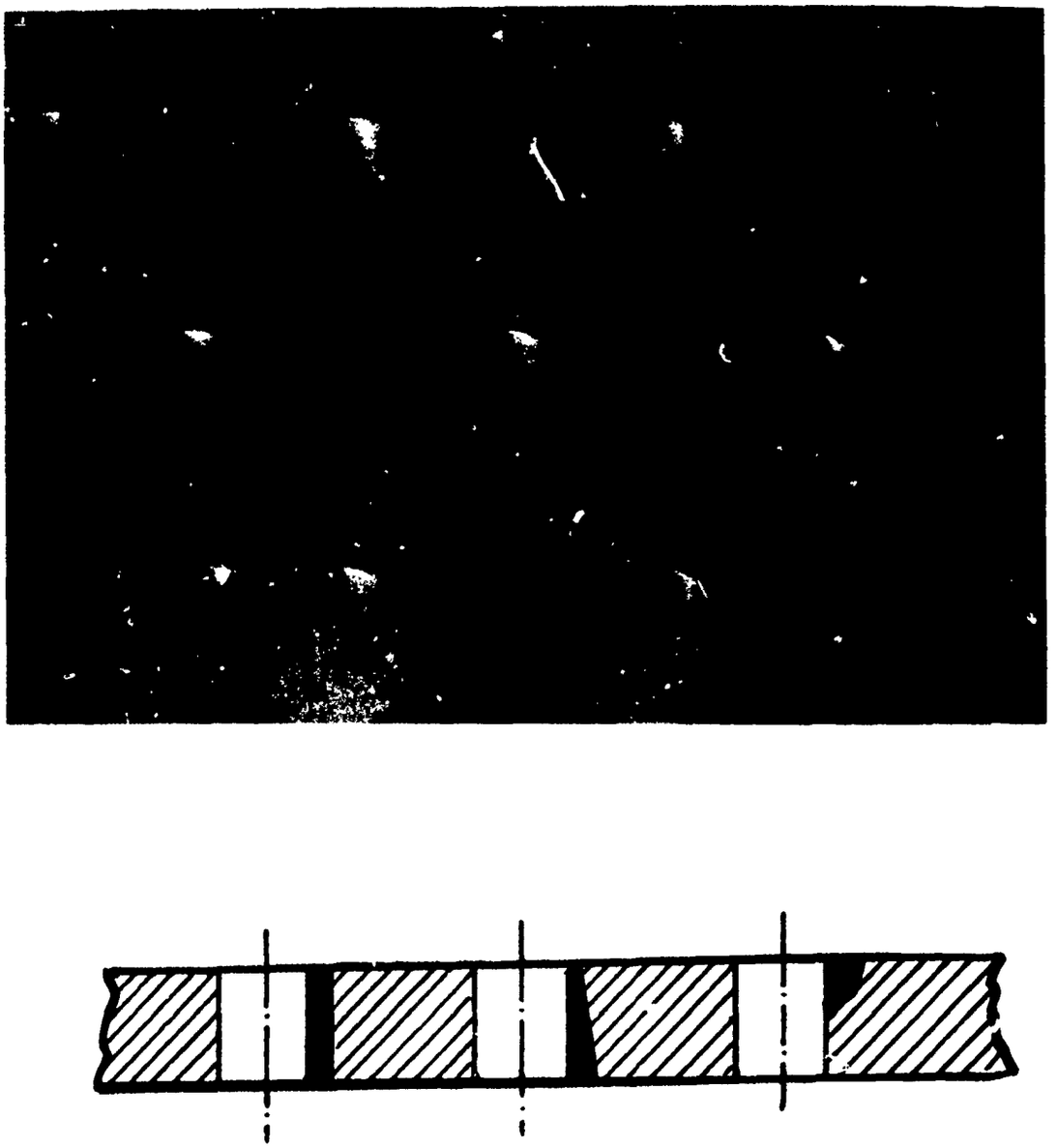

Figure 52

Detail of Typical Test Block (Steel) and Schematic Showing EDM Notch Configurations

either the MTS or Tinius Olsen. The fatigue cracks are initiated and grown in tension-tension fatigue and have an aspect ratio of approximately a = c. When the fatigue crack is grown to a pre-determined size, a hole is drilled adjacent to the fatigue crack, r-sulting in typical crack specimens. Attempts have been made to fatigue cracks initially placed in drilled holes to produce completely internal cracks, but to date have been singularly unsuccessful. The major probelm is that the high stress intensity factors associated with the immediate vicinity of the hole produce a long shallow crack totally along the depth of the hole.

A series of scans was produced using the elox specimens as well as fatigue cracks and scratches within the holes. Each of these were examined for significant signatures as described in the next section. In addition, a limited series of specimens containing crack like defects in interfaces was examined. Here the crack was produced in one plate surface near the edge and the defective hole mounted within a"stack" . The eddy current scan thus had to differentiate between the defect and the interface as well as a benign defect.

Eddy Current Results

In Figures 53 to 59, recordings for six typical slots and three typical fatigue cracks are presented. Each of these show distinct flaw indications in holes with smooth as well as rough interior surfaces. The signal was more difficult to detect with the presence of high noise due to poor machining of the hole, but the flaw indications are easily discernible from

Figure 53

Eddy Current Scan BB-1

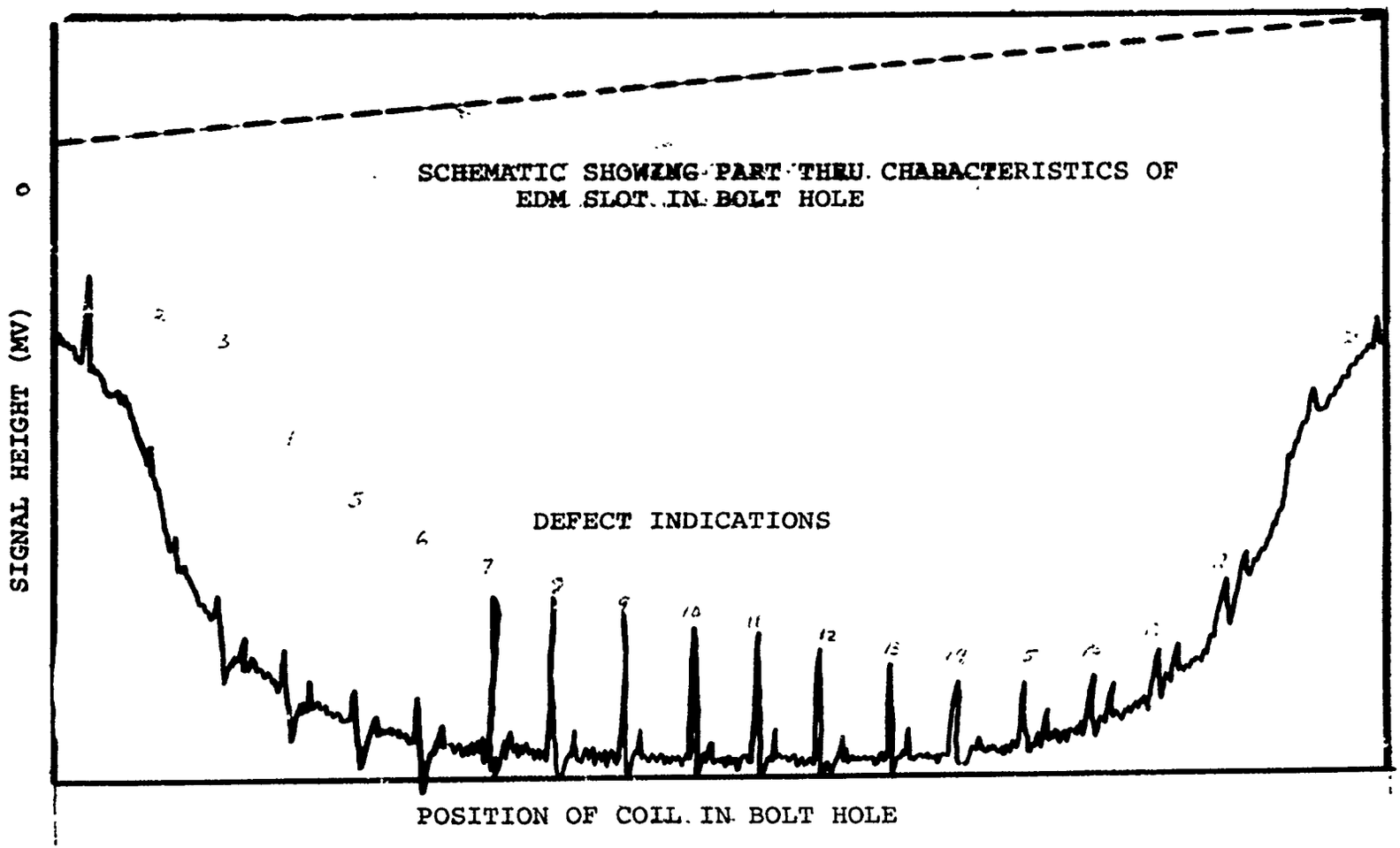

Figure 54

Eddy Current Scan BB-2

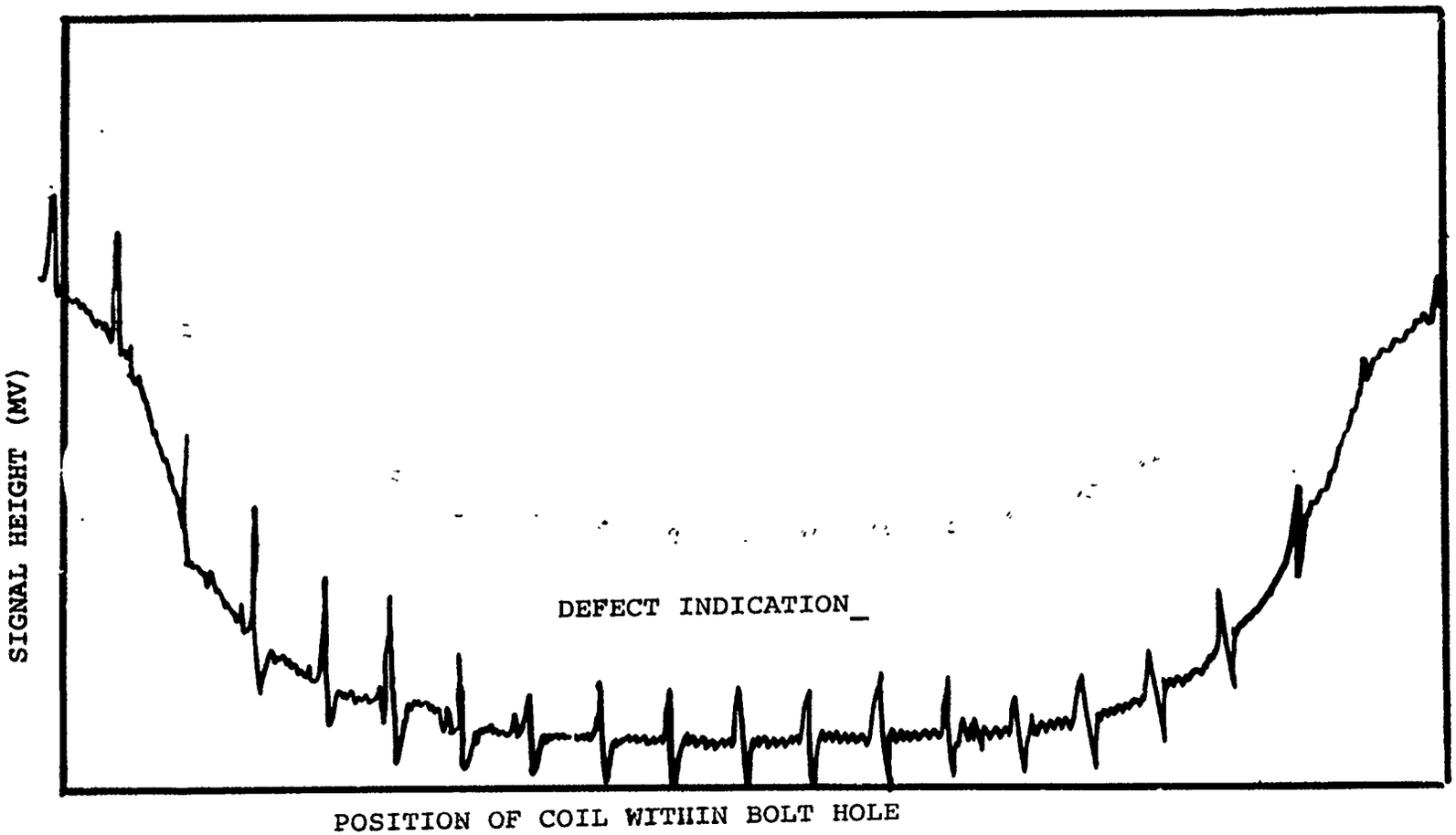

Figure 55

Eddy Current Scan BB-3

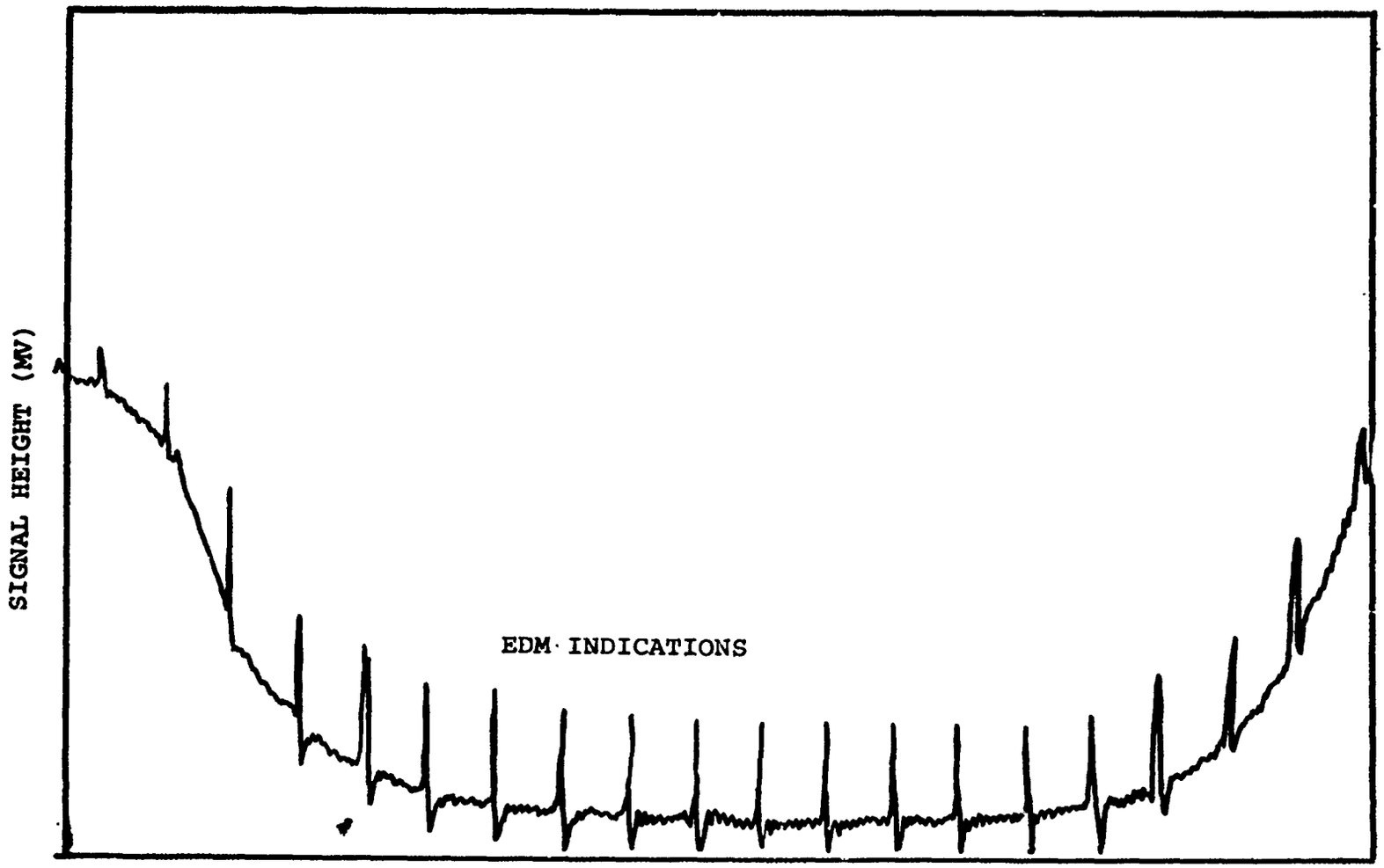

Figure 56

Eddy Current Scan AL81

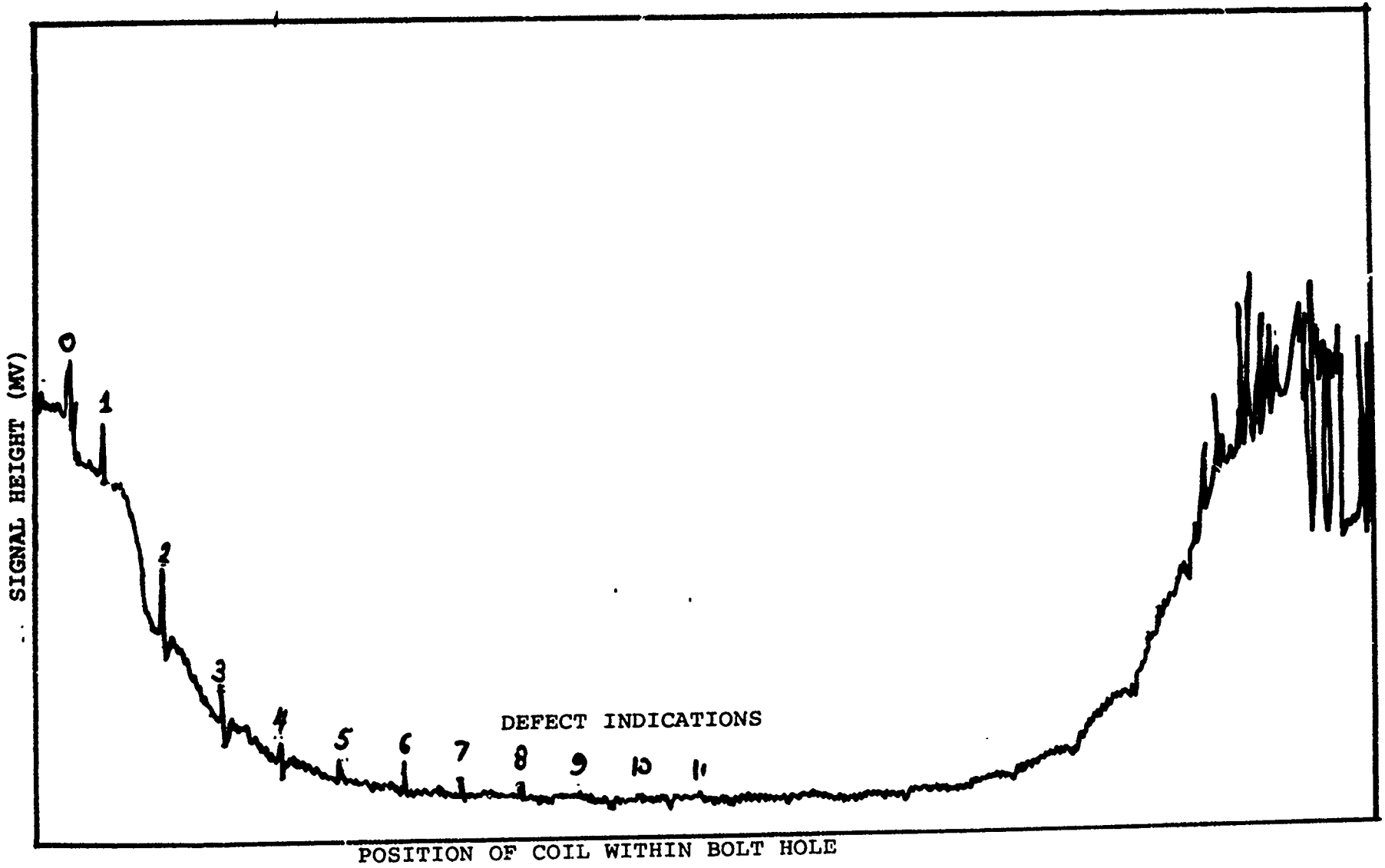

Figure 57

Eddy Current Scan AL82

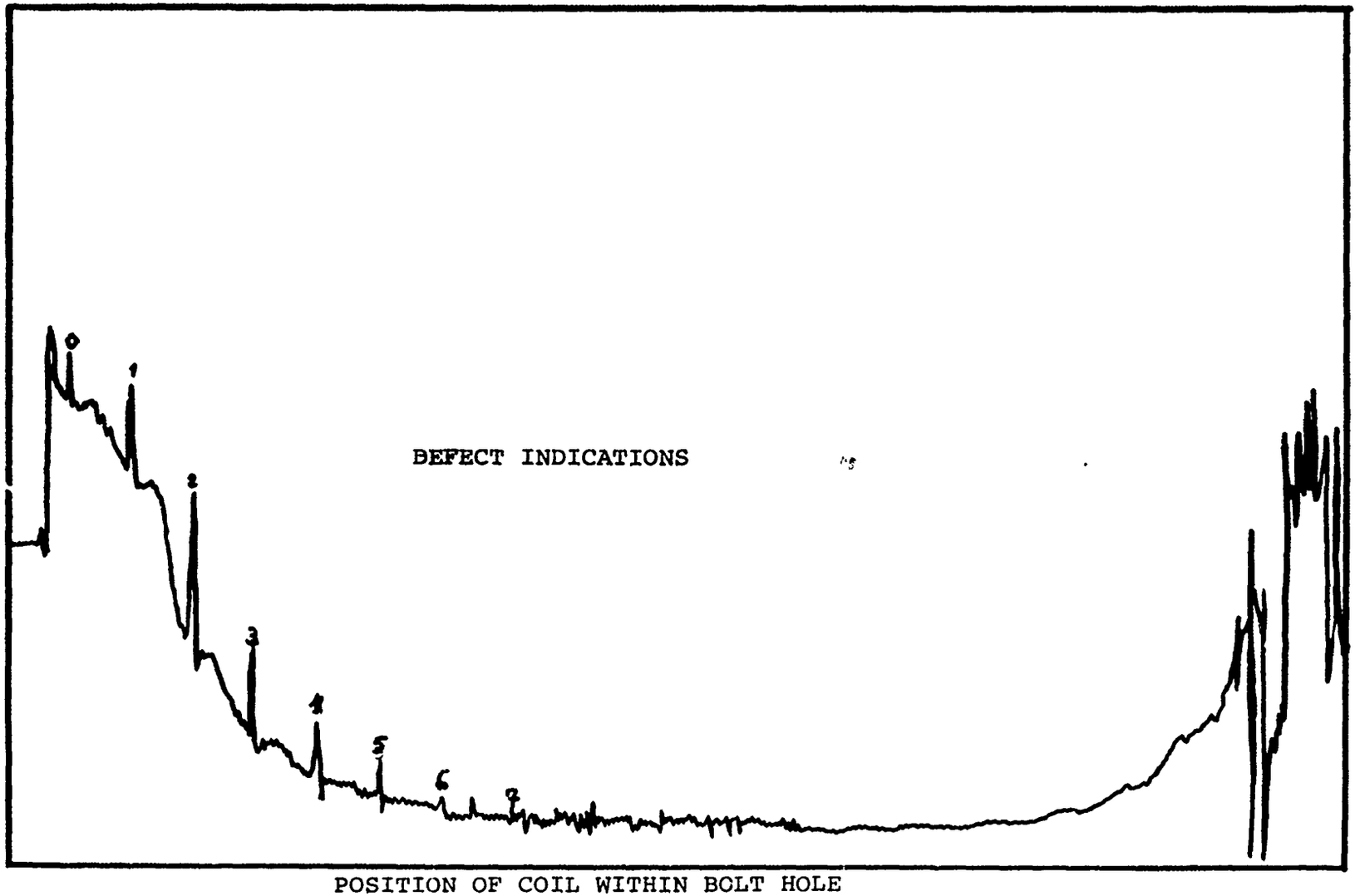

Figure 58

Eddy Current Scan AL83

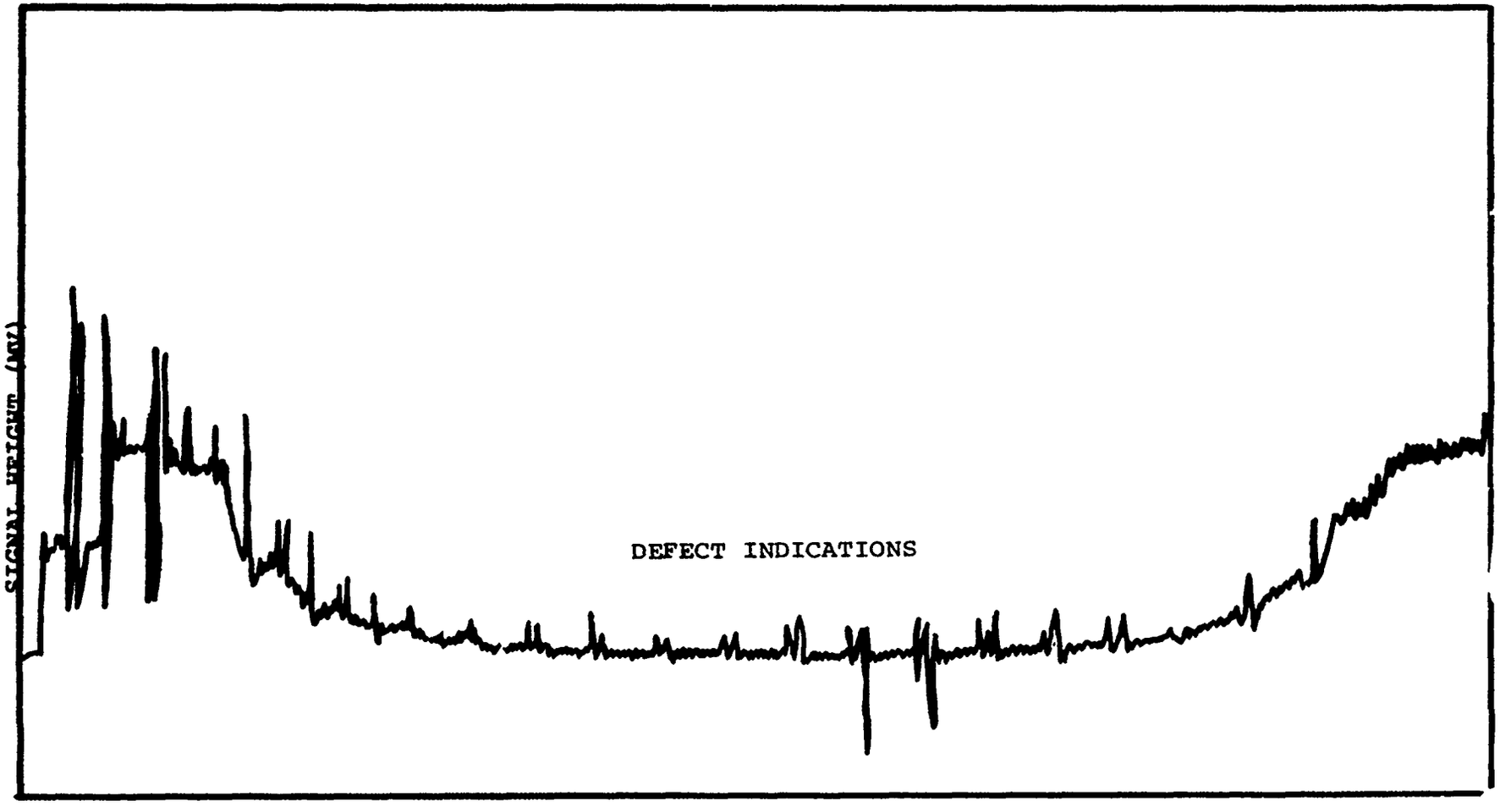

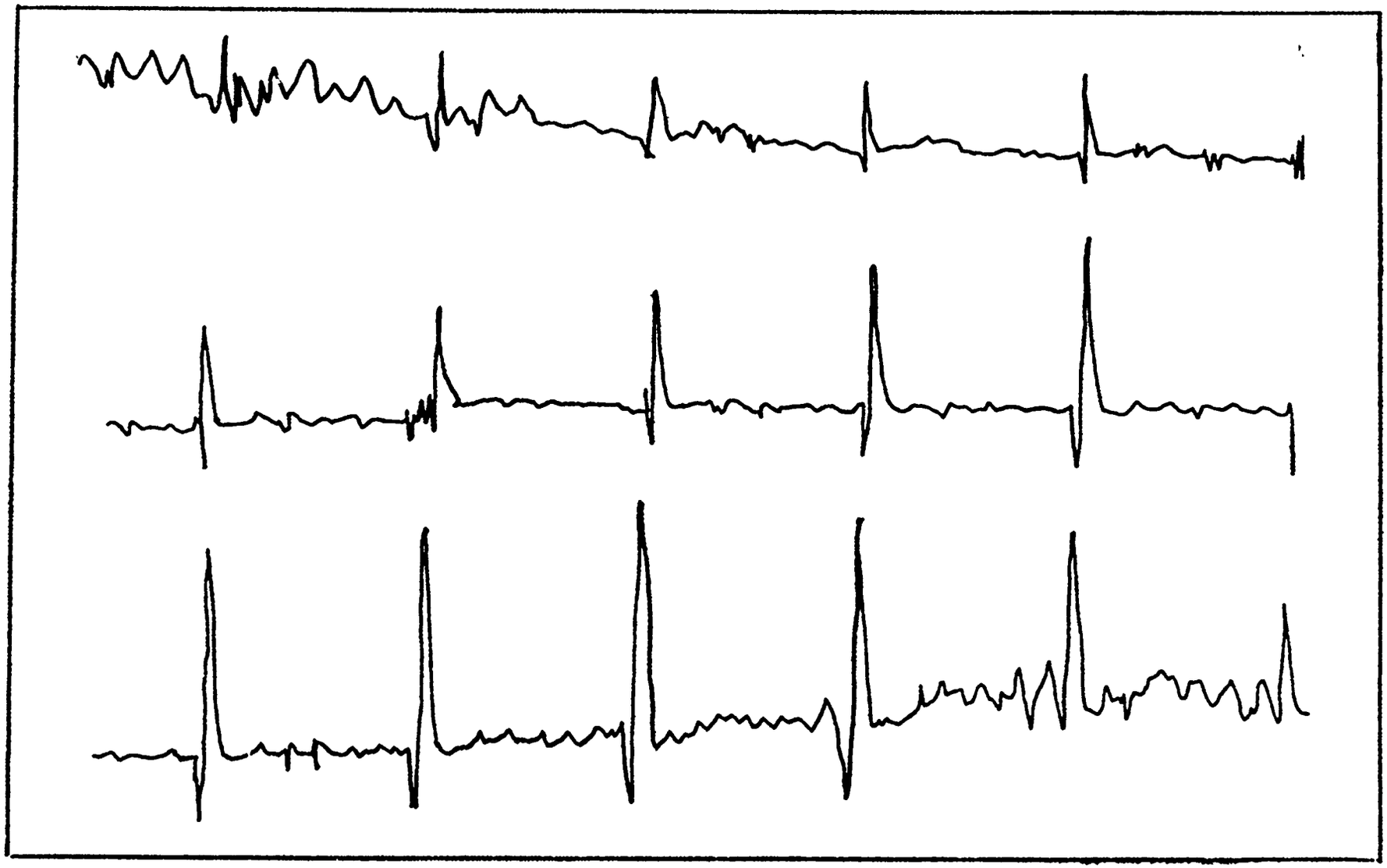

Figure 59 EDDY CURRENT SCAN

effects due to surface condition and lift off.

Figure 60 shows a reduced signal profile generated from a typical straight shank hole containing a constant depth elox slot of .037 inches.

Figure 61 shows the same typical output voltage as a function of position of the coil in the helical scan unit for a constant width, varying depth elox slot. In this figure the probe enters the specimen from the top surface. Peaks 1 through 5 show the effect of the top surface. The background noise initially increases and then decreases and the signal is initially very small, even though the crack is at its greatest depth on the near surface. Peaks 17 through 21 are the shallow portion of the crack, and here, too, the signals are small when the probe interacts with the back surface. The interior peaks all show a similar characteristic sharpness, with decreasing height as the depth of the slot decreases. Figure 13 shows another part through crack signal trace. In this case the crack does not progress completely through the back wall of the materials. This can readily be seen as peak 16 is the last observable peak and the other signals are noise indications associated with the far surface effect. The broad peaks observed in the far surface are the out of roundness of the far surface of the hole, produced by a misalignment of the hole on the back surface. This is typical of what might be expected with worn or eccentric reamers or produced in a hole that had been subjected to a tensile loading in a single direction

Figure 62 is a plot of voltage drop across the coil as a function of helical scan position for an internal part through crack. This defect is approximately 0.010 inches deep

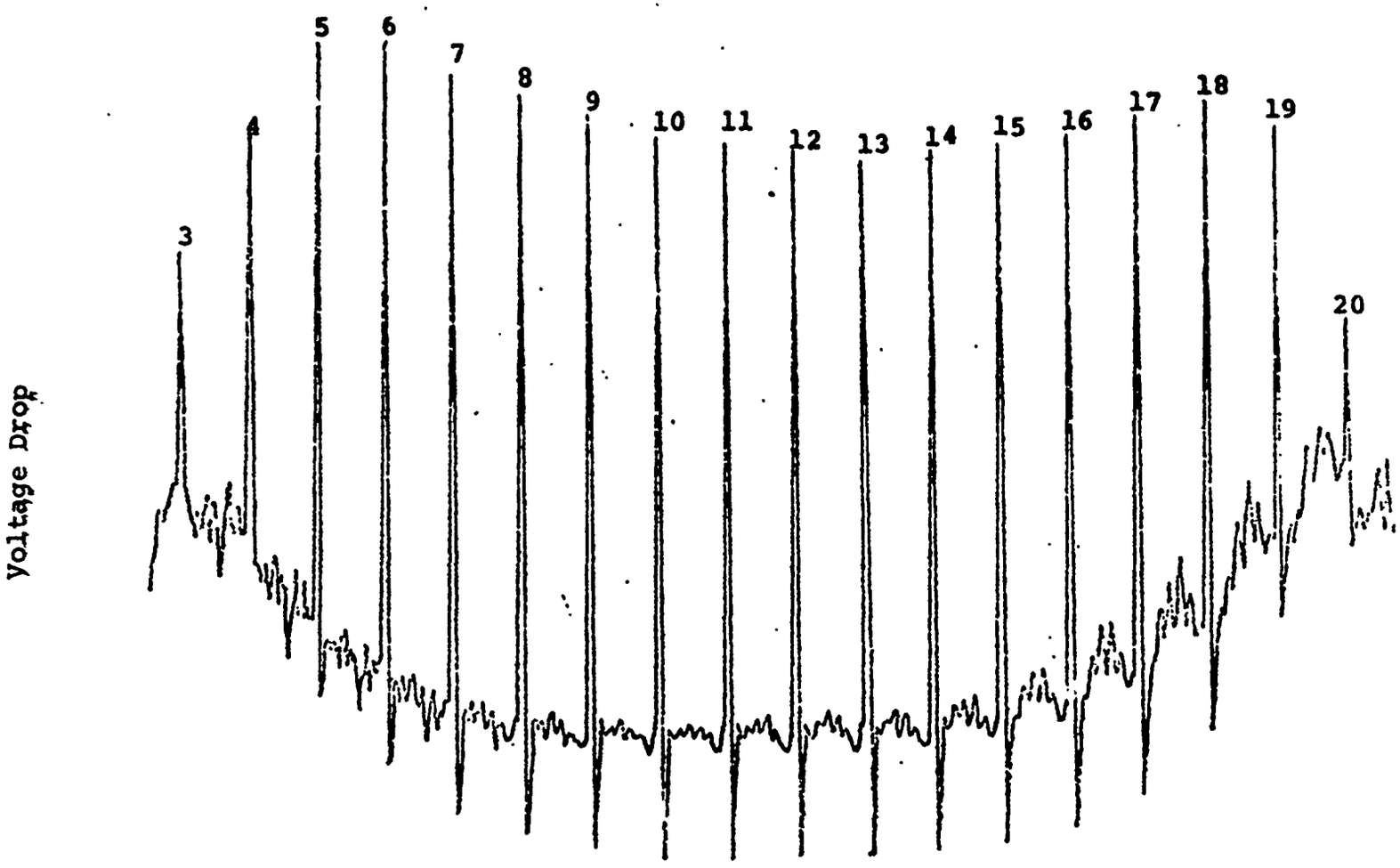

Figure 60

Signal Profile of Eddy Current Signals from
Straight Shank Hole with EDM Slot 0.037 Inches Deep

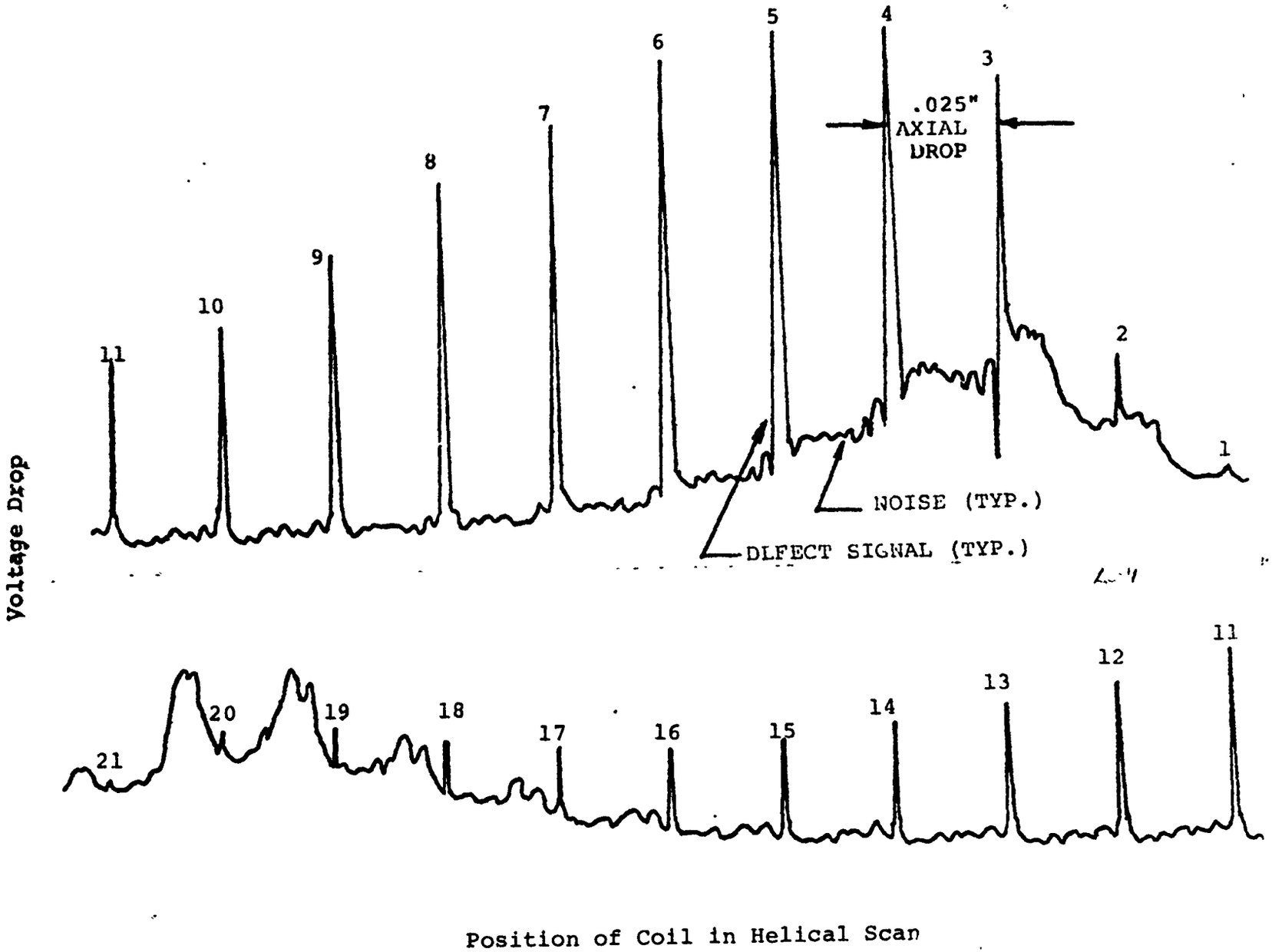

Figure 61 Signal Profile of Eddy Current Signals from Varying Depth EDM Slot

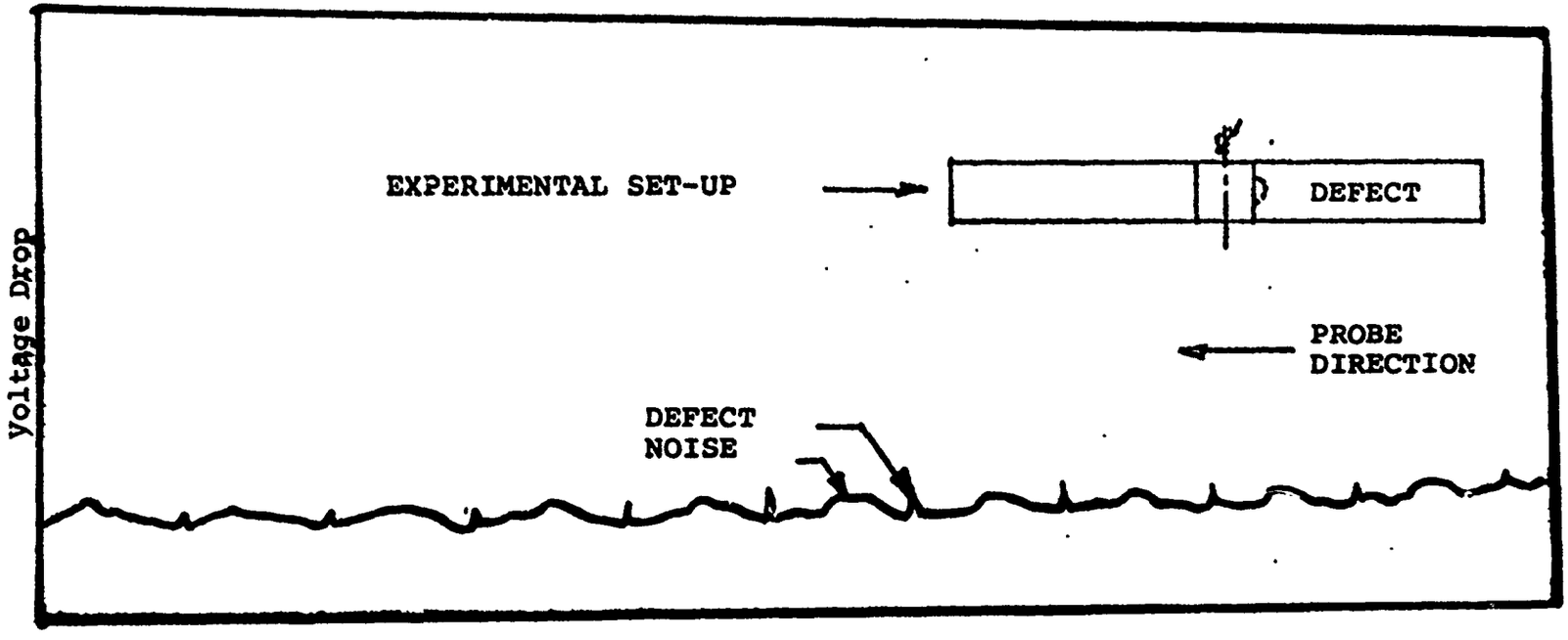

Figure 62

Signal Profile of Eddy Current Signals from Internal Defect

and less than 0.175 inches in length. The acutal length of the internal defect is not known as the specimen has not been fractured to measure the geometry on the fracture surfaces. Examination of the signal reveals that the small, sharp peaks are indicative of the crack like defect. The larger, broader peaks are due to out of round of the hole. This is assumed to be due to improper reaming of the hole. It should be noted that the out of round persists in the right hand portion of the scan, while there are no indications of a crack like defect in this portion.

Figure 63 shows a typical plot for a defect occurring within the interface of steel plates. On the right there is a defect 0.047 inches deep, on the left there is an additional defect in the lower plate 0.030 inches deep. As the scan passes the interface plate there is an abrupt transition due to the edge effect of the coil passing near the free surfaces of the specimen. As the coil centerline passes over the interface, there is a horizontal line indicative of the plate interface. The existance of an edge effect in this specimen is peculiar as the edge effects are normally considered due to the partial removal of the coil from the material as it enters the air. The normal edge effect is then due partially to the impedance and resistance changes of the material being investigated, i.e., slowly changing from steel to air. However, it appears that edge effects can be obtained even with extremely thin air interfaces as shown in the figure.

Direct Correlation of Signal Height

When one examines the signal outputs associated with the scans within the interior of the bolt hole probe, it is immediately

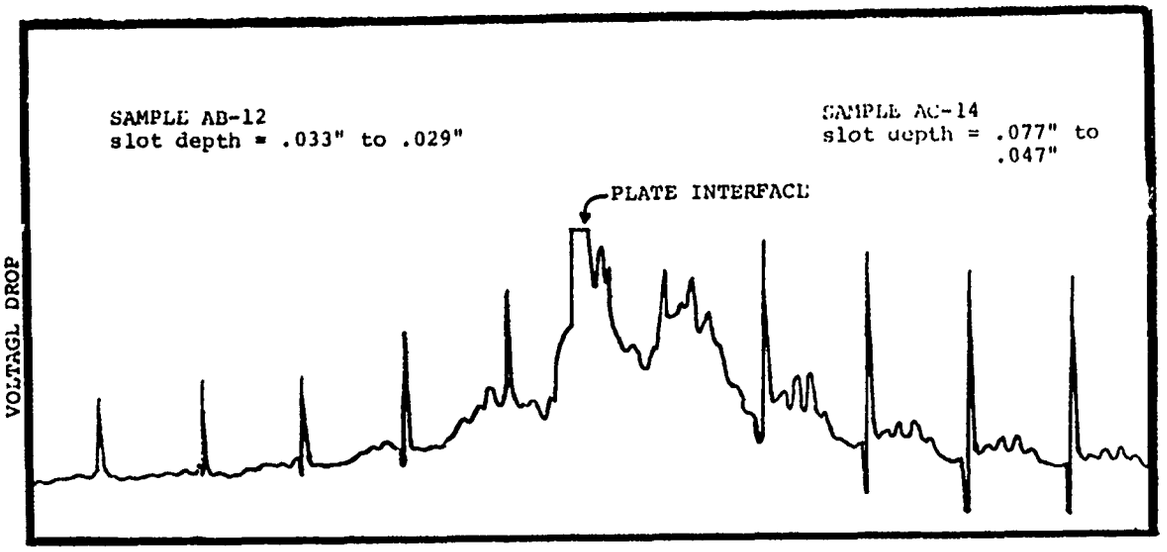

Figure 63

Eddy Current Scan Showing Plate Interface

Figure 64

PLOT OF SIGNAL PEAK HEIGHT VS

PERCENT DEPTH INTO 1/2IN PLATE

SPECIMEN AB-14

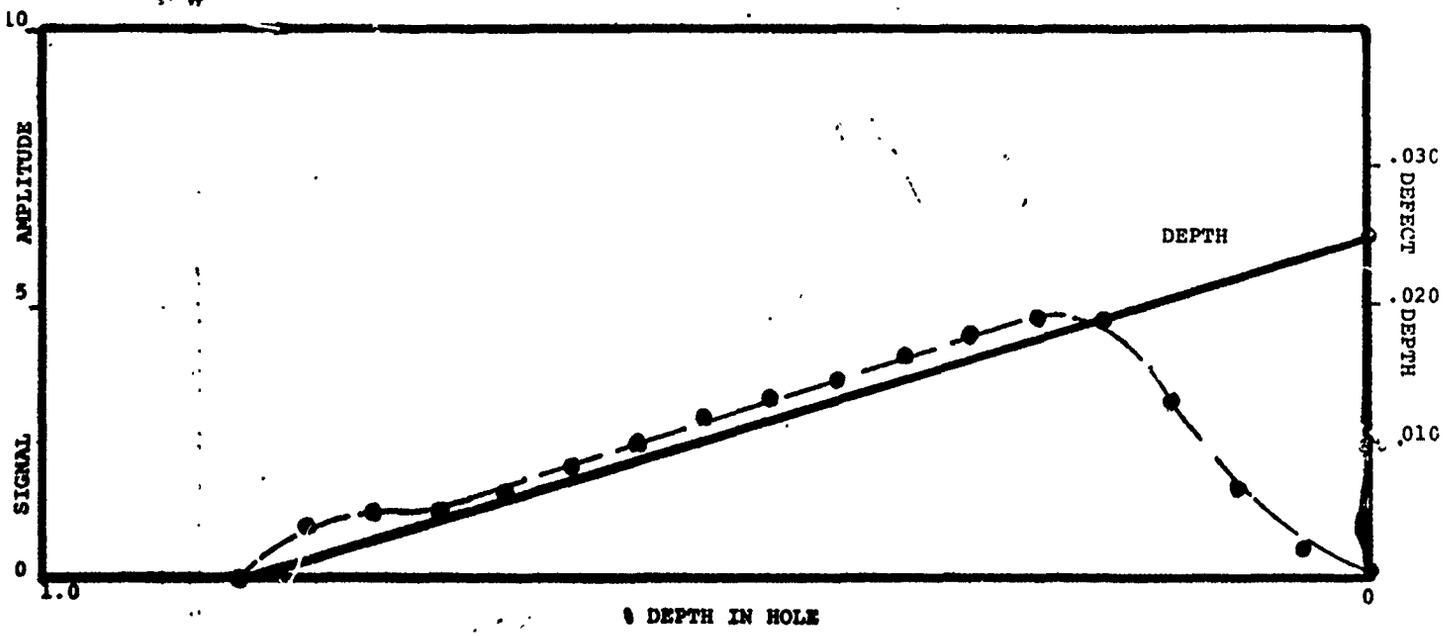

apparent that the large spikes correspond to linear defects within the bolt hole. The simple analysis is to compare the amplitude of the signals with the depth of the defect at that particular position within the bolt hole. This was initially discussed by Padilla and Parks,[27] who showed that quite accurate correlations between signal height and crack depth could be used to map the flaw geometry within a bolt hole in 7075 T651 Aluminum specimens.

Figure 64 plots the value of the mean-to-peak values for the defect indication as a function of the percent (%) depth within the bolt hole. The solid line is the calculated value of actual defect depth as obtained by measurements off of the specimen at the free edge and using the incline of the defect. It can be seen that the eddy current peak accurately measures the linear change in defect depth for about 70% of the defects linear length along the interior of the hole. Most noticeable is the edge effect at the surface of the specimen where the signal height rapidly decreases as the coil begins to interact with the free surface. Hence, the signal is rapidly decreased, even though the actual depth is about 0.025 inches. Also significant, is the slight edge effect observed as the depth of the defect approaches the interior surface of the bolt hole. Here the signal peak heights rise above the straight line portion of the curve.

If all of the data obtained from the linear portions of the peak-to-peak signals are plotted together, a calibration plot can be drawn as shown in Figure 65. The equation for the curve is given by:

$$Y = .15 + 182.8\ X$$

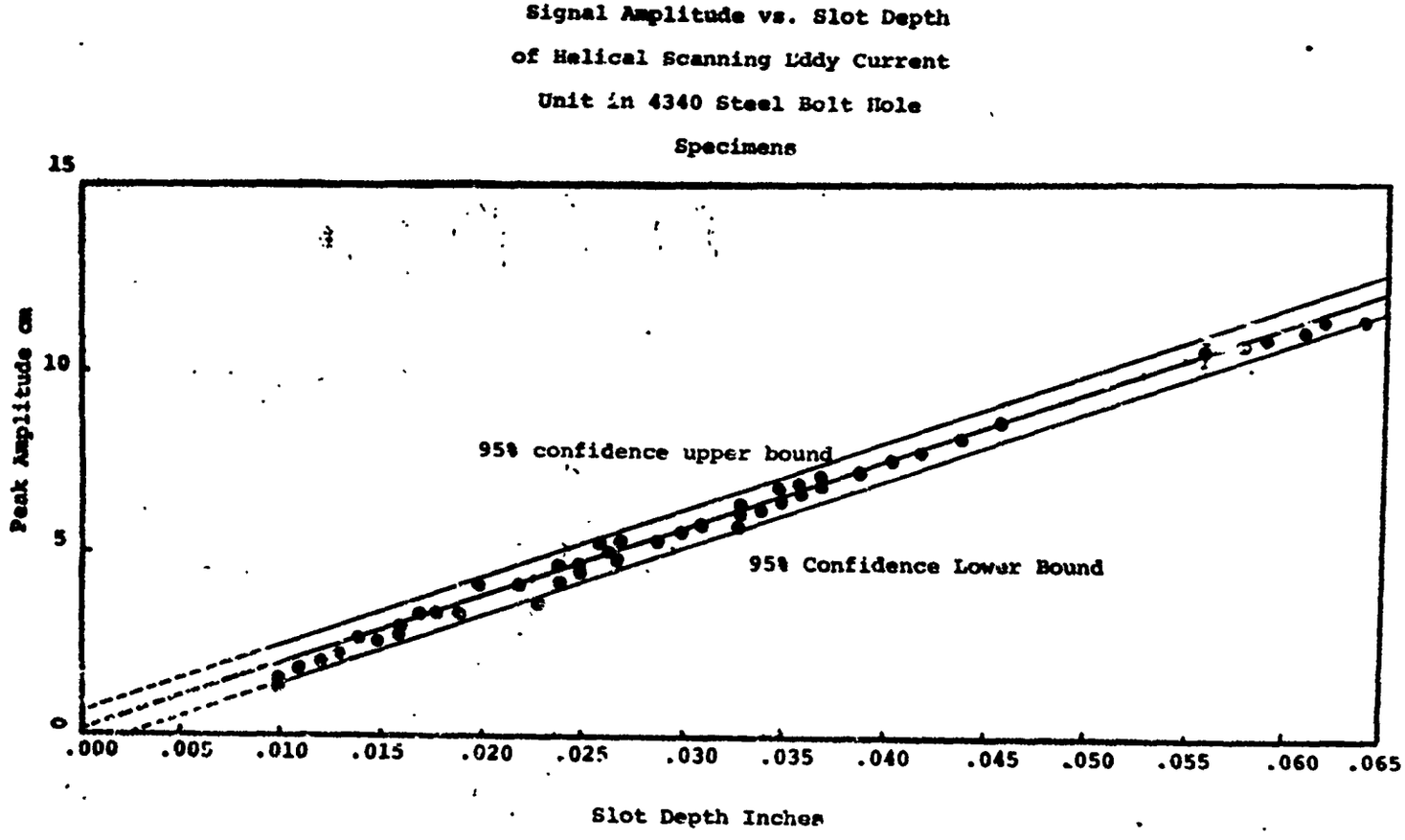
Signal Amplitude vs. Slot Depth
of Helical Scanning Eddy Current
Unit in 4340 Steel Bolt Hole
Specimens
15
10
5
0
Peak Amplitude cm
95% confidence upper bound
95% Confidence Lower Bound
.000
.005
.010
.015
.020
.025
.030
.035
.040
.045
.050
.055
.060
.065
Slot Depth Inches

Figure 65

Where Y is the peak-to-peak amplitude for the eddy current signal and X is the actual depth of the defect in inches.

The ± 95% confidence limits have also been drawn in Figure 65. This plots the deviations from the straight line that would be expected using the mean values of each reading for depth. Thus, one would expect with a 95% confidence level that given a peak amplitude of say, 5.0, the actual defect depth would lie within a range of 0.024 to 0.030 inches in depth. This requires that the signal height be adjusted by calibrating with a known depth of defect to obtain a standardized signal. Otherwise it is apparent that any desired signal peak-to-peak height could be obtained by changing the gain on the amplification for the Y coordinate.

Following Saddler[26], one can define the minimum sensitivity or minimum flaw depth that would be expected to be detected as follows: consider the standard deviation of the calibration curve of Figure 65, the value of the x intercept for the lower bound 95% confidence line indicated that there is a 5% probability of a flaw of 0.0025 inches deep existing within the specimen without obtaining a recognizable peak-to-peak signal. This means that a signal height of zero would be obtained with a defect 0.0025 inches deep at least 5% of the time. Hence, at a 95% level, a defect of 0.0025 inches deep could exist and not be distinguishable from the inherent electronic background noise.

Thus, given a known defect depth, upon which initially calibrated the system, a reasonable good approximation of the depth of the defect can be determined using Figure 65. It

should be emphasized however, that the calibration curve was obtained using EDM slots, and not fatigue cracks, and hence, if the system cannot distinguish between slots and fatigue cracks, the actual depth measurements can be in considerable error.

Transfer Analysis of Eddy Current Signals

The identification and categorization of the signals associated with different types of defects when scanned by the eddy current system are accomplished by a transfer function analysis of the particular defect signal. When one considers the integral transform f(p) of a function f(x) to be defined by the integral.[28]

$$f(p) = \int_b^a f(x)K(p,x)dx$$

Where K(p,x) is a known function of p and x is called the kernel of the transform. In this analysis, we use the complex Fourier transform defined by:

$$\int_a^b f(x)e^{ipx}dx = f(p)$$

The transform sets up a correspondence between the functions f(x) on the interval 0 x n and sequences of numbers n = 1, 2, 3...n.

Data taken in the time domain, from the peak-to-peak versus time eddy current scan unit is related to the frequency domain through the transform equations. This can be accomplished either by using a frequency analyzer or by direct integration. In this analysis, the integration was accomplished directly by digitizing portions of the input function f(x) and performing the Fourier transform directly on each digitized interval.

Suppose we are given a number N_Z(max) sample value of a

digitized eddy current signal. The calculation of its Fourier transform will give the frequency content or power spectrum of the given signal, or segment of the signal. The sample values are assumed to be zero outside of the range 0 to $N_Z(max)-1$. In this sense the Fourier transform is a finite transform and deals only with the finite record of the signal.

The calculations for the transform cannot be made for all frequencies w, but only at some finite set. It is convenient to choose the set of $N_X(max)$ frequencies given by:

$$w_K = K2\pi/N_X(max) \quad K = 0, 1, 2 \ldots N_X(max)-1$$

These correspond to values of K given by:

$$K = ejk2\pi/N_X \qquad K = 0 \ldots N_X-1$$

And the transform,

$$f(p) = \sum_{n=0}^{n=NZ\ max-1} F(n)e^{-jK2} \quad /N_X(max)$$

In this program analysis we have chosen N_Z and N_X to be possibly different from each other. This precludes the possibility of performing an inverse discrete Fourier transform which would be facilitated by making $N_Z = N_X$. However, for the sensitivity of the system used, it appears reasonable to allow the two values of sampling and frequency change to be different from each other.

After the power spectrum has been obtained for each pulse, both the input pulse and output pulse (obtained separately) the two spectrums are divided by each other. Hence, the transfer function is obtained at each value of w_K. This is to facilitate

the obtaining of the Fourier transfer function, Hence:

$$Tr(w_K) = f(p,w_K) \text{ OUTPUT}/f(p,w_K) \text{ INPUT}$$

The absolute magnitude of the transfer function is plotted as a function of the frequency as shown in Figure 66. If there were no defect present the transfer function would have a constant magnitude of unity. This means that there is simply a constant that relates the input function to the output, i.e. a simple scale change. When the defect is present, since the magnitude of the input function remains constant (since it is assumed to be a dummy input) the magnitude of the transfer represents changes due to changes in the OUTPUT function. The form of the output function then determines the location of the high spikes on the Tr(s) vs frequency curve. If there are a large number of peaks, this implies that the defect width is large, since the transform for a broad unit pulse would produce a large number of closely spaced peaks in frequency space. This is shown in Figure 65 for the transfer function of a wide EDM slot. If however, the transfer function exhibits only one or two spikes, this implies that the impulse producing the curve that is transformed is extremely narrow and tight. This would obviously be that of a crack, Figure 67.

The influence of the width of the pulse on the number of spikes in the transform is shown by comparing the power spectrum of a narrow pulse with that of a broad pulse, as is shown in Figure 68. The expression for the Fourier Spectrum for a square pulse of amplitude A and length T gives:

Figure 66

Transfer Function vs Frequency for EDM Slot

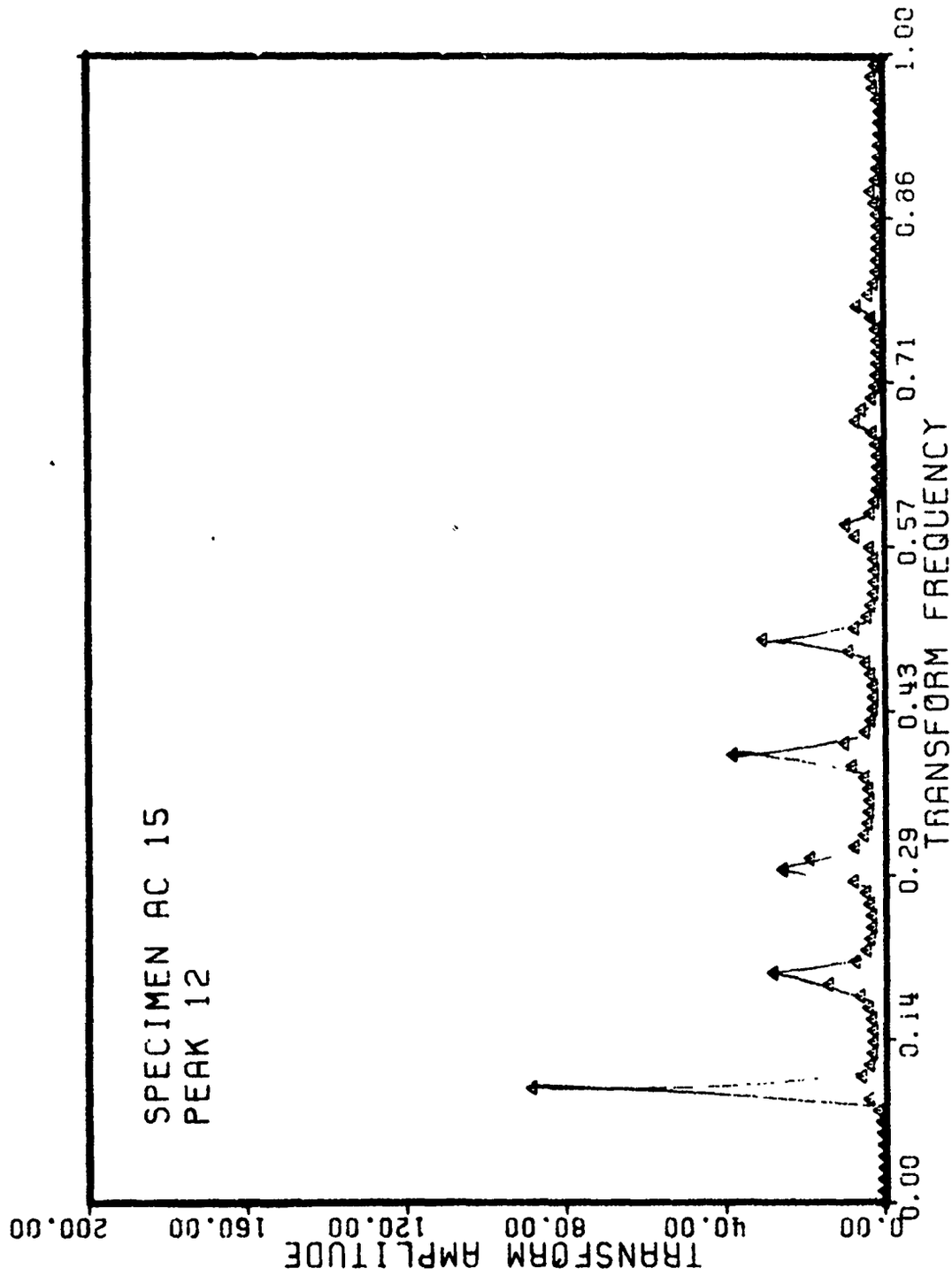

Figure 67

Transfer Function vs Frequency for Fatigue Crack

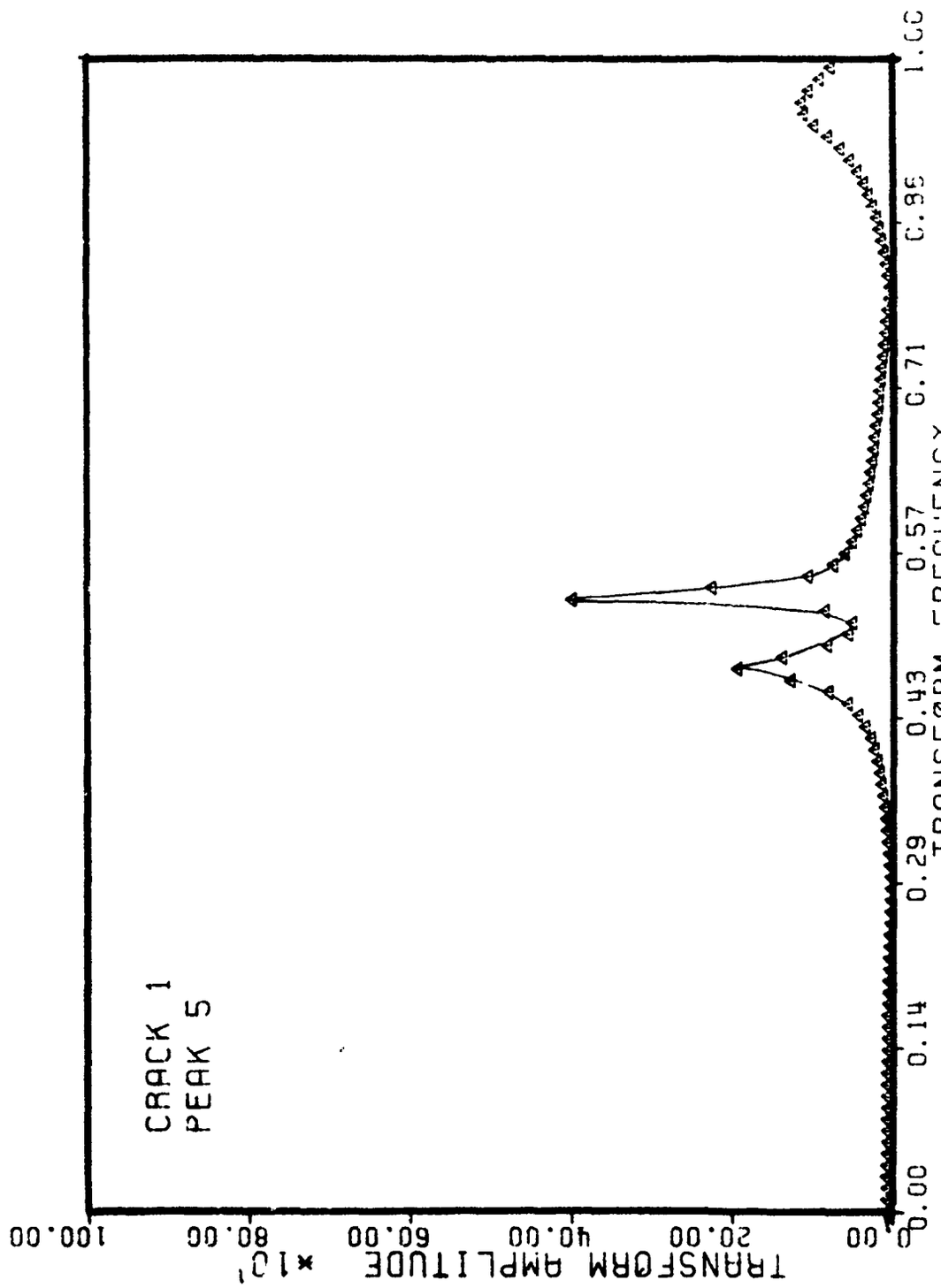

$$F(p) = \sum_{-T/2}^{+T/2} Ae^{-2\pi jip(t)}$$

or

$$\left| F(p) \right| = AT \left| \frac{\sin \pi pt}{\pi pt} \right|$$

The transfer function for this square pulse is shown in Figure 69 for peaks of two different widths. Since at the positions where the power spectrum approaches zero, the transfer function peaks, one can see that the narrow impulse will only produce one or two spikes while the wide pulse will produce many more peaks.

The Fourier transform of the actual peaks measured by the eddy current bolt hole scan are not as simple as the unit pulse peaks, since they do not have amplitudes of zero at the beginning and end of the defect pulse. A typical power spectrum of a defect is shown in Figure 70, which shows that there are particular frequencies for which the amplitudes are a minimum, but not zero as with the square pulses. Thus, it is believed that the Fourier transfer analysis measures the equivalent width of the defect as interpreted by the scan coil, and would change with different coils. This is not unreasonable, as in normal eddy current testing, the characteristics of the coil greatly influence the ability of the eddy current unit to detect, rather than measure the defect.

However, it is apparent that the transfer function approach is useful in characterizing the apparent defect width, and thus, can distinguish between wide defects and crack like defects.

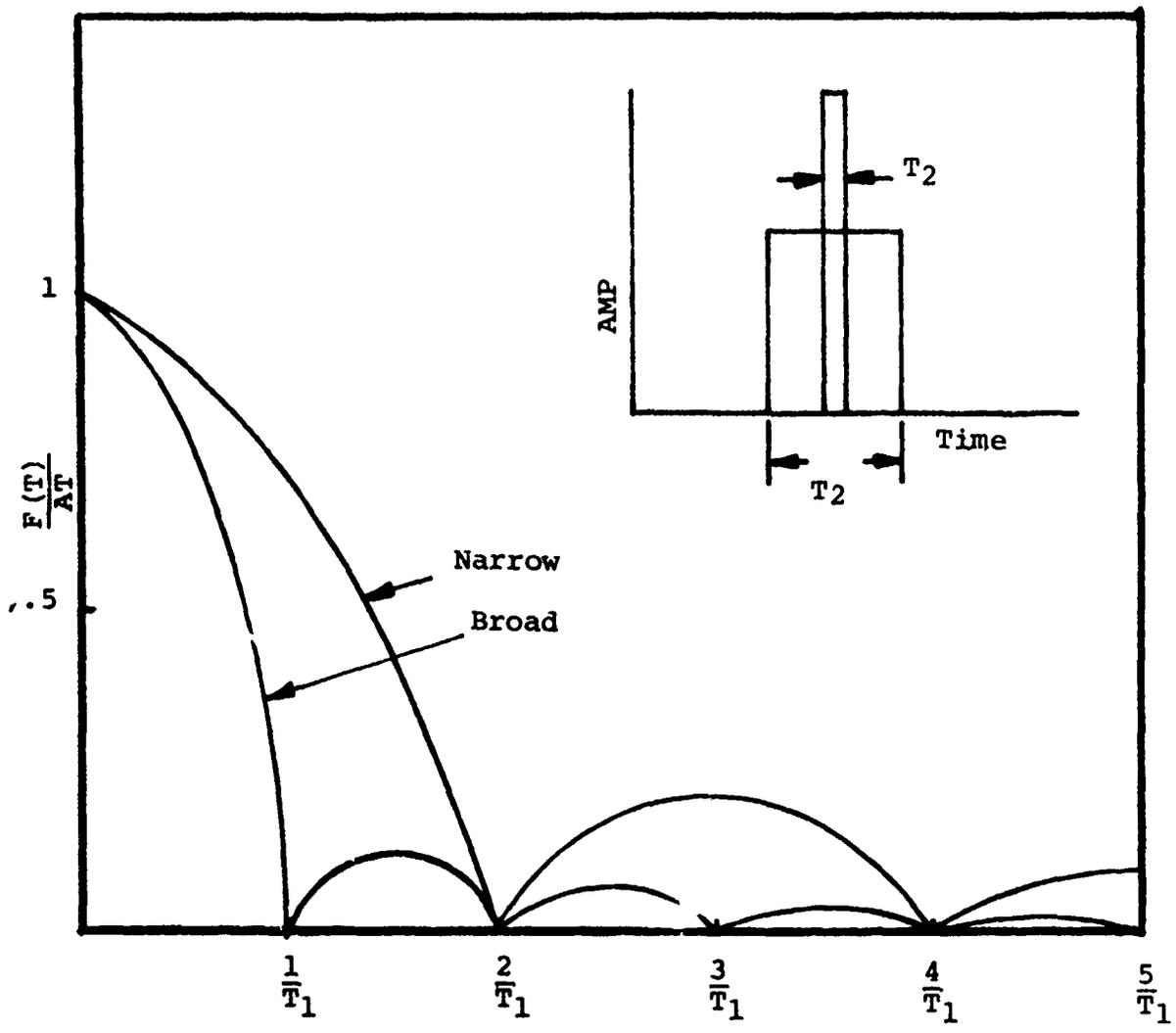

Figure 68

Power Spectrum for Narrow Pulse and Broad Pulse

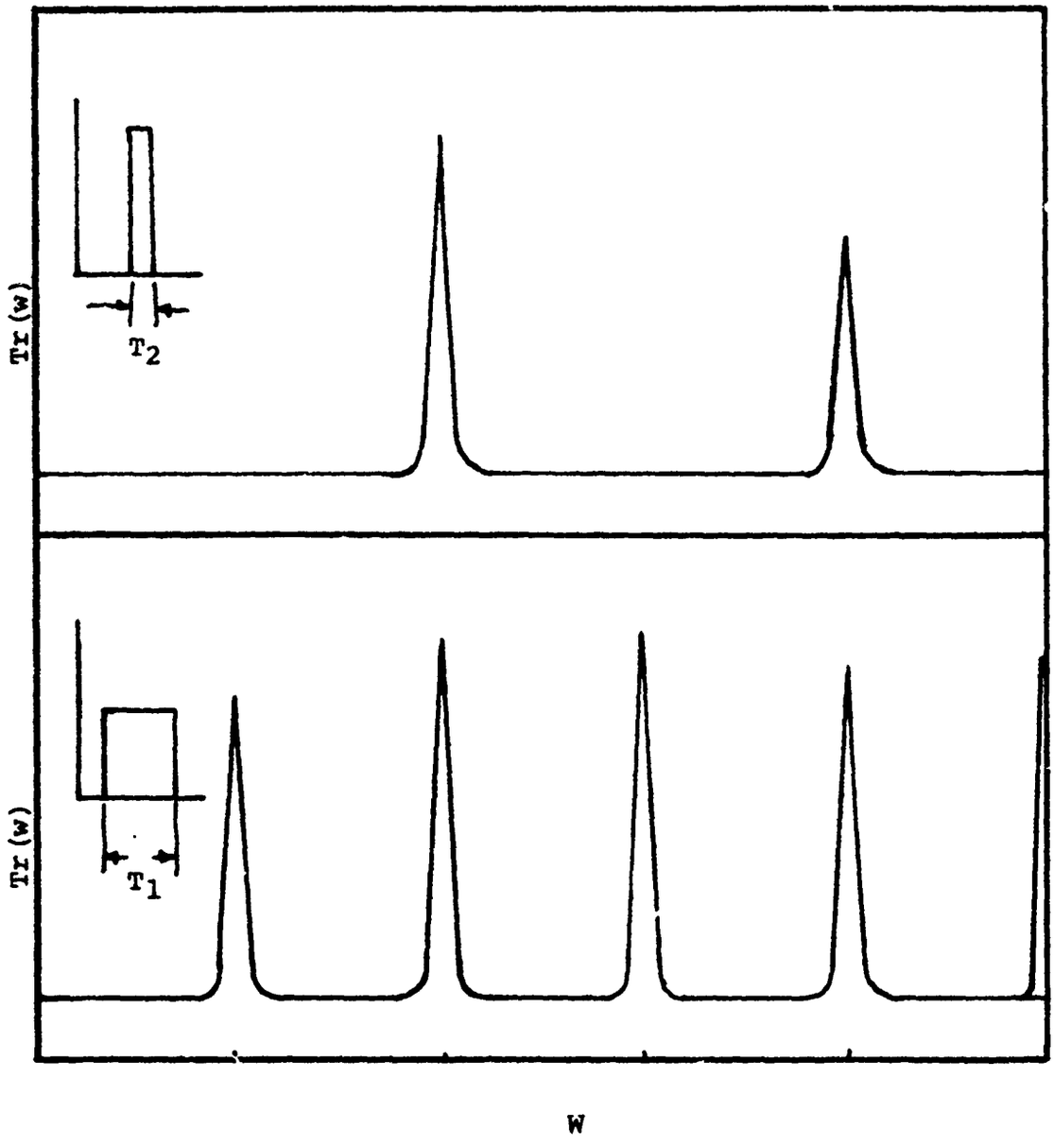

Figure 69

Transfer Function for Square Pulse

Figure 70

Power Spectrum for Eddy Current Signal of Defect

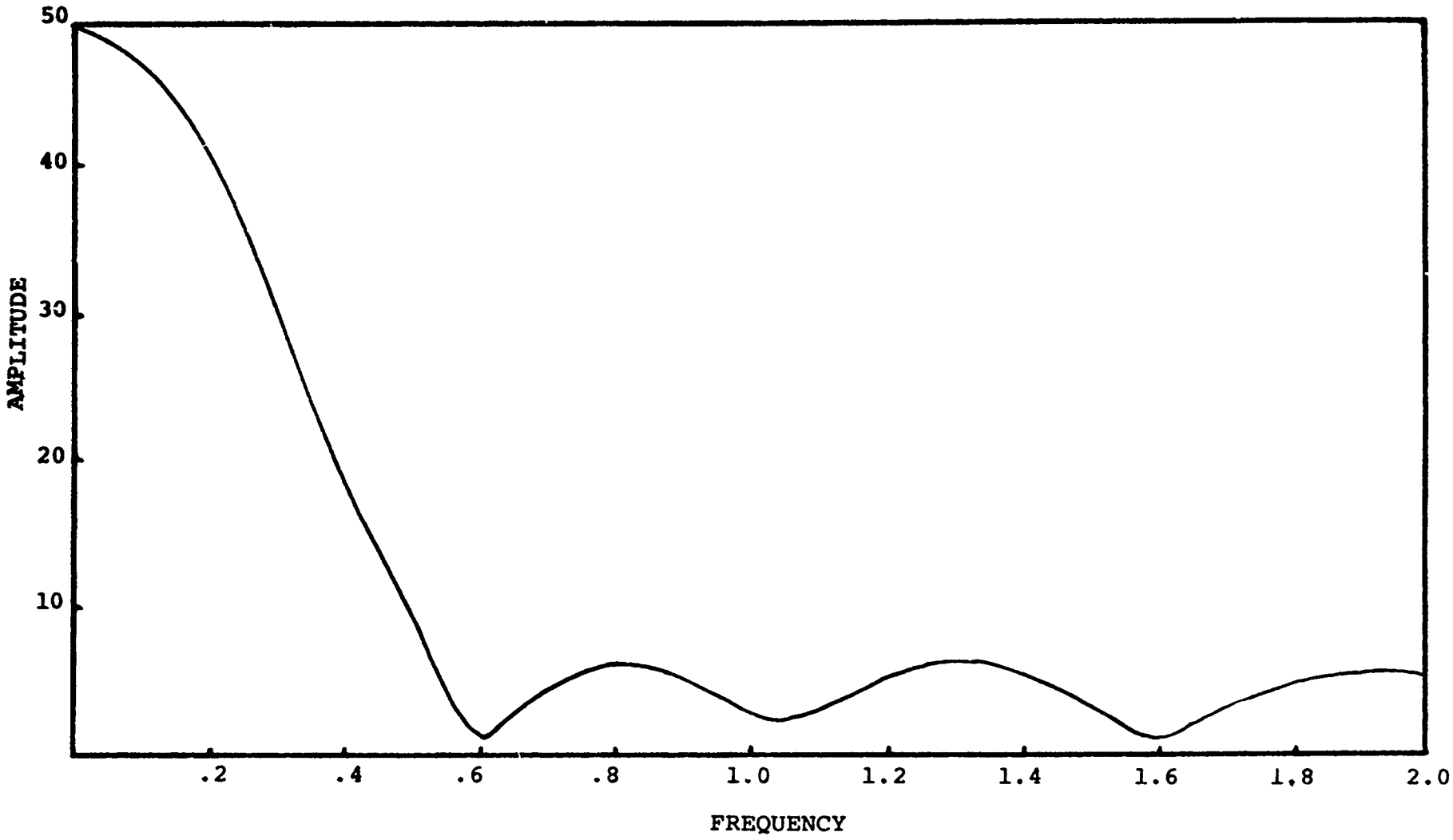

SECTION VIII

SUMMARY

Summary

The ability of ultrasonics and eddy current bolt hole probes to locate, measure and characterize the defects associated with fastener holes has been examined and shown to be of merit. At the present time it is not possible to reliably determine the size and shape of the defect, but it is very possible to determine the presence of the defect when the length of the defect is 0.030 inches or greater. These are estimates based on the measurement of fatigue like flaws eminating from fastener holes, when EDM slots or other artificial flaws are used, the potential for much smaller defect detection is increased.

It has been demonstrated that the major factors influencing the inability of ultrasonics to measure the criticality of the defect, once the defect has been found, are associated with the stress field and morphology of the crack, and not the metallurgical factors for the material. It should be recognized that metallurgical features become significant in reducing or otherwise influencing the detectability and characterization only in the vicinity of welds or diffusion bonded areas where gross attenuation-grain size changes may occur or where abrupt metallurgical phase transitions would produce erroneous reflections.

The factors that influence the measurement of criticality for ultrasonics are: stress state, prior history, loading

sequence, presence of corrosion, presence of foreign material particularly moisture. It has been shown that measurements of flaw size from the maximum amplitude reflection can be seriously in error, as the maximum reflection can increase several fold by an application of external stress opening the crack. Corrosion significantly increased the amplitude of the reflected signals from fatigue cracks, but did not influence the signals from EDM slots. This would be expected only if the amount of ultrasonic reflection from a fatigue crack was strongly influenced by the tightness and surface condition of the crack. Hence, it is strongly felt that callibration of ultrasonic response from EDM notches or flat bottom holes, while simple to perform and relatively easy to repeat, bears little actual relationship to the actual problem of characterizing tight defects.

When the presence of the defect is in the vicinity of a cutout which would be a much stronger reflector for the ultrasonic energy, such as a crack in the vicinity of the fastener hole, the identification of the defect becomes even more difficult. There are two ways that this identification problem can be solved: first to develop a complex scan unit such as the tangential scan unit developed by Boeing et all, which scans the hole with the ultrasonic beam "skimming" tangential to the larger bolt hole reflector, and second, develop a technique that identifies the presence of the defect within the greater refelcted signal of the bolt hole. The second technique was the one adopted for this program, and has been shown to be extremely effective in identifying the presence of the defect

within the bolt hole area.

The successful technique utilized the concept of the indicium, which is a measure of the total reflected signal associated with both the bolt hole reflector and the defect reflector. The indicia has been developed and discussed in detail for its role in identifying the orientation, size and position of the defect. It is seen that while the indicia suffers from the same problem as do all ultrasonic reflection techniques, i.e.major changes in reflection due to slight changes in applied stress, it holds promise for more, detailed characterization of the defect than do single maximum peak identification techniques. The indicium when combined with the transfer function concept proves itself to be as sensitive, if not more sensitive than other bolt hole inspection techniques, with the added factor that the experimental setup is extremely simple and almost identical with the standard practice for inspection of bolt holes.

The transfer function concept utilizes the Laplace or Fourier transform of the output signal from the indicia, and when the output transform is divided by a known input transform (normally an unflawed specimen or a Dirac input) greatly magnifies the differences in indicium. These differences are then related to the presence of the defect. It has been shown that the presence of a 0.030 inch defect within the 0.5 inch diameter bolt hole can be detected with a minimum of two scans. This defect is of a fatigue type crack. When EDM slots are used, defects on the order of 0.020" in length can be detected.

An additional technique exploted in the program was that of eddy current bolt hole probes. Because of the nature of the program, a simple unique design for a self calibrating helical scan unit was constructed as the first portion of this program. This unit measures the impedance changes associated with a differential eddy current coil operating at 4 Mhz within the bolt hole. These changes are recorded on a x-y strip chart record which then can be used to characterize the type of defect present. It is shown that EDM slots can use the maximum peak-to-peak signal height as a measure of the depth of the EDM slot, but again it is doubtful if such a simple technique can be applied to fatigue cracks. A parallel study showed that fatigue cracks in the bolt hole produce significantly smaller pertubations within the bolt hole scan, but these, too, can be readily identified as to their presence or absence.

When a simple Fourier analysis is performed on the specific defect signals, it has been shown that the type of defect can easily be characterized as to type. Wide defects such as EDM slots produce significantly different transfer plots than those of tight fatigue cracks. Thus, once the presence of the defect has been verified, the type of defect within the bolt hole can easily be characterized as to type.

SECTION IX

REFERENCES

1. Coffin, L., and Tiffany, C.F., AIAA Paper 175-781, 1974.

2. Mil Standard 1530, Aircraft Structural Integrity Program S-83444 Damage Tolerance Requirements.

3. Packman, P.F., Pearson, H.S., Young, G., NDT Definition of Fatigue Cracks, Journal of Materials (1972) p. 666.

4. Betz, C.E., Principles of Penetrants, Magnaflux Corp.

5. Proceedings of the Interdisciplinary Workshop on Nondestructive Testing-Materials Characterization AFML-TR 74-69.

6. Raatz, C.F., Senske, R.A. and Woodmansee, W.E., Detection of Cracks Under Installed Fasteners, AFML-TR 74-80.

7. Proceedings-Fourth Scientific Conference on Ultrasonic Defectoscopy of Welded Joints, Defectoskopia, Nov,Dec. (1970).

8. Krautkramer, J., and Krautkramer, H., Ultrasonic Testing of Materials, Springer Verlag, N.Y., 1969.

9. Yee, B.G.E., Influence of Stress on Ultrasonic Shear Wave Detection of Cracks-To be published.

10. Elber, W., Engineering Fracture Mechanics Vol. 2 (1970, p. 37.

11. Corbley, D.M. and Packman, P.F., The Effect of Single and Multiple Peak Overloads on Fatigue Crack Propagation in 7075-T6 Aluminum, International Journal of Fracture, Jan. 1973.

12. Hertzberg, R.W. and VanEuw., E.F., Met. Transactions Vol. 4 (1973) 887.

13. Corbley, D.M., Grandt, A. and Starke, E., Paper Presented at ASTM Conference on Fatigue Load Interaction, Toronto (1974) to be published as STP.

14. Giacomo, G.P., Crisci, J.R. and Goldspiel, S., Materials Evaluation, Sept.(1971) p. 189.

15. Gurvich, A.K., Ermolov, I.N., Ultrasonic Flaw Detection of Joint Welding, Kiev, 1972.

16. Throop, J.F., Crack Resistance in Thick Walled Cylinders, in Symposium on Relevence of Fracture Toughness to the Design and Reliability of Military Equipment, June 1973.

REFERENCES (Continued)

17. Clements, W.C., Schnelle, K.B., Mathematical Modeling of Dynamic Systems with Applications to Non-ideal Systems, Rept. 24. EWRE, Vanderbilt, Aug. 1969.

18. DiStefano, J.J., Stubberud, A.R., Williams, I.J., Theory and Problems of Beedback and Control Systems, McGraw Hill, 1967.

19. Libby, Materials Evaluation, 14(Dec. 1956) p.12.

20. McClung, G.O., Materials Evaluation 15(Ap. 57) p. 116.

21. Waldelich, D.L., Materials Evaluation, 27(Dec. 1970) p. 262.

22. Libby, H.S. and Cox, C.W., "Broad Band Electromagnetic Testing Methods, P.2" Geco Rept. HW 67639 (1961).

23. Robinson, B.H., Materials Evaluation, Vol. 16 (Jan. 58), p. 36.

24. Reynolds, P.M., BNF Metals Technology Centre.

25. Lloyd, E.A., An Eddy Current Instrument for Surface Inspection of Copper Housing Tubes. BNF-Rept. A1565, Sept. 1965.

26. Saddler, S., Sensitivity of Several NDT Methods AFML-TR-70, (1970).

27. Padilla, V.E. and Parks, T.W., Definition of Fatigue Crack Geometry by Eddy Current Techniques, McDonell Aircraft Rept. 1971 also, ASNT Symposium (1969).

28. Turner, C.J., "Integral Transforms in Mathematical Physics", Chapman and Hall Lt'd (1971) London.

TABLE I

DIMENSIONS OF PART THROUGH CRACKS
IN ALUMINUM FLAT PLATES

Spec #	Surface Length	Ult. Ref. Signal Height A	Ult. Ref. Signal Height RA
A66	.0438	2.0	2.0
A341	.0506	2.4	2.7
A15	.0683	2.9	3.0
A41	.0718	2.5	2.4
A46	.0834	3.0	2.8
A62	.0881	2.5	1.9
A68	.0890	3.0	2.8
A79	.0908	3.4	4.0
A20(1)	.0959	1.5	2.2
A13	.0978	2.1	3.4
A45	.0987	1.4	3.7
A12	.1045	4.2	4.2
A22(1)	.1051	2.0	2.8
A30	.1097	4.4	4.8
A50	.1126	4.4	3.8
A58	.1149	4.3	3.2
A35(1)	.1254	2.9	2.6
A39	.1345	4.8	2.7
A78	.1526	4.8	2.7
A55	.1552	4.8	4.2
A17(1)	.1560	1.0	2.8
A74	.1621	4.8	3.8
A64	.1756	5.5(2)	3.6

TABLE I (con't)

A75[1]	.3224	2.2
A78	.1045	4.2
A79	.1215	4.6
A84	.1237	4.7

(1) Additional Stresses at $R > 0$. All others fatigued $R \approx 0$

(2) Change in Sensitivity Reduced by Calibration Curve.

TABLE II

D6AC AND Ti6Al-4V SPECIMENS
WITH PTC CRACKS

Flaw Size	Cum. Obs.	Cum. Miss.	Flaw Size	Cum. Obs.	Cum. Miss.
.008	429	14	.0541	312	0
*.0105	426	11	.0550	295	0
.013	4212	8	*.2620	276	0
*.014	419	8	.0669	257	0
.015	416	8	.067	251	0
*.017	413	7	.0673	246	0
*.019	410	7	*.0700	230	0
.021	407	6	.0782	214	0
.0227	401	5	.0802	196	0
.023	398	4	.0906	180	0
.025	394	3	*.0922	164	0
.0269	358	3	.1113	149	0
.0276	384	3	.1127	134	0
.029	381	3	.1138	120	0
**.0307	378	]	.1240	101	0
.032	372	1	*.1299	93	0
*.033	368	0	**.1325	81	0
.035	364	0	.1844	73	0
.0358	357	0	.2054	62	0
.037	355	0	.2151	47	0
.0428	340	0	.2182	38	0
*.043	346	0	.2450	26	0
.047	339	0	.2500	14	0
.048	322	0			

TABLE II (con't)

Flaw Size	Cum. Obs.	Cum. Miss.	Flaw Size	Cum. Obs.	Cum. Miss.
.0497	315	0			
.0323	215	12	.1699	44	2
.0409	210	9	*.1809	33	0
.0433	203	8	.1837	24	0
*.0648	195	6	.1844	16	0
.0650	191	5	*.2265	8	0
.0716	187	5			
.0789	177	2			
.0801	171	2			
*.0840	167	2			
.0862	166	2			
.0877	156	2			
.0878	151	2			
.0886	145	2			
*.0890	140	2			
.0894	132	2			
.0926	128	2			
.0946	124	2			
*.0990	119	2			
.1000	111	2			
.1014	109	2			
.1092	105	2			
*,1070	102	2			
.1183	91	2			
.1321	81	2			
*.1426	71	2			

TABLE II (con't)

.1472	61	2
.1626	49	2

* Examined by Shear Wave Indicia

** Broken Open in Tests

TABLE III

PART THROUGH FATIGUE CRACKS
NEAR BOLT HOLES

4340 STEEL

	Defect Length				
SFF1	.015	.020	SFF7	.045	.052
SFF2	.012	.041	SFF8	.050	.035
SFF3	.015	.035	SFF9	.022	.045
SFF4	.032	.044	SFF10	.038	.045
SFF5	.020	.025	SFF11	.032	.048
SFF6	.030	.044	SFF12	.022	.028

7075 T6AL

BAL1	.025	.040
BAL2	.032	.045
BAL3	.018	.025
BAL4	.045	.055
BAL5	.021	.070
BAL6	.040	.038
BAL7	.012	.030
BAL8	.018	.022
BAL9	.080	.045
BAL10	.055	.062
BAL11	.080	.075
BAL12	.072	.082

TABLE IV

EDM NOTCHES

TYPE AA	Spark Cut .005 Monel Wire	
AA1	.030 x .005	CD
AA2	.010 x .005	CD
AA3	.020 x .005	CD
AA4	.030 x .005	CD
AA5	.040 x .005	CD
AA6	.050 x .005	CD
TYPE AB		
AB1	.007 x .037	CD
AB2	x .015	CD
AB3	.008 x .043	6°
AB4	.008 x .055	6°
AB5	.008 x .027	30°
AB6	.008 x .033	30°
AB7	.007 x .043	30°
AB8	.013 x .026	30°
AB9	.014 x .041	30°
AB10	.015 x .032	30°
AB11	.014 x .023	CD
AB12	.014 x .033	CD
AB13	.013 x .037	CD
AB14	.013 x .025	10°
TYPE AL		
AL1	.030 x .010	10°
AL2	.050 x .010	10°

TABLE IV (Continued)

	a Length	c Depth	w Width
AC1	.015	.030	.005
AC2	.020	.030	.005
AC3	.030	.030	.005
AC4	.018	.005	.005
AC5	.030	.005	.005
AC6	.055	.005	.005
AC7	.020	.010	.005
AC8	.031	.010	.005
AC9	.048	.010	.005
AC10	.026	.020	.005
AC11	.035	.020	.005
AC12	.047	.020	.005
AD1	.010 x .008		
AD2	.026 x .003		
AD3	.034 x		
AF1	.007 x .008		
AF2	.020 x .008		
AF3	.039 x .008		
AC13	.063 x .008		
AC14	.077 x .010		
AC15	.053 x .010		
AC16	.039 x .010		
AC17	.047 x .010		
AC 18	.056 x .010		

TABLE IV (Continued)

AE1	.019 x .009 x .008	
AE2	.019 x .010 x .005	
AE3	.018 x .020 x .005	
AG1	.032 x .009	CD
AG2	.010 x .025 x .006	
AG3	.015 x .006	CD
AI1	.020 x .009	
AI2	.021 x .010 x .008	
Ai3	.020 x .020 x .006	

TABLE V

STEEL EDM NOTCHES OUT OF 0.5" BOLT HOLES

A Transducer Focused on Defect at Top of Plate
B Transducer Focused on Defect at Bottom of Plate

Defect Length (9) in. avg.	Signal Height (Arbit. Units) A (avg. of 5rdgs)	B (avg. of 5rdgs)
.015	1.5	1.5
.017	1.6	1.6
.020	1.8	2.0
.022	1.8	2.1
.023	2.0	2.1
.027	2.1	2.3
.030	2.2	2.5
.032	2.3	2.6
.037	2.6	2.9
.040	2.8	SAT
.050	3.0	SAT

TABLE VI

STEEL FATIGUE CRACKS OUT OF 0.5" BOLT HOLE

Defect Length A	Defect Depth C (estimated by micrometer)	Maximum at Xi Signal Height Arbitrary Units (avg. 5 readings)
.015	.022	1.5
.022	.035	1.6
.032	.040	1.8
.037	.040	2.0
.041	.040	2.3
.044	.042	2.3
.052	.050	2.5

TABLE VII

PART-THROUGH FLAWS

SPECIMEN	TOP DEPTH	BOTTOM DEPTH	WIDTH	DEPTH LENGTH OF FLAW INTO PLATE INCHES
AB-3	.043	0.00	.008	0.42
AB-4	.055	.0035	.007	0.50
AB-5	.027	.000	.007	0.047
AB-6	.033	.000	.008	0.063
AB-7	0.43	.000	.007	0.078
AB-9	.041	.000	.014	0.078
AB-10	.032	.000	.015	0.063
AA-2	.010	.007	.009	0.50
AC-13	.063	.008	.010	0.50
AC-14	.077	.047	.010	0.50
AC-15	.053	.009	.010	0.50

TABLE VIII

EFFECT OF 5% SALTWATER CORROSION
ON ULTRASONIC SIGNALS (ALUMINUM)

FATIGUE CRACKS

Spec #	Orig Signal	12 hrs.	24 hrs.	48 hrs.
A79	4.6*	5.2*	5.3*	5.3*
A84	4.7*	5.6*	5.6*	5.8*
A55	4.2*	6.0*	6.0*	6.2*
A68	3.0	4.5	4.8*	4.8*

*SENS (2.0)

EDM NOTCHES

Spec #	Orig Signal	12 hrs.	24 hrs.	48 hrs.
NA27	2.0	2.0	2.0	2.0
NA24	2.4	2.4	2.4	2.4
NA32	2.8	2.8	2.8	2.8
NA41	2.9	2.9	2.9	2.9

TABLE IX

EFFECT OF SIGNAL LEVEL ON REJECTS BY EDDY CURRENT
vs VISUAL IDENTIFICATION

Signal Level	Number of Eddy Current Rejects (N_e)	Number of Visual Rejects (N_v)	Ratio N_e/N_v
5.0	4	13	.30
4.75	8	8	1.0
4.5	14	10	1.4
4.25	35	13	2.6
4.0	56	15	3.77
3.75	67	6	11.2

TABLE X

CONSTANT DEPTH AND WIDTH

SPECIMEN	DEPTH INCHES	WIDTH
AB-11	.023	.014
AB-12	.033	.014
AB-13	.037	.013
AA-3	.022	.009
AA-4	.034	.009
AA-5	.045	.016
AA-6	.052	.011

TABLE XI

VARYING DEPTH NEAR SURFACE FLAWS

SPECIMEN	a DEPTH	b AXIAL DEPTH
AC-4	.018	.005
AC-5	.030	.005
AC-6	.058	.005
AC-7	.020	.010
AC-8	.031	.010
AC-9	.048	.010
AC-10	.026	.020
AC-11	.035	.020
AC-12	.047	.020